



Jimma University
Jimma Institute of Technology
Faculty of Mechanical Engineering

**Design and Optimization of PCM integrated Solar Water Heating System:
Case Study Limmu Gennet Hospital**

By: Oluma Wolde Tolosa

This Thesis is Presented to the School of Graduate Studies at Jimma University as a Partial Fulfillment of the Requirements for Obtaining a Master of Science Degree in Mechanical Engineering with a Specialization in Thermal System Engineering.

Sep., 2023
Jimma, Ethiopia



Jimma University
Jimma Institute of Technology
Faculty of Mechanical Engineering

**Design and Optimization of PCM integrated Solar Water Heating System:
Case Study Limmu Gennet Hospital**

By: Oluma Wolde Tolosa

This Thesis is Presented to the School of Graduate Studies at Jimma University as a Partial Fulfillment of the Requirements for Obtaining a Master of Science Degree in Mechanical Engineering with a Specialization in Thermal System Engineering.

Main advisor: Balewgize Amare Zeru (Asst. Prof)

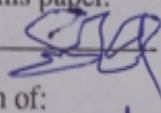
Co-advisor: Nebyou Bogale (Asst. Prof)

Sep., 2023
Jimma, Ethiopia

Declaration

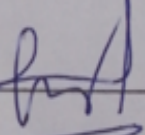
I, the undersigned, sincerely declare that this research paper titled "Design Optimization of the Water Storage Tank by Thermal Stratification Integrated with PCM for Solar Water Heating System as Thermal Storage through CFD Simulation (A Case Study of Limmu Gennet Hospital)" is my original work. I have conducted this research under the supervision of Balewgize Amare (Asst. Prof.) and co-advisor Nebiyou Bogale (Asst. Prof.). I confirm that this work has not been submitted for the award of any academic degree or similar qualification at any other institution or university.

I further affirm that all the sources I have used or quoted in this research have been appropriately indicated and acknowledged. I take full responsibility for the accuracy and integrity of the information presented in this paper.

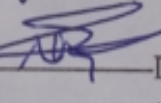
By: Oluma Wolde Tolosa Signature  Date 23.10.23

The work has been done under the supervision of:

1. Main Advisor

Balewgize A. Zeru (Asst. Prof.) Signature  Date 23.10.23

2. Co-advisor

Nebiyou Bogale (Asst. Prof.) Signature  Date 23.10.23

3. External Examiner

Name Samson M. Atnaw (PhD) Signature  Date _____

4. Internal Examiner

Tarakegn Limore (MSc) Signature _____ Date _____

5. Chair Person

Eshetu Tadese (MSc) Signature _____ Date _____

Acknowledgment

First and foremost, I would like to express my truthful gratitude to God for granting me the opportunity to complete this research and for guiding me through all the challenges and triumphs along the way. I would like to extend my heartfelt appreciation to my advisor, Balewgize Amare (Asst. Prof), and Co-advisor Nebiyu Bogale (Asst. Prof.), for their unwavering support, invaluable advice, and guidance throughout the entire duration of this research. Their expertise and encouragement have been instrumental in shaping the direction and success of this study.

I would also like to acknowledge the Jimma University Institute of Technology Department of Mechanical Engineering for their support and resources that have greatly contributed to the completion of this research.

Furthermore, I am deeply grateful to all my classmates and friends who have provided me with their insightful comments, suggestions, and encouragement throughout the course of this research. Their camaraderie and support have been invaluable.

Lastly, I would like to express my profound appreciation to all my teachers who have imparted their knowledge and wisdom upon me, helping me grow both academically and personally.

Without the support and guidance of these individuals, this research would not have been possible. I am truly grateful for their contributions and am honored to have had the opportunity to work with such wonderful people.

Abstract

Solar energy is abundant renewable energy available everywhere, environmentally friendly and easily harnessed, and used for domestic and industrial water heating applications. Since this energy is alternating, a thermal energy storage system is required to store the energy for later use. Many authors optimized TES (K. Kumar et al., 2021) (Karuthedath et al., 2020). However, they did not consider the effects of the inlet design of a HWT to store large amounts of energy. In this study, the diameter and height of the HWT were calculated from the total volume of hot water required for the hospital which was found to be 38.88m³. Using this volume, height and diameter of HWT are 4.64m and 2.32m. A total volume of 5.8m³ PCMs was designed and integrated into latent Shell and tube TES by modeled Solidworks2020. The site solar energy analyzed from 2017 to 2021 collected from Jimma Metrology Agency temperature of cold and hot water was 295K and 375K, respectively. In this work, three models of HWT were studied with different inlet designs to optimize HWT and enhance the thermal stratification of hot water tanks. Model 1 was designed with an ordinary inlet pipe, while model 2 was perforated. However, in model 3, holes were used as inlet and outlet. A detailed simulation was performed by ANSYS FUEENT 19.2 independently for each model with the same mass flow rate of 1.31 kg/s and inlet temperature of cold and hot water 295K and 375K, respectively.

CFD result indicated that efficiency of model 2 was improved from 53.1% to 56.2% compared to model 1 and 49.9% to model 3. In model 1, around six layers are seen; in model 2, only one layer is observed.

Key words: solar water heater, hot water tank, thermal stratification, PCMs, perforated pipe, normal pipe, CFD, Solidworks2020.

Contents

Declaration	i
Acknowledgment	ii
Abstract	iii
List of Abbreviations, Symbols, and Nomenclatures	iv
1 Introduction	1
1.1 Statement of the Problems	4
1.2 Objectives of the Study	5
1.2.1 Main Objective	5
1.2.2 Specific Objectives	5
1.3 Scope and Limitations	6
1.3.1 Scope of this Study	6
1.3.2 Limitations of this Study	6
1.4 Significant of the Research	6
2 Literatures Review	7
2.1 Concepts of Solar Water Heaters	7
2.1.1 Different Types of Solar Water Heating Systems	9
2.2 Review of Solar Water Heater Parts	10
2.2.1 Collectors for Solar Energy	10
2.2.2 Flat Plate Collectors	10
2.2.3 Evacuated Tube Collector	11
2.3 Thermal Energy Storage (TES)	12
2.3.1 Thermal Energy Storage Types	12
2.3.2 Sensible Heat Energy Storage (SHES)	13
2.3.3 Storage of Latent Heat Energy (SLHE)	13
2.4 Phase Change Materials (PCM)	14
2.4.1 Classification of PCM	14
2.4.2 Thermo-Physical Properties of (Solid-Liquid PCMs)	16
2.4.3 Properties and Phase Change Material Selection	17
2.4.4 Phase-Change Materials for the Storage of Thermal Energy (TES-PCMs)	17

2.5	Related Previous Work	18
3	Methodology and Materials	31
3.1	Description of Study Area	31
3.2	Data Collected from Limmu Genet General Hospital and Specific Location	32
3.2.1	Assessment of Daily Hot Water Demand of the Hospital	33
3.2.2	Regular Hot Water Consumption Outline (Pattern)	36
3.3	Storage Capacity of Hot Water Tank	38
3.4	Materials and Methods	39
3.4.1	Material Selection	39
3.4.2	Design of Hot Water Storage Tank	41
3.4.3	Thickness Optimization Hot Water Tank	42
3.4.4	Optimization of Insulation Storage Tank Thickness	44
3.5	Selection and Design of Paraffin PCMs	47
3.5.1	Selection of Paraffins as PCMs	47
3.5.2	Mechanism of Thermal Energy Storage System	48
3.5.3	Assumption for Latent Heat Thermal Energy Storage System and Design Consideration	48
3.5.4	Design of Phase Change Materials PCM	49
3.6	Energy Storage Unit	49
3.6.1	Selection Geometric Parametric of Shell and Tube	49
3.7	Modeling and Optimization of Hot Water Storage Tank by Thermal Stratification	51
3.7.1	Modeling of Inlet Pipe for Inlet Design Optimization	52
3.8	Proposed Solar Water Heating System Integrated with Different Com- ponents	54
4	Available Solar Radiation Assessment of Limmu Gennet	56
4.1	Basic Sun-Earth Angle Relationship	56
4.2	Average Monthly Day-to-day Solar Energy on Horizontal Surface	59
4.2.1	Monthly Average Diffuse Radiation (H_d) on A Horizontal Surface	64

4.2.2	Monthly Average Global Radiation (H_T) on Horizontal Surface	64
4.2.3	Monthly Average Beam Radiation (H_b) on Horizontal Surface	65
4.3	Monthly Average Hourly Global Radiation on a Horizontal Surface	66
4.3.1	Average Monthly Hourly Diffusion Radiation on Horizontal Surface $I_d \left(\frac{w.h}{m^2} \right)$	66
4.3.2	Average Monthly Hourly Beam Radiation on Horizontal Surface $I_b \left(\frac{w.h}{m^2} \right)$	66
4.3.3	Hourly Solar Energy Estimation on Inclined Surfaces	67
4.4	Evaluating the Effectiveness of Flat Plate Solar Collectors	69
4.5	Mathematical Energy modeling on flat plate solar collectors	70
4.5.1	Theoretical Design of Collector	71
4.5.2	Determining the Overall Heat Loss Coefficient of Solar Collectors (U_L)	71
4.6	Theoretical Collector Efficiency Factors	79
5	CFD Simulation Analysis of Hot Water Storage Tank	83
5.1	Pre-Processing	84
5.1.1	Geometry	84
5.1.2	Generation of Mesh	85
5.1.3	Mesh Independent Test	86
5.2	Boundary and Initial Condition	88
5.3	Governing Equation and Assumption	89
5.4	Selection Turbulence Flow Model	90
5.5	Setup	90
5.6	Defining Material Properties	90
5.7	Operating and Boundary Conditions	91
5.8	Solution Methods	92
5.9	Solution Initialization	92
6	Result and Discussion	93
6.1	Hot Water Storage Tank CFD Analysis	93

6.2	Temperature Distribution or Contours Profiles	93
6.3	Pressure Contours or Distribution Profiles	96
6.4	Streamlines or Velocity Distribution Profiles	99
6.5	Variation of Outputs with Mass Flow Rates	102
6.6	Comparisons of Hot Water Storage Tank with Stratification and Without Stratification	105
6.7	Comparisons of Thermal Stratification Hot Water Storage Tank with Experimental Results	107
7	Conclusion and Recommendations	109
7.1	Conclusion	109
7.2	Recommendations	110
	References	111
A	Appendix	115
A.0.1	Analyzed average monthly sunshine hours of Limmu Gennet for five years	115
A.0.2	The monthly average daily solar radiation on the horizontal sur- face (H_o)	116
A.0.3	General thermodynamic characteristics of PCMs(Zhang et al., 2018)	116
A.0.4	Summary technical data designed thermal and hot water tank. .	117
A.0.5	Questionnaire	118

List of Tables

2.1	Summary of Literature Reviews.	27
3.1	Information collected from Limmu Gennet General Hospital	32
3.2	Average hot water requirement for international hospital appliances (Fuentes et al., 2017)	33
3.3	Water consumption (hot) of Limmu Gennet General Hospital per room .	35
3.4	Total hot water consumption of Limmu Gennet general Hospital per rooms	36
3.5	Physical properties of mild steel	40
3.6	Desirable Thermophysical properties of selected paraffin.	48
4.1	Standard suggested average days for months and values of n by months	60
4.2	Average monthly sunshine hours of Limmu Gennet (2017-2021)	61
4.3	Average sunshine hour duration (2017-2021)	61
4.4	Hour Angle (W_s).	63
4.5	Maximum possible daily hours sunshine duration (N).	63
4.6	Monthly average diffuse radiation (H_d) on a horizontal surface	64
4.7	Month average everyday global radiation ($kwh/m^2/da$) on horizontal surface	64
4.8	Monthly Average Beam Radiation ($kwh/m^2/da$) on Horizontal Surface	65
4.9	Monthly average hourly global radiation on the horizontal surface $I \left(\frac{w.h}{m^2} \right)$.	66
4.10	Diffusion radiation on horizontal the surface $I_d \left(\frac{w.h}{m^2} \right)$	66
4.11	Beam Radiation on Horizontal the Surface $I_b \left(\frac{w.h}{m^2} \right)$	67
4.12	Average angle of incidence	67
4.13	Average zenith angle	68
4.14	Summary of average temperature five years analysis of the site	68
5.1	Nodes number and elements versus different mesh sizes	86
5.2	Three properties of liquid water and materials (mild steel and fiberglass)	91
5.3	Thermo-physical properties of working fluid (liquid water) and solid materials (mild steel and fiber glass.	91

6.1	Mass flow rate vs outlet with normal pipe (model 1)	102
6.2	Mass flow rate vs outlet with perforated pipe inserted (model 2)	103
6.3	Mass flow rate Vs outlet without insert pipe (model 3)	104
6.4	Mass flow rate vs outlet for each model	106

List of Figures

2.1	Active solar water heating system (Rasha and Science, 2020)	7
2.2	Passive water heating with solar energy (Rasha and Science, 2020)	8
2.3	Classification of solar water heating system	9
2.4	Flat plate collectors (Rasha and Science, 2020)	10
2.5	Evacuated tube collectors (Rasha and Science, 2020)	11
2.6	Types of thermal energy storage	12
2.7	Classification of phase change materials	14
2.8	Temperature-time curve of PCMs a) charging and b) discharging processes	17
2.9	Standard heating curve	18
2.10	Schematic indication of PCM in water storage (Huang et al., 2019)	21
2.11	Heat storage tank with Equalizer	24
2.12	Schematic diagram of hot water storage tank	26
3.1	Geographical location of Limmu Kossa (Diro, 2019).	31
3.2	Variation of consumption load with different rooms	35
3.3	Total variation of hot water load in different rooms	36
3.4	Regular hot water consumption pattern in an hour per day	37
3.5	Proposed model for the hot water storage tank	47
3.6	Component and inner structure of proposed model for PCMs shell and tube heat exchanger	50
3.7	Fully assembly of the proposed model for PCMs shell and tube heat exchanger a) indicates solid full structure and b) indicates transparent inner visualization structure	51
3.8	Dimension and diagram of the inlet pipe.	52
3.9	Perforated Inlet Pipe	54
3.10	Normal Inlet Pipe	54
3.11	Proposed solar water heating system integrated with different component	55
4.1	Hour angle (Maleki et al., 2017)	57
4.2	Definition solar azimuth angle (Maleki et al., 2017)	58
4.3	Average monthly sunshine of Limmu Genet for five years	61

4.4	Hourly sunshine duration of Limmu Genet (Bar chart)	62
4.5	Hourly sunshine duration of Limmu Genet (Graph)	62
4.6	Solar radiation of Limmu Genet on the horizontal surface	65
4.7	Typical liquid flat plate collector (Klevinskis and Buinskis, 2011)	69
4.8	Sheet and tubes (Thermal and Engineering, 2019)	80
5.1	Steps of analysis CFD	83
5.2	CFD geometry model of hot water storage tank designed with a normal pipe inserted.	84
5.3	a) Normal pipe used in model 1 b) Perforated pipe used in model 2.	85
5.4	CFD geometric model of hot water storage tank constructed without inserting inlet pipe.	85
5.5	Mesh generation and visualization of different mesh sizes.	86
5.6	The selected Finner mesh element size's view	87
5.7	Variation of outlet temperature with mesh size elements.	88
6.1	Model 1, Normal pipe inserted	94
6.2	Model 2, Perforated Pipe inserted	95
6.3	Model 3, with holes instead of inlet pipe	96
6.4	Model 1, Pressure contours hot water storage tank constructed normal pipe inserted.	97
6.5	Model 2, Pressure contours hot water storage tank constructed perforated pipe inserted.	98
6.6	Model 3, Pressure contours hot water storage tank holes instead of inlet pipe.	99
6.7	Model 1, Streamlines of hot water storage tank with normal inlet pipe.	100
6.8	Model 2, Streamlines of Hot Water Storage Tank with Perforated Inlet Pipe.	101
6.9	Velocity distribution of model 3 HWST holes instead of inlet pipe	101
6.10	Mass flow rate Vs outlet temperature for model 1	102
6.11	Mass flow rate Vs outlet temperature for model 2.	103
6.12	Mass flow rate Vs outlet temperature for model 3.	104
6.13	Mass flow rate Vs outlet temperature for each model	106
6.14	Comparison of CFD results with experimental results	108

List of Abbreviations, Symbols, and Nomenclatures

Abbreviations

PCMs	Paraffin phase change of materials
HST	Hot Water Tank
LHTES	Latent Heat storing thermal energy
SHS	Storing Sensible Heat
TES	Sensible Heat Storage of Thermal Energy
LHS	Thermal Energy Latent Heat Storing
CFD	Computational Fluid Dynamics
HWLL	Laundry Hot Water Consumption
HWLK	Kitchen Hot Water Consumption
HWLR	Restaurant Hot Water Consumption
HWLS	Shower Hot Water Consumption
HLC	Heat Loss Cost
CMS	Material Cost
HTF	Fluid Transfer heating
OC	Overall cost

Symbols

ρ_m	Material Density (kg/m^3)
μ_d	Material Dynamic viscosity (Pas)
β_{th}	Coefficient of Thermal Expansion (k^{-1})
τ	Glass Cover Emissivity
α	Absorptivity (Glass Cover)
ϕ_s	Location of the Site (Latitude)
θ_{zs}	Angle (Zenith)
ω_h	Angle (Hour)

Nomenclatures

c_{pw}	Water specific heat capacity
K_s	Material thermal conductivity (w/mk)
V	Volume (m^3)
m_s	Mass of substance (kg)
Q	Quantity of heat (J)
H_c	Coefficient of Heat Transfer (w/m^2k)
A_c	Area of Collector (m^2)
A_r	Area of absorber (m^2)

m_{fr}	Flow rate (of mass) (kg/s)
T_{f0}	Final Outlet Collector (Fluid Temperature)
T_{sgc}	Stagnation Collector (Temperature) (K)
Re	Reynolds numbers
N_U	Nusselt number

Chapter 1

Introduction

Most rural areas in developing countries use fossil fuels and biomass for water heating systems in domestic, hospitals, hotels, etc. However, since the fast-decreasing abundance of fossil fuel and increasing demand for it, there is a need to explore alternative energy sources. Biomass application is directly related to deforestation, which leads to ozone layer destruction, which causes environmental pollution worldwide. The use of electric energy for water heating systems is very costly. Another problematic use of electric power for such purposes is the lack of gridlines, especially in rural areas of developing countries. Energy costs and water heating operations are rising significantly, reducing profitability and depletion of fossil fuel resources. In Ethiopia, local water heating systems heavily rely on electric power, fossil fuels, and biomass as their primary energy sources. However, the decreasing availability of fossil fuels and the environmental impact of biomass usage have created a need for alternative energy sources. Additionally, using electricity for water heating is expensive and inaccessible in many rural areas. This energy has led to intensifying costs and reduced fossil fuel resources. Given the global energy crisis and its link to climate change, research has focused on sustainable energy sources such as solar energy, wind power, rainfall, and waves. Solar energy, in particular, is cost-effective and environmentally friendly (Thermal and Engineering, 2019). Utilizing solar energy for domestic and industrial water heating can save money, reduce reliance on imported oil, and contribute to a sustainable future (Repository, 2014).

Modern systems are designed to capture solar power and use heat transfer fluid for immediate storage. In settings like hospitals, where hot water is needed for various applications, solar energy can be stored in thermal energy accumulators like hot water tanks or heat storage tanks, as well as in energy-storing materials like phase change materials (PCMs). PCM allows constant solar energy consumption, even on days without direct sunlight. Thermal energy storage systems are designed to store excess solar energy during periods of high availability, such as during sunny days, and release it when there is a demand for hot water or heating. TES allows for a constant energy supply even when direct sunlight is unavailable (Zhang et al., 2018).

Thermal energy storage (TES) is essential for renewable energy systems, particularly solar systems, to overcome the issue of mismatched supply and demand. Numerous studies have highlighted the potential for optimizing the performance of components in solar water heaters to reduce the additional energy requirements for domestic hot water heating systems. As a result, TES has emerged as a significant area of research within the solar energy utilization technology field. TES is a critical component of solar heating systems and plays a crucial role in maximizing the efficiency and effectiveness of these systems. (Wang, 2019).

When it comes to applications involving individual and communal waste heat recovery and other-temperature heating like Air-Source pump (ASHP) water heaters, centralized systems are interested in the thermodynamic quality of the recovered energy. Due to the low energy storage capacity per unit mass of water and significant temperature fluctuations in heat storage, the efficiency of solar energy utilization is reduced (Majumdar and Saha, 2019) (Wang, 2019). To increase uses of the latent heat of phase-change materials used to release and store the heat energy during off-day times. It also contains large heat storage density, a wide range of temperature coverage, and relatively low cost. It is used as latent heat energy storage, improving the total energy capacity of heat storage tanks. Thermal energy storage can be divided into two categories: latent and sensible. Among these types, latent heat thermal energy storage (LHTES) offers several advantages, such as high storage capacity, low storage volume, isothermal operation during charging and discharging phases, and minimal variation in operating temperature (Abokersh, 2018). The conventional method of solar-powered water heating typically involves a tank for storing water and conserving thermal energy by holding it as sensible heat. Still, heat energy is stored by sensible thermal energy storage, which requires a large volume and expensive insulating technique. On the other hand, the drawback of latent heat thermal energy storage is that it is difficult to modify. For this problem, combined sensible and latent heat thermal energy storage techniques can be used, benefiting from the advantages of both types. One approach is to place phase change material (PCM) capsules within the water TES tank. Encapsulation enhances heat transfer between the PCM and the surrounding medium, overcoming the PCM's low thermal conductivity (Abokersh, 2018).

Thermal stratification is crucial for optimizing solar water heaters in domestic hot water systems. It involves creating distinct layers of cold and hot water within the storage tank, with cold water at the bottom and hot water at the top. This stratification is achieved through density variation and gravitational effects (K. Kumar et al., 2021). Another method of thermal stratification is reducing fluid turbulence, which affects thermal energy inside the storage tank. However, the thermally stratified hot water storage tank is affected by factors ratio of height-to-diameter, the structure of the storage tank, and the water's flow rate. Limmu General Hospital is located in the rural area of the country. It primarily uses biomass and fossil fuels for hot water heating systems. In addition to this, it uses two standby generators to overcome these problems. Using a solar water heating system is the best alternative source of energy. The application of solar energy for water heating systems and others in this area is unknown. So, solar energy application for this hospital is critically recommended. Many authors worked on solar water heating systems at different places by different methodologies (Thermal and Engineering, 2019) (Supply et al., 2016b). Most of them did not focus on remote areas to solve the problem of the rural community. (Wang et al., 2020) worked on an experimental study on improving stratification in heat storage using an equalizer and PCM unit. A novel equalizer was used to regulate the flow rate of inlet cold water at the bottom of the water tank. However, the hot water flow rate into the water tank also dramatically affects the system, and this study did not indicate the hot water flow rate of the system.

This study is focused on the inlet design of a hot water storage tank to optimize its uniform temperature inside the hot water storage system to obtain a constant hot water temperature outlet integrated with the PCM solar water heating system. Consumption of hot water data is gathered from the hospital and analyzed, solar energy data is taken from Jimma zone metrology and analyzed, and materials are selected to design a water storage tank and modelled by solid work software. Computational fluid dynamics CFD simulation is used to know the temperature distribution inside it and the efficiency of newly modelled hot tanks for storing water equipped with different pipe inlets.

1.1 Statement of the Problems

In nearly all regions of Ethiopia, the rural healthcare center greatly depends on biomass, fossil fuel, and electrical power for water heating. However, utilizing biomass results in the destruction of forests, which causes environmental pollution. In contrast, in addition to high payment costs in town, scarcity of electrical power is a significant problem in the rural areas. To reduce these problems, using optimized solar energy devices as a substitute is the best solution for water heating water systems.

Limmu Genet General Hospital uses biomass, fossil fuel, and electric power for its water heating system. The availability of electric power is rare since it is far from the electric gridline. The hospital uses two standby generator, which consumes more than 200 liters daily and requires high maintenance costs. To reduce this problem and traditional ways of water heating systems and dependence on electric power, solar water heating systems and energy storage systems (TES) as thermal storage are promising and important. Many studies were conducted in this area with different methodologies (Thermal and Engineering, 2019) (Supply et al., 2016b). Many of them did not focus on remote regions to solve the problem of the rural community. Most research has been done on integrated water heating systems using phase-change substances for storing hot water as thermal energy storage through sensible heat during peak off sunlight. This drawback is that they need large volumes and expensive insulation materials to store hot water (Sarkar and Bhattacharyya, 2012). But, the latent heat-storing method has a high cost for modifications to the system (Abokersh, 2018).

It is necessary to optimize hot water technology design for a continuous hot water supply an adequately designed hot water tank stores solar energy for constant application. Thermally stratified hot water tanks improve the efficiency of storage tanks to reduce the problem of energy storage deficiency during instability between supply and demand (Bouzaher et al., 2019). Thermal stratification of the hot water storage tank's design affects the effectiveness of hot water tank technologies. Therefore, this research mainly focuses on design optimization and CFD analysis of tanks for storing hot water.

1.2 Objectives of the Study

1.2.1 Main Objective

The main objective is to study design and optimization of PCM integrated solar water heating system for limmu gennet hospital to collect constant hot water temperature inside hot water storage tank.

1.2.2 Specific Objectives

- To collect data of solar radiation from appropriate nearby meteorology analysis the data, to compute the daily average solar radiation, the monthly average solar radiation, the solar azimuthal angle, zenith angle and optimum tilt angle of selected site.
- To collect data of hot water demand of the hospital and analysis the data, to compute the demand of hot water for each room such as kitchen, shower, and laundry and total demand of hot water consumption.
- Numerical designing of diameter and height of shell and tubes, numbers of tubes required, volume and mass of PCM required, material and insulation selections and SolidWorks modeling of thermal energy storage integrated with PCM.
- Numerical designing of diameter and height hot water tank and SolidWorks modeling of the hot water tank with normal inlet pipe, perforated inlet pipe and holes as inlet to predict effects of inlets on hot water storage tank and perforated inlet pipe as inlet design optimization to reduce high turbulence.
- To analyze the site solar radiation to compute the local global solar radiation, temperature of cold and hot water and numerical analysis of flat plate solar collector, to calculate total heat loss, useful energy gain.
- To compare hot water storage tanks with stratification, without stratification and experimental results of related work.

1.3 Scope and Limitations

1.3.1 Scope of this Study

This work is limited to the study selected Limmu Gennet Hospital weather conditions. Numerical designing and modelling of hot water storage tank and inlet pipes to investigate the thermal behaviour of storage tank. It also includes thermal energy storage integrated PCM numerical modelling and designing and collecting data from the hospital and metrology agency to analyze the amount of hot water consumption and availability of solar energy.

1.3.2 Limitations of this Study

This study is limited to the design and modelling of the hospital's hot water storage tank and thermal energy storage tank. Experiment analysis, hot water distribution for different rooms, and cost analysis are not included because of time. CFD is used to investigate the influence of inlet pipes on a hot water tank performance system.

1.4 Significant of the Research

This study's core advantage is introducing the uses of solar energy applications in rural areas integrated with PCM and the effect of the inlet structure on hot water storage tanks. Generally, the outcome of this work is to:

- Promote solar energy application in rural areas.
- Enhance clean energy uses from solar energy.
- Reduce the independence of imported fuel energy for different applications.
- Introduce phase change materials as the best energy storage for continuous energy supply.
- Improve a clean environment by reducing the use of fossil fuels replaced by solar energy.

Chapter 2

Literatures Review

2.1 Concepts of Solar Water Heaters

The solar water heating system is the interconnection or integration of several components, such as solar collectors, thermal and hot water energy storage devices, pumps, valves, and other details for water and space heating applications (Benli, 2016). The core advantages of components are to collect or capture solar energy and change it into valuable heat energy (Supply et al., 2016a). The energy from the sun can be captured by modern devices utilized to warm water for immediate use or as a storage medium. There are different types of solar water heating systems. Active and passive solar water heating systems are commonly known (Vinubhai, 2014).

i. Active System (Forced Circulation)

Mechanical forces such as pumps, valves, and controllers circulate liquid water into the system. Based on the working fluid transported, it can be direct or indirect systems (Rasha and Science, 2020).

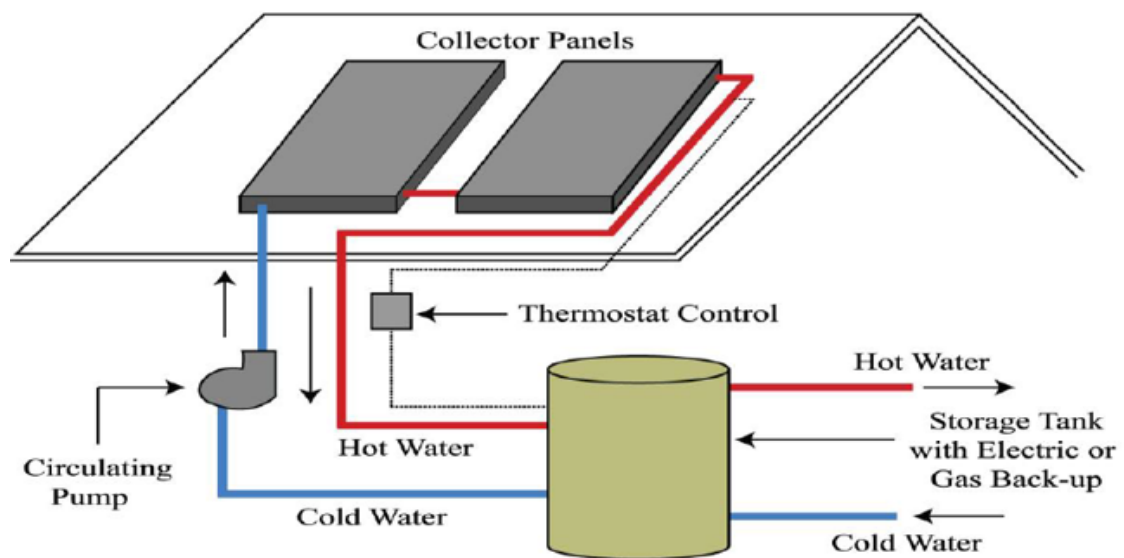


Figure 2.1: Active solar water heating system (Rasha and Science, 2020)

Direct System (Open Loop)

Water is directly heated as it flows into the solar collectors, and the pump transports the heated fluid into the system (Rasha and Science, 2020). The water storing tank can be positioned below or above the solar collectors. In this system, a single or double tank can keep water.

Indirect System (Closed Loop)

The heat exchanger or solar collectors heat water as it passes between collectors and storage tanks. The ethylene glycol solution is also used as the medium of heat exchange and liquid water. In addition, silicone oils and refrigerants can also be used if non-potable or toxic, as the medium of the double wall heat exchanger must be installed. This heat exchanger may be located inside the storage tank or externally. High-temperature prevention is needed in this system, and the air is used as a working medium to avoid such temperatures and overheating in summer and freezing in winter.

ii. Passive System

Mechanical forces such as pumps are not required to transport water into the system. It is less expensive and has a low maintenance cost compared to active systems. The passive system can be further classified as thermosiphon and integrated collected storage (Herez et al., 2020).

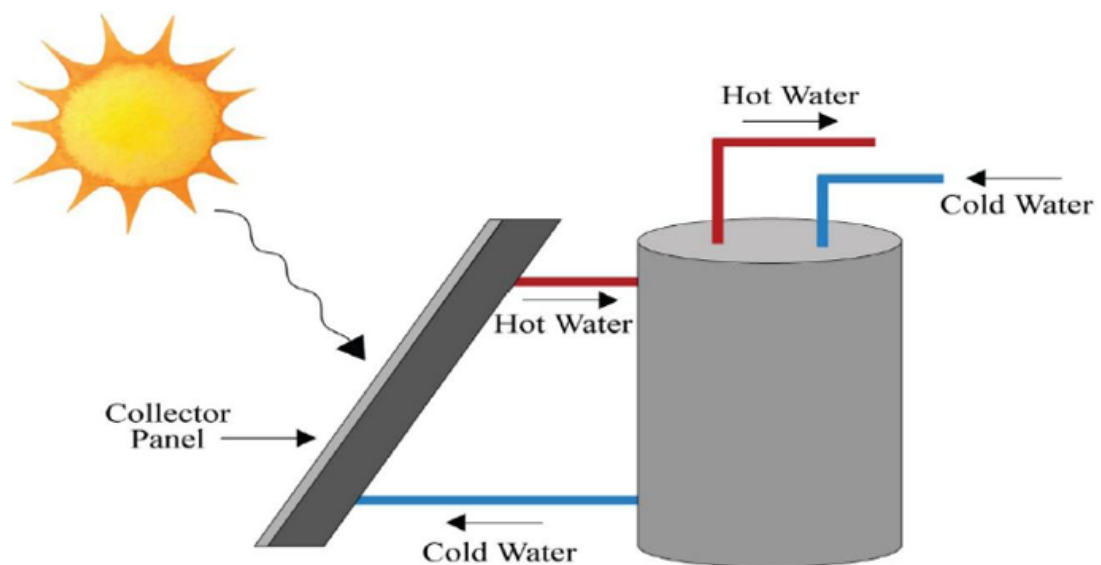


Figure 2.2: Passive water heating with solar energy (Rasha and Science, 2020)

Thermosiphon System

Mechanically simple since pumps or other parts are not required to transport fluid into the system. The water storage tank is located above the solar collectors, and as the liquid is heated into it, which is less dense, it expands up to the hot water storing tank, and cold water having higher density flows down into collectors (Supply et al., 2016b).

Integrated Collector Storage System or Batch System

In this case, the storage tank is used as a solar collector since water is directly heated in the insulated box water storing tank by sunlight. Pumps do not need to circulate water through the system; it is less expensive and less maintenance.

2.1.1 Different Types of Solar Water Heating Systems

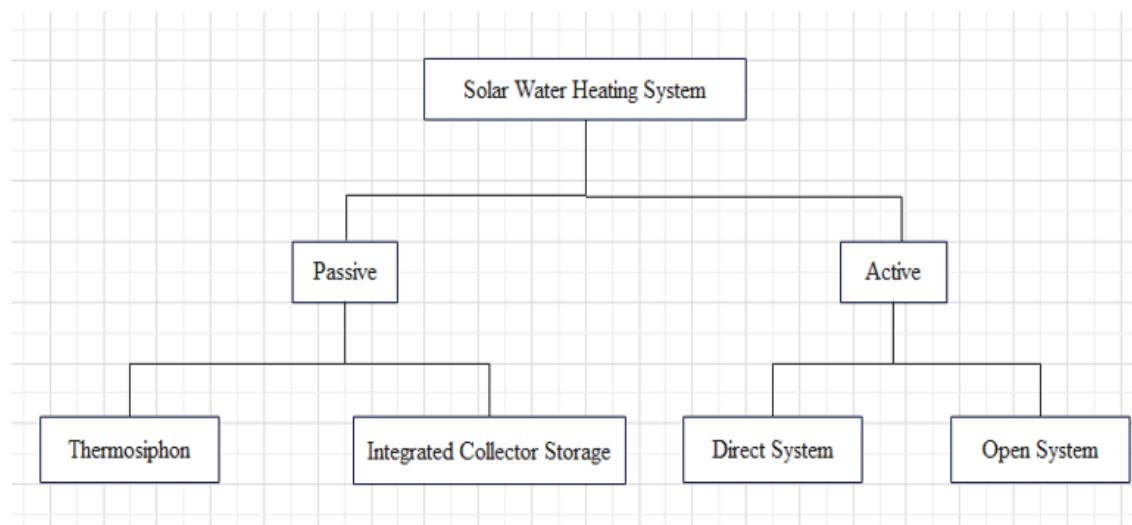


Figure 2.3: Classification of solar water heating system

This study selects a thermosiphon system because no electrical or mechanical pump is required to move fluid through an open or closed system. This system uses natural convection or conduction to circulate fluid from high to low heat and vice versa by differential pressure between atmospheric pressure and a hydrostatic pressure vacuum created by density difference across different temperatures.

2.2 Review of Solar Water Heater Parts

2.2.1 Collectors for Solar Energy

It is the device used for storing or collecting solar radiation from the sun and transforming it into valuable energy (Dupeyrat et al., 2011).

The most common solar energy collectors utilized in solar water heating systems are:

- Flat plate collectors (FPCs)
- Evacuated tube collectors (ETCs)

2.2.2 Flat Plate Collectors

This device was made up of glazed and unglazed parts. Glazed solar collectors comprise components such as insulation, copper tubes, and weatherproofed boxes that may be dark and glass plate covers (Aisa and Science, 2017). Because of its straightforwardness (simple), cost-effectiveness, simple design, and ease of installation compared to various other solar collector types, collector for flat plates is the most effectively used for residential and domestic hot water applications and used to circulate working fluid by natural convection techniques (Mahanta, 2020). Another advantage of this collector is its capability to deliver a sufficient amount of hot water at the appropriate temperature and no need for tracking to the sun since both direct and diffusive solar radiation is absorbed within it (Thermal and Engineering, 2019).

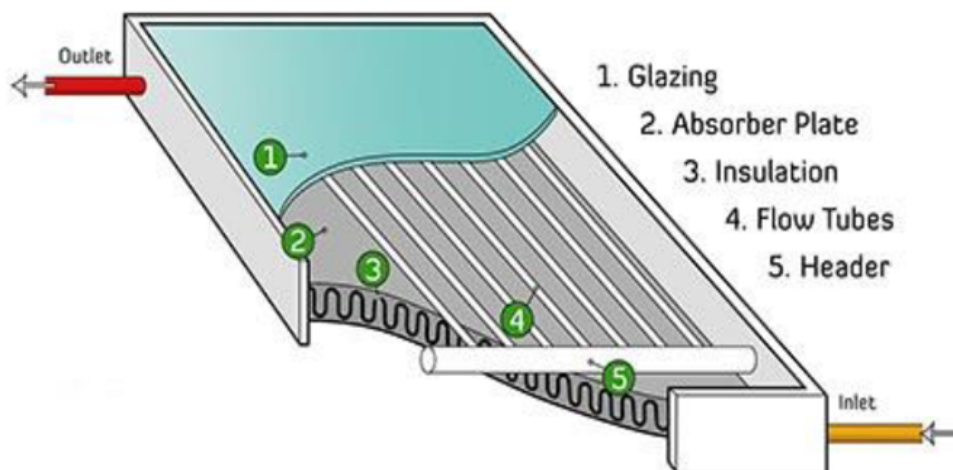


Figure 2.4: Flat plate collectors (Rasha and Science, 2020)

2.2.3 Evacuated Tube Collector

These collectors have higher efficiency than FPC due to decreased heat loss compared to FPC. Because of its high initial cost makes it less competitive than FPC (Engineering, 2021). The components of these collectors have Evacuated tubes to minimize heat losses, copper heat pipes for quick heat transfer, and aluminum housing to support other parts and maintain the system's integrity. Its absorber tube's design systems make it a more efficient shape, absorbing up to 16% more energy than FPC (Islam et al., 2013).

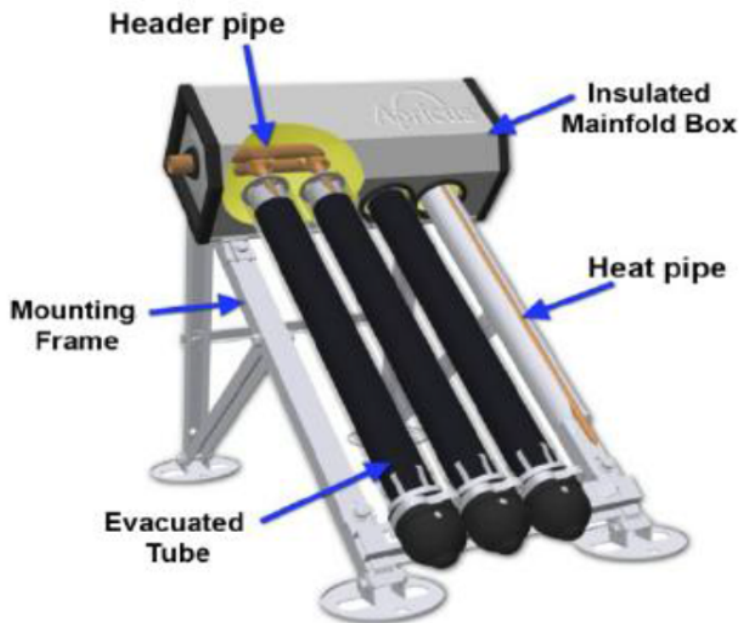


Figure 2.5: Evacuated tube collectors (Rasha and Science, 2020)

In this study, a flat plate solar collector is selected because of its cost-effectiveness, simple design, and ease of installation compared to various other solar collectors. This collector is most effectively used for residential and domestic hot water applications within required temperature ranges and to circulate working fluid by natural convection techniques; direct and diffusive solar radiation absorbed within it of tracking to the sun is not needed (Thermal and Engineering, 2019). This collector is not a concentrating collector used for water and space heating in a building and when the required temperature is below $250F^{\circ}$ sufficiently instructed. This temperature range is enough for water heating used by the hospital, so reducing the cost and complexity of designing a flat plate collector is recommended in this study.

2.3 Thermal Energy Storage (TES)

This device is used to store the production of energy for night use. Since the sun's energy is most of the appointed time accessible, unrestricted, environmentally clean, and critically favorable alternate accessible energy source since earliest records, it is intermittent (Nash et al., 2017). The magnitude and availability of solar energy depend on time and that site's meteorological location. Solar energy applications using water heating, such as hospitals, space heating, and other industrial and domestic purposes, are limited to sunlight and zero at night. The maximum water demand is warmed throughout the day and at night (Naidu et al., 2016). However, when solar radiation becomes noon, it is no means of energy for the rest of time, particularly during the night. So, thermal energy storage is required to fulfill inconsistent solar energy and meet energy demands at all times. The goal of a thermal energy system is to store all forms of power that can be applied to various applications (Zhang et al., 2018). In addition, TES is also used to increase the performance and consistency of the system, increase overall efficiency, improve the economy, and reduce pollution in the atmosphere.

2.3.1 Thermal Energy Storage Types

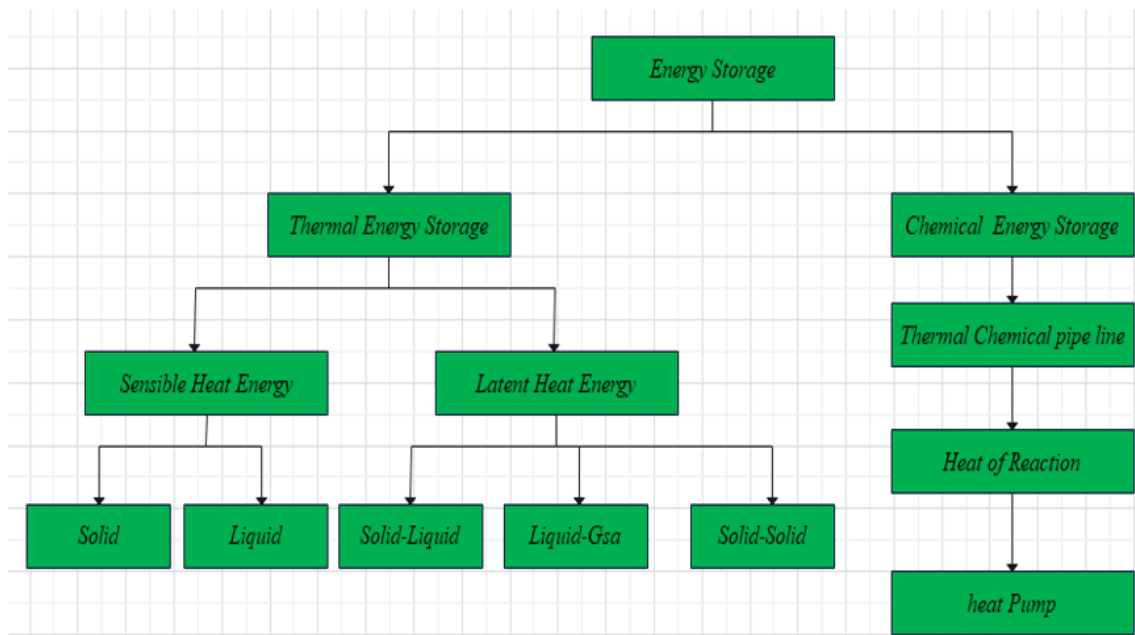


Figure 2.6: Types of thermal energy storage

2.3.2 Sensible Heat Energy Storage (SHES)

In this system, thermal energy is stored by increasing the temperature of solid-phase or liquid-phase materials. The specific heat of a substance is used to keep heat energy because of temperature differences. The hot water tank is the best thermal energy storage compared to others, such as phase change and thermos-chemical storage and storage of medium because of its low cost and high specific heat capacity for sensible heat needed to be stored (Rasha and Science, 2020).

The amount of heat stored is based on the thermal capacity of the substance and the temperature difference during the process (Zhao et al., 2018).

$$Q_{sensible} = \int_{T_1}^{T_2} mc_p dT \quad (2.1)$$

$$Q_{sensible} = mc_p \Delta T \quad (2.2)$$

where, $Q_{sensible}$ total heat stored (KW), m masses heat storing materials (kg/s), c_p specific heat storing material (kJ/kg.C°) and ΔT temperature difference (C°).

2.3.3 Storage of Latent Heat Energy (SLHE)

To overcome the challenge of sensible heat energy storage, latent heat energy storage is developed to provide a high storage capacity and target-oriented discharge temperature. The heat energy is absorbed or released under constant temperature and the phase transition of materials from the solid state to the liquid form (Rasha and Science, 2020). Energy storing capacity with PCM, latent heat energy storage combines sensible and latent heat storage, as shown by the following equation (Lasmar, A. 2018).

$$Q_{LHES} = \int_{T_1}^{T_m} mc_{p,s} dT + m\Delta H_{PCM} + \int_{T_m}^{T_2} mc_{p,l} dT \quad (2.3)$$

$$Q_{LHES} = m[c_{p,s}(T_m - T_i) + \Delta H_{PCM} + c_{p,l}(T_m - T_i)] \quad (2.4)$$

Where, $Q_{Latentheat}$ in (KW) , m of PCM (kg), $c_{p,ss}$ and $c_{p,ll}$ for PCM in solid and liquid KJ/kg.C°, T_i and T_2 are the initial and final temperature of PCM respectively (C°) and ΔH_{PCM} latent heat of fusion PCM temperature, T_m melting temperature (C°) of PCM. (Thermal and Engineering, 2019).

In this study, LHES is selected due to its capacity to store heat and high energy density at a constant temperature related to the phase transition temperature of PCM. LHES involves a phase transition of the PCMs from solid-gas, liquid-gas, solid-liquid, and solid-solid as they heated to the temperature of phase transition (Zhang et al., 2018 and Lasmar, A. 2018).

In general, because of their small change in volume, easy handling, higher thermal energy density, compactness, constant temperature phase change, and melting and freezing, they can repeated for unlimited time cycles with no change in thermos-physical properties of materials' solid-liquid phase change is widely used for domestic water heating application (Thermal and Engineering, 2019).

2.4 Phase Change Materials (PCM)

Phase change materials are known for their high capacity for energy storage, the slight change in operating temperature because of the phase transition PCMs at the melting point, and isothermal properties during the charging and discharging process Lasmar, A. (2018). Their energy-storing mechanisms combine both sensible and latent (Abu-Hamden and Alnefaie, 2019). The practical energy-storing tool is based on initial and end temperature conditions. In contrast, latent energy-storing involves phase change and heat enthalpy increases in temperature and latent heat resulting from phase transitions (Zhang et al., 2018). The quantity of energy stored is determined by (2.4).

2.4.1 Classification of PCM

Phase change materials mainly used LHTES can be classified as shown in the figure based on their chemical composition (Abu-Hamden and Alnefaie, 2019).

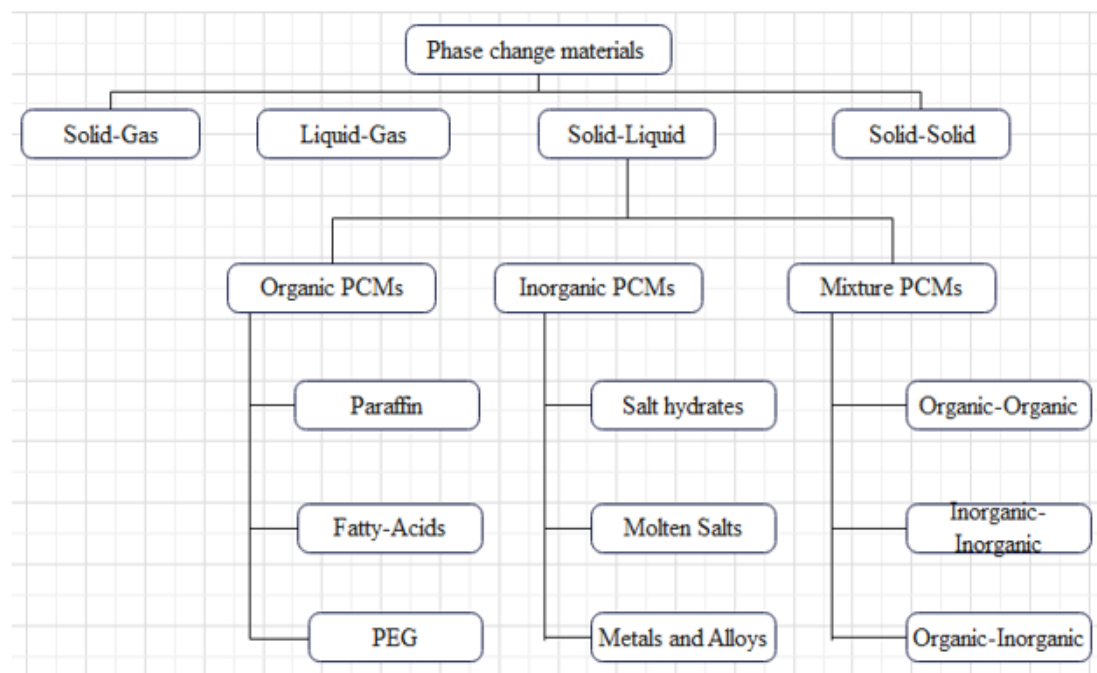


Figure 2.7: Classification of phase change materials

Solid-liquid PCMs are categorized as organic, inorganic, and combination PCMs

1. Organic PCMs

Organic solid-liquid PCMs have unique properties such as melting, a narrow phase change temperature range, self-nucleation, high thermal energy density, and no or minimal phase segregation, making them suitable for energy storage (Abu-Hamden and Alnefaie, 2019). However, the main challenges with solid-liquid PCMs are low thermal conductivity and the risk of leakage (G. S. Kumar et al., 2016). Therefore, further research is needed to improve thermal conductivity and prevent PCM leakage.

i. Paraffin Wax: Is a mixture of traditional n -alkanes cheaper than pure n -alkanes. It has crucial thermophysical properties such as low vapor pressure, self-nucleation, no or minimal phase segregation, chemical inertness, high heat density, and a wide range of phase change temperatures (18 to $71C^\circ$), making it suitable for thermal energy storage (Das, 2018).

Fatty Acids: Such as capric acid, lauric acid, stearic acid, and arachidic acid, are widely used as PCMs. They have melting temperature ranges from 30 to $74C^\circ$ and latent heat ranges from 140 to $208Jg^{-1}$ (Zhang et al., 2018). One advantage of fatty acids is that they can form eutectic mixtures, allowing the phase change temperature to be adjusted (Series and Science, 2021).

iii. Polyethylene Glycol (PEG): Polyethylene Glycol (PEG) has a large latent heat capacity, thermal and chemical stability, no corrosiveness, no supercooling, low vapor pressure, and appropriate phase change temperatures (Das, 2018). The temperature change of PEG was controlled by adjusting its molecular weight. However, the latent heat decreases for PEG with a molecular weight above 10000 due to decreased crystallinity caused by longer molecular chains (Zhang et al., 2018).

2. Inorganic PCMs

These are grouped into salt hydrate, salt metals, and alloys and relatively have twice as latent compared to organic PCMs, heat storage apiece unit volume, higher thermal conductivity, and lower cost.

i. Salt Hydrates: Salt hydrates are a type of eutectic mixture. They have several advantages, including a high latent heat per unit volume, relatively high thermal conductivity, and minimal volume variation during phase change. Salt hydrates consist of water and inorganic salts, represented by the formula $AB_n H_2O$ (Faraj et al., 2020).

ii. Molten Salts: These are used for high-temperature applications ranging between 100 and 450 for low and medium-temperature range steam generation in industrial applications. They decompose at a temperature greater than 550 (Abu-Hamden and Al-nefaie, 2019).

iii. Metals and Alloys: Including aluminum alloys, magnesium alloys, and copper alloys, possess high melting points exceeding 300 and are highly competitive for high-temperature thermal energy storage (TES) applications (El-shibari, n.d.).

However, these liquids and metals exhibit significant instability regarding their chemical properties.

3. Eutectic Mixture PCMs

Are classified into their group: - organic with organic, inorganic with inorganic, and organic with inorganic. The addition of homogeneous and heterogeneous salts can be achieved to decrease the high melting point of molten salts. The added salts serve as nucleons, inducing the solidification of the liquefied salty under supercooling conditions (Bazri et al., 2019). The liquefied salts hurried/precipitated around the introduced nucleons, and their freezing temperature added to salts also reduced the melting point that resulted from interfering with the unique configuration of the molten salts and weakening the forces between molecules (Zhang et al., 2018).

2.4.2 Thermo-Physical Properties of (Solid-Liquid PCMs)

The key performance parameters for phase change materials (PCMs) include their phase change temperature, latent heat, thermal conductivity, density, thermal reliability, thermal and chemical stability, and compatibility with the container (Zhang et al., 2018). When the temperature of the environment is higher than the melting point of the PCM, the PCM absorbs heat until its temperature matches that of the domain (Wang, 2019). This results in the formation of an isothermal temperature profile. The freezing point of the PCM is crucial in determining the amount of heat released during the discharging process (Liu et al., n.d.).

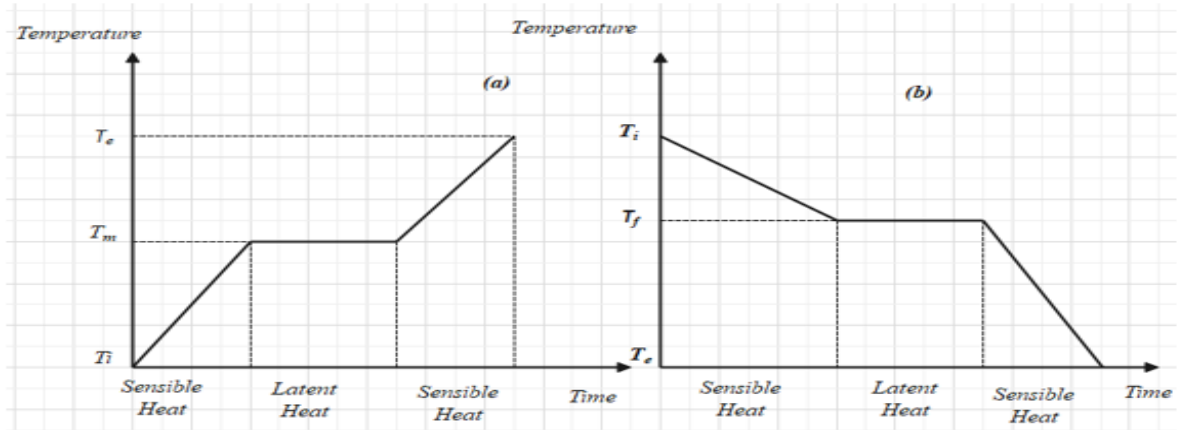


Figure 2.8: Temperature-time curve of PCMs a) charging and b) discharging processes

2.4.3 Properties and Phase Change Material Selection

Phase change materials used in the design of LTES should possess certain important characteristics. These include suitable melting points within the desired temperature range, which is typically between -5 to 190°C . Additionally, these materials should be able to undergo frequent melting and freezing without experiencing phase division or a reduction in their thermal material properties. Organic materials such as fatty acids and Paraffin are commonly used in energy storage systems due to their ability to meet these requirements (Thermal and Engineering, 2019) as listed in Appendix A.0.3.

2.4.4 Phase-Change Materials for the Storage of Thermal Energy (TES-PCMs)

PCMs are undertaking solid-liquid phase change within the restricted thermal application. While absorbing energy from the nearby their phase changed from solid to liquid state, even though remaining almost at a fixed temperature. At the melting temperature, the atomic bonds break and the material changes from a solid to a liquid phase. The reverse process, known as solidification, occurs when the material releases energy to its surroundings. The energy involved in these melting and solidification cycles is called the latent heat of fusion, which can either be released or absorbed. This process continues as the solid transitions through a liquid phase and then the temperature increases to the boiling point as sensible heat. Once the liquid reaches the boiling point, vaporization occurs and the material transitions from a liquid to a vapor phase until the phase change is complete, releasing latent heat. Further heating during this process results in superheated vapor, which takes the form of sensible heat.

Compared to fusion, evaporation requires more energy in the form of latent heat (Lasmar, 2018). The amount of energy gained or lost during the melting-solidification cycle depends on the rate at which the material undergoes latent melting and can be expressed in units such as J/g or kJ/kg . This process is influenced by the energy gained or lost by the material during melting, the mass of the substance, and the average temperature at which the material melts.

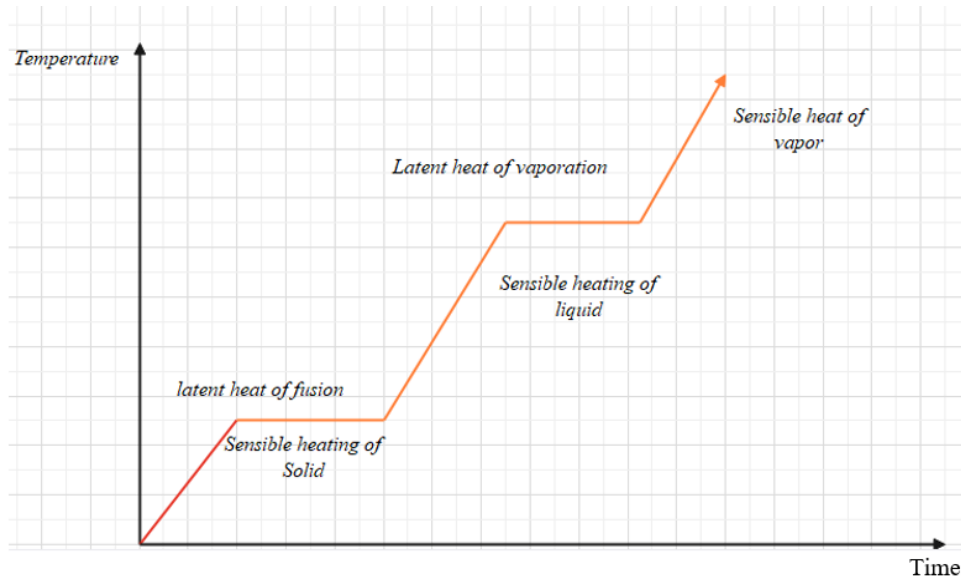


Figure 2.9: Standard heating curve

2.5 Related Previous Work

(Bazri et al., 2019 worked on an analytical and comparative study of the charging and discharging processes in a latent heat TEST for a solar water heater system. This research examined the compact design of a solar water heater with an integrated latent heat storage tank using evacuated heat pipe solar collectors. The collectors are connected directly to the tank containing paraffin phase change materials (PCMs). The study involved two steps: first, the system uses mathematical equations for modelling to understand its thermal performance, and second, a comparative investigation was conducted to analyze the system's performance using different PCMs, climatic conditions, and flow rates. Different PCMs, such as PCMA, PCMB, and PCMC, are based on their ability to produce the highest outlet water temperature. The study was conducted to compare the model with the conventional system. In the baseline system and for the best chosen PCM, the system's efficiency is between 32% and 42% on low solar radiation days.

At the same time, it ranges around $40 \pm 3\%$ on high radiation intensity days. The efficiency of the new design for all three types of PCMs on a typical sunny day is 36 – 54%. This efficiency increases to 47 – 58% on a cloudy/rainy day. This condition is inverse for the conventional system. The overall average efficiency of the proposed method is increased from 10 – 58% for all three different PCMs compared to the baseline.

(Bouhal et al., 2019) They worked on numerical modelling and optimization of thermal stratification in solar water hot water storage tank applications. The study aimed to evaluate the thermal stratification within a conventional hot water storage tank by incorporating multiple flat plates with varying angles into a vertical storage tank operating under dynamic conditions. Two different configurations based on plate position and slopes were compared using computational fluid dynamics (CFD) analysis. Performance parameters such as temperature evolution, Richardson number, and stratification number were calculated and compared between the two configurations. They showed that thermal stratification inside the storage is based on the flat plates positions, and increasing the number of flat plates inside the storage tank does not establish suitable thermal stratification. They also proved that superior thermal performance is achieved when the flat plate is maintained at the middle height of the storage tank, and a flat plate at different angles improves thermocline structure development.

(Shinde et al., 2019) They worked on heat transfer characterization and optimization of latent heat thermal storage systems using fins for medium-temperature solar applications. Their study used numerical analyses to predict the thermal efficiency of a latent heat thermal energy storage system using phase change materials (PCMs) for medium solar applications. This system is a shell and tube heat exchanger designed to store $1100kW/h$ for one hour. The PCM used in the shell side is a commercial organic material (A164), and a thermic oil (Hyperperm 600) is utilized as the heat transfer fluid that flows through the tubes. A 3D numerical modelling technique was developed to characterize the behavior of the PCM during solidification, and it was determined that heat transfer in the PCM is primarily governed by conduction during solidification. The study aimed to assess the impact of different fin parameters on the thermal performance of a latent heat thermal energy storage system using phase change materials. The research found that increasing fin thickness and number improved heat transfer rate, while fin height had minimal effect above a specific size. The optimal design for the given operating parameters was a system with 24 fins, each $1mm$ thick and $7mm$ high.

(Bouzaher et al., 2019) During the dynamic mode, they worked on thermal stratification inside an aspherical water storage tank. This research aimed to evaluate the efficiency of a novel storage tank model using a CFD solver. The tank had a diameter of $0.4m$ and a volume of 268 liters, with an inlet diameter of $0.02m$. A passively moving plate is installed at the tank axis to enhance the discharge flow rate while maintaining tank stratification. The study first compared the tank's performance with a diffuser to the new plate model. Then, it examined the impact of the hinged baffle material on the tank's thermal characteristics. These materials are wood, aluminum, and copper. Dynamic meshing was utilized to prevent mixing cold and hot water during plate movement. The findings revealed that the interaction between incoming cold water and stored hot water resulted in a thick thermocline layer influenced by the intensity of the mixing process. Additionally, tanks equipped with hollowed wood baffle cases exhibited higher temperature stratification than others.

(Wang, 2019) studied the influence of inlet structure on thermal stratification in a heat storage tank with PCMs. Furthermore, the study developed a heat storage tank with a volume of $60l$ and an aspect ratio of 1.68 based on the temperature of PCMs 331.15 of sodium acetate trihydrate. The thermodynamic characteristics were measured at a temperature of 353.15 and an inlet temperature of 278.15 . CFD was used to simulate the discharging process of the heat storage tank and experimentally verified. The impact of PCM position on thermal stratification was analyzed for different flow rates, considering parameters such as Richardson and MIX numbers. In the water discharge process, dimensionless time ($t^* = 0.1 - 0.7$) the distance between the isothermal surface 278.15 and 352.15 isothermal surface in PCM4, PCM3, and PCM2 and PCM1 increased by 6.56 , 7.2 , 8.98 and $12.34cm$ respectively. They also found that mixing hot and cold water increases with a higher PCM position, improving the thermal stratification in heat storage tanks. The half-life of PCM is prolonged with increasing inlet flow rate. The simulation results for filling efficiency and Richardson number were higher than the experimental results, while the MIX number was below the practical value.

(Huang et al., 2019) worked on an experimental investigation on thermal stratification characteristics with PCMs in solar water tanks. The research focused on integrating phase change materials (PCMs) in a thermal storage tank with an initial temperature of $353.15K$ and an inlet water temperature of $278.15K$.

The tank was filled with sodium acetate PCMs of 325.15 with a supercooling temperature below $278.15K$. The study examined the impact of PCM position on thermal

stratification at various flow rates ($0.06, 0.18, 0.3, 0.42, \text{ and } 0.54 \text{ m}^3 \text{ h}$) over increasing dimensionless time. The results indicated that the position of the PCMs significantly influenced thermal stratification in the tank and that increasing the inlet flow rate prolonged the half-life of the PCM. Additionally, the simulation results for filling efficiency and Richardson number were higher than the experimental values, while the MIX number was lower than the experimental results. They also studied fill efficiency to compare with energy efficiency, MIX number, and Richardson number to characterize the stratification of the thermal tank. From their experimental result, when the water tank's temperature increased from 278.15 to 353.15 , the energies of the water tank and PCMs tank were 18.81 and 19.34 MJ , respectively. At the same flow rate, increasing the PCMs close to the inlet improved the tank's thermal stratification. At a high flow rate, cold-hot water mixing increased, and the tank's thermocline thickness increased, weakening the thermal stratification.

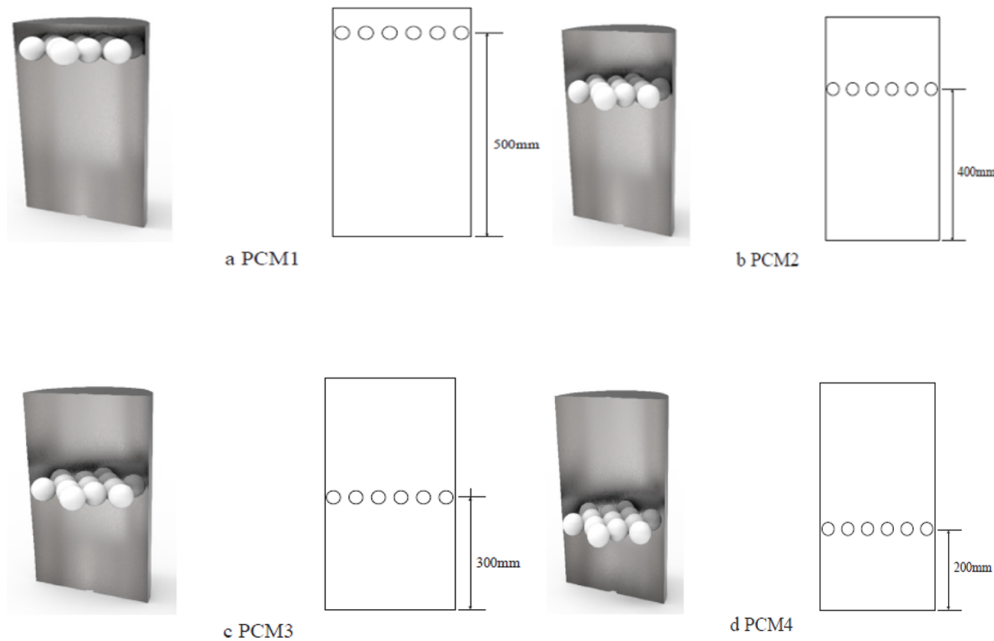


Figure 2.10: Schematic indication of PCM in water storage (Huang et al., 2019)

Theeb et al. (2020) studied the thermal effects of using various metal disks inside a liquid PCM thermal storage system. The temperature of PCM in TES at different inlet temperatures of ($340, 350, \text{ and } 360 \text{ K}$) and primary, smooth disk, and perforated disk were studied with three values of the water flow rate of ($0.0281, 0.0303, \text{ and } 0.0557 \text{ L/s}$). Experimental and numerical study of TES was examined and compared with each other.

They obtained an excellent agreement from the results. The finding indicated that increasing the water flow rate could cause faster melting PCM, and the optimum liquid value flow rate is obtained at $0.0303L/s$. The result also indicated that a smooth disk with $7.5cm$ causes increases in the temperature of the PCM faster than another diameter. They recommended that using metal smooth disks inside liquid PCM containers will add significant heat in large-scale systems.

(Neri et al., 2020) worked on numerical simulation and validation of a commercial hot water tank integrated with PCMs based on a storage unit. The researchers conducted a numerical and experimental analysis of a hybrid latent-sensible heat storage tank consisting of a commercial hot water tank integrated with PCM macro-encapsulation to enhance the overall thermal capacity of the sensible water tank. They developed three different numerical models and validated them experimentally. The first model was based on the enthalpy porosity method and simulated the charging and discharging of the PCM storage unit in a climatic chamber. The second model provided a 1D description of the water storage tank without PCM. The third model combined the first and second models to simulate the entire PCM water thermal storage system. The third model was validated through an experimental test involving the insertion of 94 modules of PCMs into a water tank and observing its thermal behavior for three days. The researchers found that the hybrid thermal storage system could not fully utilize the heat potential of PCM, as 40% of it changed its phase due to adverse effects on heat transfer from thermal transport properties.

(Louanate et al., 2020) They were designed and analyzed efficient STE (storage of thermal energy) using phase change material. They created and fabricated a TES tank and paraffin wax PCMs enclosed in stainless steel balls, and the PCM's high specific heat capacity is used to store latent heat for later application. Temperature measurements are taken using a type thermocouple along with an indicator. Numerical analysis was done using the CFD Software Analysis Fluent to solve the mismatch of abundant solar energy available during the daytime. The experiment was done on a thermal storage system using PCM (paraffin wax) and water as heat transfer fluid to calculate the efficiency of the storage system. They concluded that using different PCMs with higher latent and better insulation materials, such as glass wool, can increase efficiency.

(Karuthedath et al., 2020) worked on analyzing the evacuated tube collector types of solar water heater static and dynamic modes of operation. The researchers utilized a 3-D transient pressure-based numerical simulation with a Newtonian laminar solver and UDF to analyze the discharge rate in both charging and discharging modes. Their findings were validated through experimental data, which aligned with the experimental results. This approach allowed for a comprehensive understanding of the roles of discharge rate in the thermal stratification of hot water storage tanks. The work considered five different flow rates (i.e., 3, 5, 7, 10 and 15 *Lpm*) to determine the effect on the temperature profile during the dynamic mode of operation. As flow rate fluid increases during discharging, the stratified layers are disoriented and lead to rapid mixing, which results in a drop in the outlet temperature. They found that low fluid flow rates maintain thermal stratification in the tanks, with only a gradual decrease in outlet temperature. This study highlights the importance of flow rate in determining thermal stratification in hot water storage tanks.

(Wang et al., 2020) worked on an experimental study on improving stratification in heat storage using an equalizer and PCM module. Furthermore, the researchers modelled a novel balance with different positions of PCM balls and flow rates. They measured the influence of the heat storage tank using dimensionless time. They analyzed the thermal characteristics of the HST with different inlet structures, such as variations in flow rates, using parameters like Richardson number, fill efficiency, and MIX number. The results demonstrated that the water inlet structure with the equalizer stabilizes the heat output and effectively enhances the thermal stratification of the heat storage tank. Based on the exact position of the PCMs ball and inlet flow, the Richardson number and fill efficiency of HST with equalizer are more significant than those of the water tank with a typical inlet structure, but the MIX number is smaller. The FE decreases by 8.6% as the inlet flow rate increases from 1 *L/min* to 9 *Lmin*. Placing the PCM with an equalizer closer to the inlet flow results in a 1.3% increase in fill efficiency compared to a standard water tank. The use of the equalizer also enhances thermal stratification in the heat storage tank, reducing cold-hot mixing and improving overall thermal stratification.

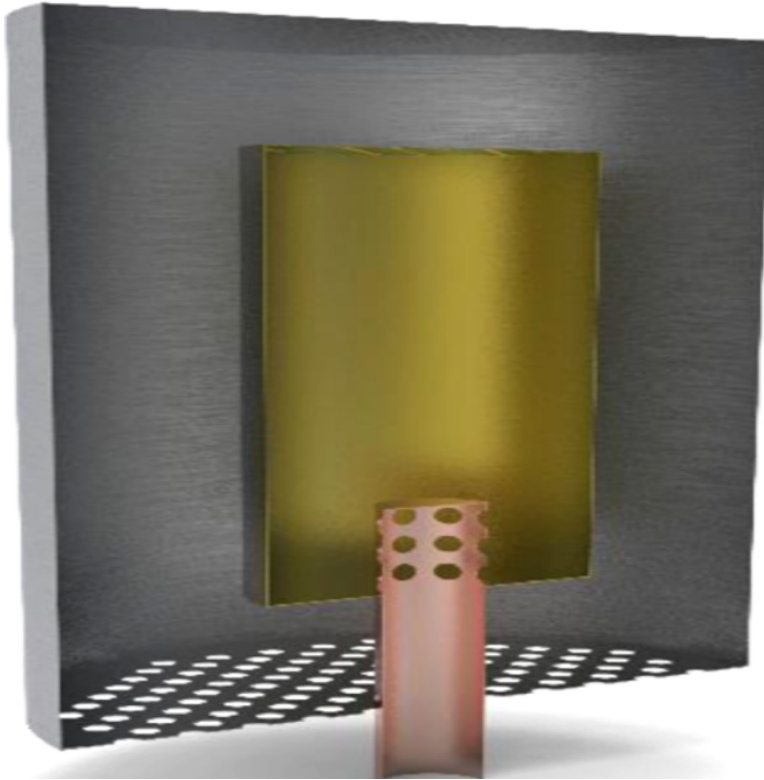


Figure 2.11: Heat storage tank with Equalizer

(Madadi et al. (2021) worked on integrating phase change material in the storage tank of a solar water heater to maintain a constant hot water output temperature. The mathematical model bed of PCM with a diameter $0.3m$ and length of $0.6m$ for $300l$ of hot water was validated with experimental data. The modelled beds of PCMs were coupled to the overall solar water heating system model, and the outlet temperature from the SWH unit at any time enters the bed. A solar collector integrated with a PCM bed in a hot water store for seven h of operation with a bed diameter $0.3m$ consisted and length of $0.6m$ consistedm for $300l$ hot water with a temperature of 60 and $\pm 2C^{\circ}$ was produced. At a high flow rate of water through the system, hot water produced at the outlet bed does not reach the melting temperature of PCM, so hot water cannot be created at constant temperature. To overcome this problem, they used multiple collectors in series. When they used two collectors in series for eight hours of system operation, $60C^{\circ}$ of hot water was achieved. By using two consecutive collectors, the systems performance is increased by more than double that of a single collector. From their result, the number of collectors in a series configuration is based on the amount of water required and latent heat, as well as the melting point of PCM.

(Malec et al. 2021) studied the influence of cold-water inlets and obstacles on the energy efficiency of the hot water production process in a hot water storage tank. They experimentally prepared seven different cold-water inlets for the water storage tank and used two obstacles inside the tank at three different heights. These inlets are straight forward inlet, elbow directed upwards, and inlet elbow directed downward, inlet elbow directed upwards with a single plate, inlet elbow directed downward with a single plate, inlet elbow directed upwards with a double plate and inlets elbow directed downward with a double plate. They tested for different profiles of hot water consumption to know the temperature in the domestic hot water tank. The results indicated that the elbow facing downward with a single plate gives the best advantages, with a 3 – 8% increase in energy efficiency compared to the primary inlet type. The result also showed that the use of obstacles inside the tank at its lower parts improved the system's energy efficiency by up to 15% compared to the variant without partition.

(K. Kumar et al., 2021) studied investigating thermal stratification in a vertical hot water storage under multiple transient operations. The researchers also conducted a transient numerical investigation of a domestic multi-source hot water tank under three dynamic operational modes: charging, continuous delivery, and discharging. The hot water tank has a volumetric capacity of 210 liters with inlet and outlet ports at the bottom and top of the tank. It is connected with two alternative sources via a heat exchanger coil to maximize energy efficiency and one electric ring to raise hot water temperature. A 2D model of the double-coiled, vertical-shaped HWT was simulated by ANSYS fluent and validated with experimental data. Dimensionless stratification and Richardson numbers are calculated and compared for each operation case. The result showed that thermal stratification depends on the location of the heating source inside the tank under the given operational mode. In both continuous delivery and charging ways, the degree of stratification is improved when the heat exchanger coil installed at the upper portion of the tank is functioning. They concluded that the highest degree of thermal stratification occurred when the heating source was in the upper part of the tank. They also observed that in charging mode, a Stratifier was used to improve thermal stratification, while in continuous delivery mode, higher mixing occurred due to the constant flow of water. In discharging mode, the thermocline layer moved upward over time as hot water was unloaded from the top of the tank.

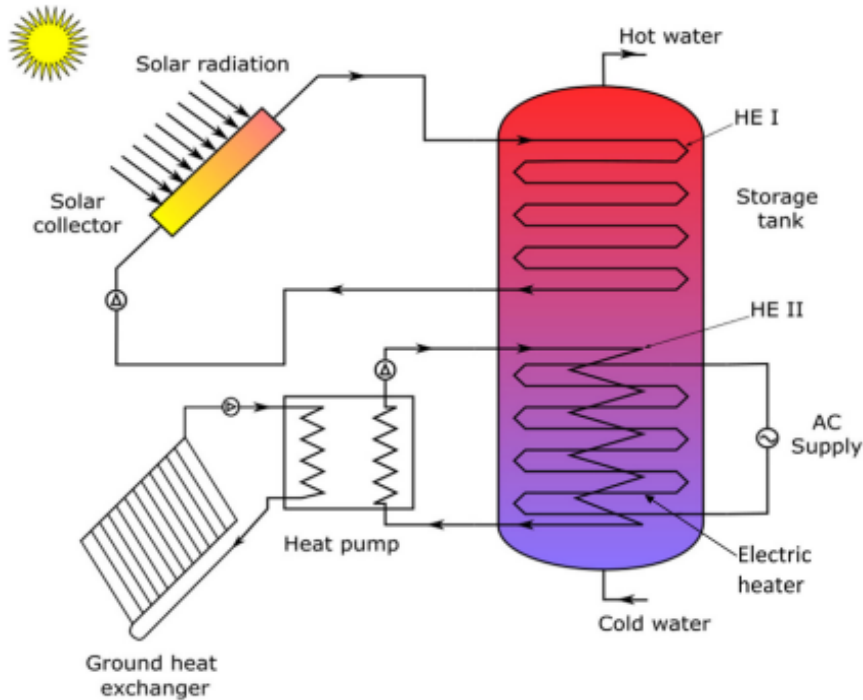


Figure 2.12: Schematic diagram of hot water storage tank

(Gao et al., 2021) worked on the numerical and experimental investigation of thermal stratification characteristics affected by the baffle plate in the thermal storage tank. The researchers aimed to study the impact of a central hole-type baffle plate on the thermal stratification of a heat storage tank. They utilized the response surface method to optimize the structural parameters and performed experiments to assess the thermal stratification during the charging process. Numerical simulations are used to calculate the temperature and flow fields within the tank and analyze various structural parameters on mixing stratification and Richardson numbers. Their findings indicated that the interaction factors that significantly influenced three evaluation indices were the baffle aperture and inlet velocity, baffle position and inlet velocity, and baffle position and baffle aperture. The Richardson number was used in their model for optimization objectives, and the optimal parameter combination optimized by the expected function was a baffle location of 0.79, a hole of 0.80, and an inlet velocity of $0.2m/s$. They also demonstrated that the numerical simulation was consistent with the experimental results. The baffle position and baffle aperture had the most significant impact on the mixing number.

Authors	Year	Works or studies	Methods	Results Achieved	Variation
Bazri et al.,	2019	An analytical investigation of the new design of heat pipe solar heater integrated with latent heat storage tank	Mathematical Equation and MATLAB Modeling	The overall efficiency of the system with PCMs over conventional	Parametric comparison
Bouhal et al.,	2019	Numerical demonstrating and optimizing of thermal stratification of water tank for domestic application.	Insertion of a flat plate at different angles inside the water storage tank.	Results Achieved	Experimental
Bouzaher et al.,	2019	A new model of a spherical heat storage tank.	The comparative studies between the tanks with typical diffusers and the new moving plate model.	Temperature diffusion and the thermocline thickness depend on the baffle material. The tank equipped with a hollowed wood baffle case was higher compared to others	Comparative analysis

Table 2.1: Summary of Literature Reviews.

Huang et al.,	2019	An experimental investigation effect of phase change material on thermal stratification characteristics of the water tank	The effect of the position of the PCMs on thermal stratification at different flow rates (0.06, 0.18, 0.42, and $0.5m^3h$) Increasing PCM close to the inlet led to better thermal stratification of the tank.	Increasing PCM close to the inlet led to better thermal stratification of the tank	Experimental
Shinde et al.,	2019	Numerical analyses to investigate the thermal characteristic of latent heat energy (LHTES) by phase change material (PCM) for medium temperature solar applications.	The 3D mathematical prototypical.	Increased rate of heat transfer with fin thickness and number but least effect fin height on the enhancement of heat transfer in PCM above a certain height	Mathematical modeling
Neri et al.,	2020	Numerical simulation and validation of commercial hot water tanks integrated with phase material-based storage units.	By Macro encapsulation of PMC into a commercial hot water tank.	An increased overall thermal capacity of a sensible water tank.	Experimental.
Theeb et al.,	2020	Thermal effect of using various metals inside liquid-PCM thermal storage system.	Numerical analysis with ANSYS fluent software for simulation.	Metal smooth disks inside liquid-PCM containers will add a significant mean gain more heat in large-scale systems.	Experimental.

Louanate et al.,	2020	Experimental and Numerical Studies TES using paraffin wax PCMs.	Temperature measurement using a T-type thermocouple with an indicator. Numerical analysis using CFD Software ANSYS Fluent	Possibility of PCMs during off-loads and release the same during load.	Experimental + Numerical
Karuthedath et al.,	2020	Analyzed the evacuated tube collector types of solar water heater static (stagnant) and dynamic (retrieval) modes of operation.	3D transient numerical modeling using CFD	3D transient numerical modeling using CFD	Experimental
Wang et al.,	2020	Experimental study on the enhancement of stratification in heat storage using an equalizer and PCM module	Modelling of novel equalizer with different positions of PCM balls and flow rates	Placing the PCM with an equalizer closer to the inlet flow results in a 1.3% increase in fill efficiency compared to a standard water tank.	Experimental
Malec et al.,	2021	The effect of obstacles and Cold water inlet on the energy efficiency of the hot water production procedure in a hot water storage tank	They experimentally prepared seven different cold-water inlets for the water storage tank and used two obstacles inside the tank at three different heights	The use of obstacles inside the tank at its lower parts improved the system's energy efficiency by up to 15% compared to the variant without partition.	Experimental

Kumar et al.,	2021	Thermal stratification of hot water storage tank during charging mode.	Thermal stratification of hot water storage tank during charging mode.	Improve the level of stratification Separated of hot and cold water	Experimental
Gao et al.,	2021	The effect of baffle plates on thermal stratification experimentally.	Numerical simulation design of baffle aperture the Richardson number	The baffle position and aperture had the greatest influence on the mixing number.	Experimental

Many studies have been conducted on hot water storage tanks experiential, analytically, and numerically. Most methods are used to optimize and maintain thermocline thickness thinner, by the aspect height to diameter ratio, the storage tank configuration, whether horizontally or vertically, placing obstacles inside the storage tank, using stratifies and baffle. However, the inlet structure of the water storage tank has a significant impact on the thermal efficiency of the system, which needs further studies. In this study, careful design and analysis of the inlet structure of the hot water tank were investigated to maintain the constant output temperature at the outlet side and thus enhance thermal stratification.

Chapter 3

Methodology and Materials

3.1 Description of Study Area

In terms of the study area, Limmu Kossa district is located at latitude $8^{\circ}09'60.00'' N$ and longitude $37^{\circ}09'60.00'' E$, with an elevation of $1773m$ above sea level. It is bordered by Limmu Seka district to the north, West Chora Botor to the northeast, Nadhi Gibe to the southeast, Manna and Karsa districts to the south, and Buno Bedele zone and Gomma district to the west. It is the largest and most populous district in the region, with 70% of its area characterized by a sub-tropical climate and 15% by a temperate agro climate. The average annual temperature in the district ranges from $18 - 23c^{\circ}$ (Diro, 2019).

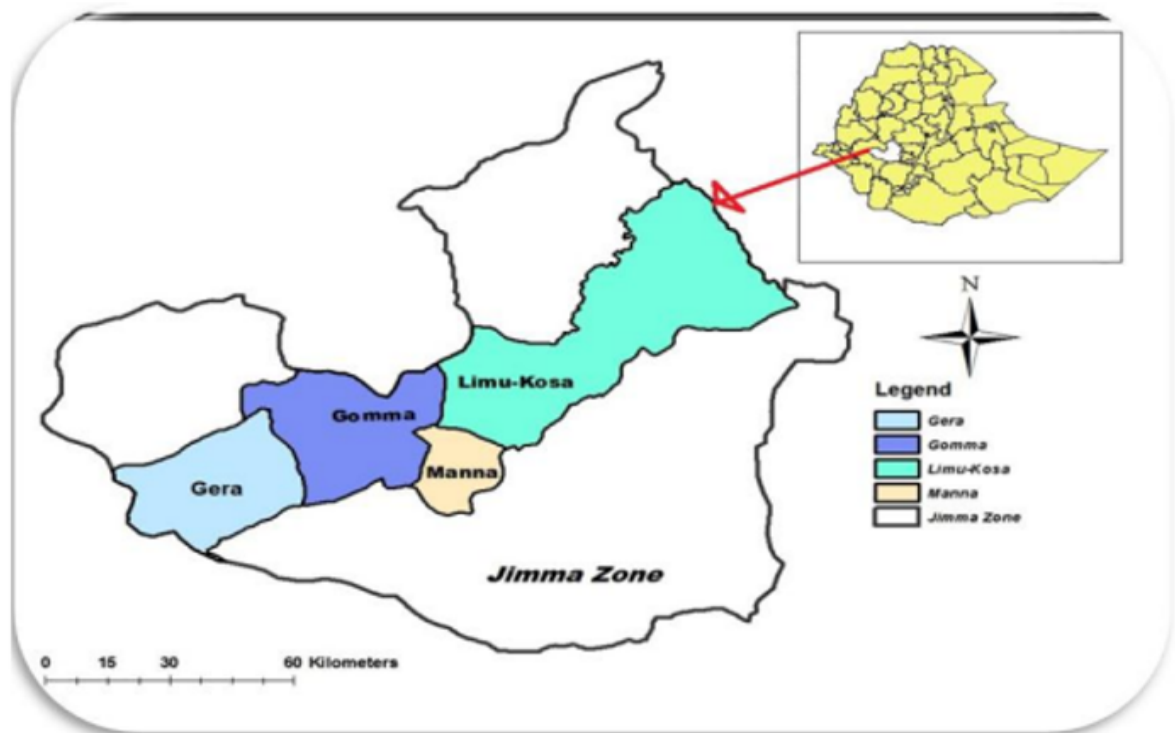


Figure 3.1: Geographical location of Limmu Kossa (Diro, 2019).

3.2 Data Collected from Limmu Genet General Hospital and Specific Location

Limmu Genet is the administrative center of Limmu Kossa district, which is 75 kilometers from Jimma town and 421 from Addis Ababa and the second particular town of the Jimma zone, surrounded by different rural kebeles. Since there is no solar water heating system in the hospital's history, fuels, biomass, and electric power for water heating systems are sources of energy. No measuring instruments for hot water consumption in the hospital are found; getting accurate information is impossible. Direct interviews take the information with the medical director of the hospital and staff workers by preparing questionnaires to estimate the amount of hot water required for the hospital. The load consumption is based on standard assumptions and estimation of international hot water requirements for hospitals without recorded data. The hospital provides service for more than 786,500 people and 90 bedrooms, with each room containing eight beds, two laundries, one kitchen, and restaurants, and has 90 total beds.

Table 3.1: Information collected from Limmu Gennet General Hospital

Parameters	Appliance					
	Kitchen	Shower			Restaurant	laundry
		Patient	Medical staff	Student		
Number of rooms	1	90	25	15	1	2
Person per room	12	4	4	8	12	7
Occupancy	100%	95%	60%	25%	100%	100%
Source of energy	<i>Fuel + electric + biomass</i>					

3.2.1 Assessment of Daily Hot Water Demand of the Hospital

Due to a lack of accurate measurement devices in the hospital, estimating regular hot water demand for different appliances is based on standard requirements. Two types of domestic hot water extractions are generally considered: tempered and untampered. Untampered hot water is used directly without mixing cold water, such as dishwashers and washing machines, with temperature measurements ranging from 55°C to 60°C. On the other hand, tempered hot water is created by mixing hot water with cold water to reach a comfortable end-use temperature for sinks, baths, and showers, with temperature measurements ranging from 40°C to 45°C (Fuentes et al., 2017).

Table 3.2: Average hot water requirement for international hospital appliances (Fuentes et al., 2017)

Demand	Standard hot water demand for different appliance			
	Kitchen	Shower	Laundry	Restaurant
Hot water demand	280 L/kitchen	60 L/person	490 L/laundry	120 L/Restaurant
Temperature	50 °C	43 °C	60 °C	50°C

In the hospitals, the water usage of each system is calculated individually and then added to obtain the total hot water consumption. This calculation is necessary to design and optimize the storage tank and collector area. The hot water demand for each appliance can be determined by multiplying the number of rooms per appliance's water consumption.

$$HWD = \text{Number of rooms} * \text{water per appliance} \quad (3.1)$$

Laundry Service service in hospitals is a process that consumes a significant amount of energy. It provides clean linen for patients and staff and operates twice daily, in the morning and evening. The hot water demand for laundry can be calculated separately using appropriate methods.

Laundry hot water consumption (HWLL)

$$HWLL = (\text{Number of room}) * (\text{water room}) * (\text{Occupancy rate}) \quad (3.2)$$

$$HWLL = 2 * 490L/day * 1 = 980L/day$$

Kitchen Hot Water Consumption (HWLK)

This hot water is used for cooking food and washing equipment at a temperature up to 50°C is calculated as follows.

$$HWLK = \text{Number of the room} * (\text{water room}) * (\text{Occupancy rate}) \quad (3.3)$$

$$HWLK = 1 * 280L/day * 1 = 280L/day.$$

Restaurant Hot Water Consumption (HWLR)

This is used for cooking restaurant and washing equipment at a temperature up to 50°C is calculated as follow.

$$HWLR = \text{Number of the room} * (\text{water room}) * (\text{Occupancy rate}) \quad (3.4)$$

$$HWLR = 1 * 120L/Restaurant * 1 = 120 \text{ litres per restaurant.}$$

Shower Hot Water Consumption (HWLS)

This includes shower for patient room, medical staff, and students room at a temperature of 43°C and it is calculated as follows for each room.

$$HWLS = (\text{Number of room}) * (\text{Person room}) * (\text{water room}) * (\text{Occupancy}) \quad (3.5)$$

$$\text{Patient shower load (PSL)} = 90 * 4 * 60L/person * 0.95 = 20520 \text{ litres per a day.}$$

$$\text{Student shower load (SSL)} = 15 * 8 * 60L/person * 0.25 = 1800 \text{ litres per a day.}$$

$$\text{Medical staff load (MSL)} = 25 * 4 * 60L/person * 0.6 = 3600 \text{ litres per a day.}$$

$$\text{Laundry workers shower (LWS)} = 2 * 7 * 60L/person * 1 = 840 \text{ litres per a day.}$$

$$\text{Kitchen workers shower (KWS)} = 1 * 12 * 60L/person * 1 = 720 \text{ litres per a day.}$$

$$\text{Restaurant workers shower (RWS)} = 1 * 12 * 60L/person * 1 = 720 \text{ litres per a day.}$$

Overall hot water consumption of hospital is the summation of each appliances

$$THWLL = HWLL + HWLK + HWLR + HWLS. \quad (3.6)$$

The above hot water load for shower (HWLSH) consists of the shower for the patient, students, medical staff, laundry workers, and kitchen and restaurant workers.

$$HWLSH = PSL + SSL + MSL + LWS + KWS + RWS. \quad (3.7)$$

$$HWLSH = 20520 + 1800 + 3600 + 840 + 720 + 720 = 28,200 \text{ litres per a day.}$$

Thus, the overall hot water consumption for hospital is calculated as:

$$THWLL = HWLL + HWLK + HWLR + HWLS. \quad (3.8)$$

$$THWLL = 980 + 280 + 120 + 28,200 = 29580 \text{ litres per a day}$$

Table 3.3: Water consumption (hot) of Limmu Gennet General Hospital per room

Appliances	Services				Total
	Laundry	Kitchen	Restaurant	Shower	
Hot water demand (L/day)	980	1800	120	28,200	29,580

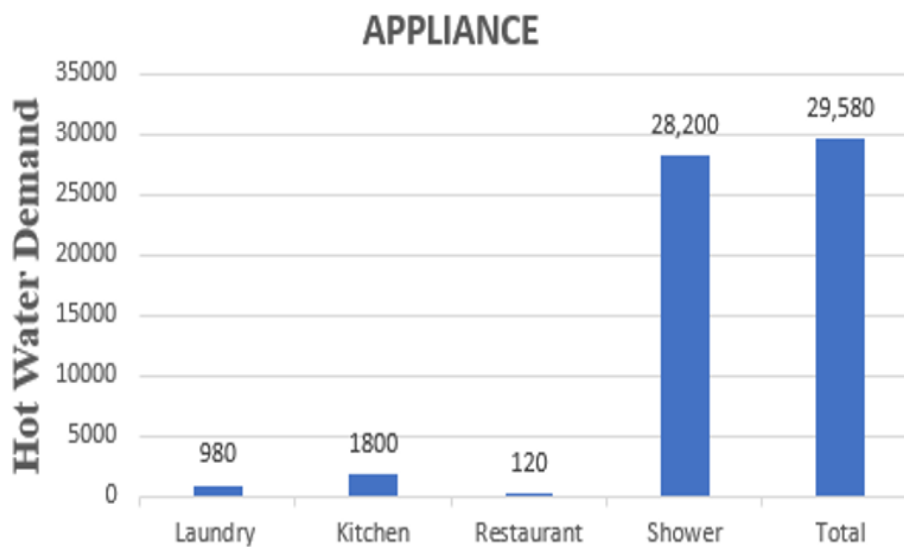


Figure 3.2: Variation of consumption load with different rooms

The calculated value is a multiple of the factor of 1.25, representing one-fourth of the total calculated daily and weekly hot water demand of the hospital to account for potential fluctuations in daily and weekly hot water consumption.

$$HWLL = 1.25 * 980 = 1,225 \text{ litres per a day}$$

$$HWLK = 1.25 * 1800 = 2,250 \text{ litres per a day}$$

$$HWLR = 1.25 * 120 = 150 \text{ litres per a day}$$

$$HWLS = 1.25 * 28.200 = 35,250 \text{ litres per a day}$$

Finally, the optimized total hot water required for the hospital is summed as follows:

$$THWLL = HWLL + HWLK + HWLR + HWLS$$

$$THWLL = 1225 + 2250 + 150 + 35250 = 38875 \text{ litres per a day}$$

Table 3.4: Total hot water consumption of Limmu Gennet general Hospital per rooms

Appliances	Services				Total
	Laundry	Kitchen	Restaurant	Shower	
Hot water demand (L/day)	1,225	2,250	150	35,250	38875

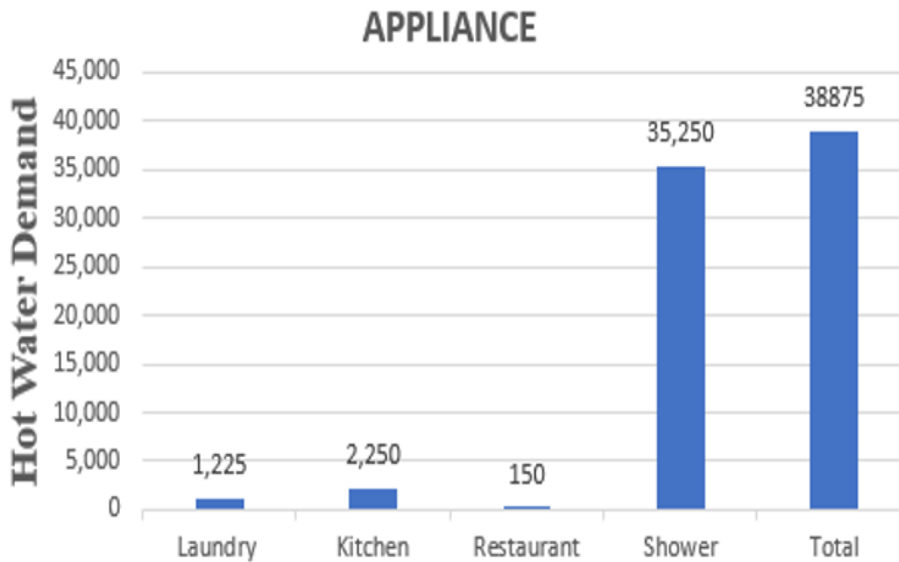


Figure 3.3: Total variation of hot water load in different rooms

3.2.2 Regular Hot Water Consumption Outline (Pattern)

Each service, such as the restaurant, kitchen, and laundry, consumes hot water in the morning, mid-day, and evening, but most showers happen morning and evening. Large water consumption occurred in the morning. Because of this unknown demand, an additional 8% is added to the morning hot water load pattern. So, the everyday hot water load pattern is determined as below.

$$HWLL = 1.25 * 980 = 1,225 / 3 = 408.34 (1.10\% \text{ morning}, 1.10\% \text{ mid-day}, \text{ and } 1.10\% \text{ evening})$$

$$HWLK = 1.25 * 1800 = 2,250 / 3 = 750 (1.93\% \text{ morning}, 1.93\% \text{ mid-day}, \text{ and } 1.93\% \text{ evening})$$

$$HWLR = 1.25 * 120 = 150 / 3 = 50 (0.13\% \text{ morning}, 0.13\% \text{ mid-day}, \text{ and } 0.13\% \text{ evening})$$

$$PSL = 20520 / 3 = 6840 (17.59.00\% \text{ morning}, 17.59\% \text{ mid-day}, \text{ and } 17.59\% \text{ evening})$$

$$SSL = 1800 / 2 = 900 (2.32\% \text{ morning}, \text{ and } 2.32\% \text{ evening})$$

$$MSL = 3600 / 2 = 1800 (4.63\% \text{ morning}, \text{ and } 4.63\% \text{ evening})$$

$$LWS = 840 / 2 = 420 (1.08.00\% \text{ morning}, \text{ and } 1.08\% \text{ evening})$$

$KWS = 720/2 = 360(0.93\% \text{ morning, and } 0.93\% \text{ evening})$

$RWS = 720/2 = (0.93\% \text{ morning, and } 0.93\% \text{ evening})$

Total percentile value

Morning load = $(1.1 + 1.93 + 0.13 + 17.59 + 1.93 + 2.32 + 4.63 + 1.08 + 0.93 + 0.93)\% + 8\% = 40.57\%$.

Mid-day load = $(1.1 + 1.93 + 0.13 + 17.59) = 20.75\%$

Evening load = $(1.1 + 1.93 + 0.13 + 17.59 + 1.93 + 2.32 + 4.63 + 1.08 + 0.93 + 0.93)\% = 32.57\%$.

Morning load = 40.57%

Mid-day load = 20.75%

Evening load = 32.57%

Distribute 6.11%

Morning load = $40.57\%(38875) = 15,771.771Ltr/day$

Mid-day load = $20.75\%(38875) = 8066.56Ltr/day$

Evening load = $32.57\%(38875) = 12,661.59Ltr/day$

Over distribute = $6.11\%(38875) = 2,375.26Ltr/day$

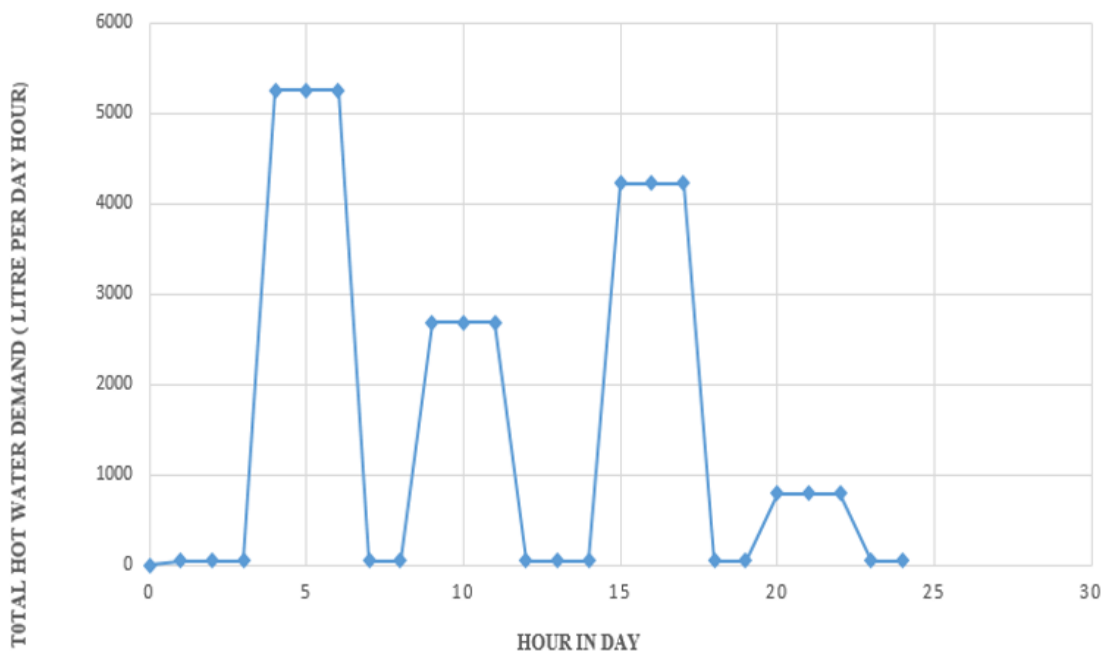


Figure 3.4: Regular hot water consumption pattern in an hour per day

The above graph shows the hospital's daily hot water load pattern for different appliances. A large amount of hot water is consumed in the morning (40.57%), and a small amount is consumed in mid-day (20.75%). It shows that most fluctuating probability occurs in the morning because most activity requires more hot water than other times, as data taken from the hospital indicates.

3.3 Storage Capacity of Hot Water Tank

Storage capacity hot water tank at uniform temperature is given

$$Q_w = \dot{m}c_p\Delta T \quad (3.9)$$

Where: Q_w = total heat capacity of the storage tank [kwh]

\dot{m} = Volume of the storage tank [m^3].

ΔT = Temperature difference between cold and hot water temperature [K].

The mass of water to be heated is calculated from the following equation.

$$\rho = \frac{m}{v} \quad (3.10)$$

Where ρ in kg/m^3 the density of water, m total masses in kg , and v volume in liters (l). of water respectively. From hot water load of laundry

HWLL

$$m_L = \rho * v = 1000 \frac{kg}{m^3} * 1.225m^3 = 1225kg$$

where, m_L Shows the mass of water required for Limmu Gennet Hospital hot water load analysis **HWLK**

From hot water load of kitchen

$$m_L = \rho * v = 1000 \frac{kg}{m^3} * 2.250m^3 = 225kg$$

From the hot water load of the Restaurant

HWLR

$$m_R = \rho * v = 1000 \frac{kg}{m^3} * 0.150m^3 = kg = 150kg$$

From hot water load of shower

HWLS

$$m_s = \rho * v = 1000 \frac{kg}{m^3} * 35.25m^3 = kg = 35250kg$$

Total masses of water (m_T)

$$m_T = m_L + m_k + m_R + m_s \quad (3.11)$$

The total number of masses is 38,875kg, which is equal to the total volume of water calculated in the above section $v = 38,875$ liters, which is equivalent to $\dot{m} = 38.88m^3$ and then from equation (3.9), energy capacity storage water can be determined as follows. Taking the C_p of water $4.2kwh/(m^3k)$, hot and cold-water temperature $60C^\circ$, and $22C^\circ$ respectively. .

$$Q_w = 38.88m^3 * 4.2kwh/m^3k * (333 - 295)$$

$Q_w = 6205.25kwh$ is the total energy daily required.

Number of Flat Plate Solar Collectors

The following can be determined as the total area of the flat plate collector.

$$A_{total} = \frac{Q_{HWD}}{\eta_{th}I_T} \quad (3.12)$$

Where Q_{HWD} is total hot water demand, η_{th} is thermal efficiency, I_T Represent average solar radiation intensity.

Based on the duration of sunshine hours for nine hours per day, the total number of flat plate collectors was determined by dividing the entire area by unit area.

$$\text{Number of collectors} = \frac{A_{total}}{A_c} \quad (3.13)$$

The total number of flat plate collectors is 217 units.

3.4 Materials and Methods

3.4.1 Material Selection

The selection of materials for the storage tank is vital since it is the core of the whole system. The key issues affecting material selection are durability, safety, performance, cost, resistance to corrosion, etc. Hot water storage tanks can be made from different materials, such as mild steel, steel, fiberglass, stainless steel, copper, etc. These materials and their related properties vary from tank to tank based on their application.

Vessel the shell that comprises and stores the water and can withstand the extreme pressure of at least $400kPa$.

Mild steel because of its low carbon content, is somewhat strong compared to its price related to the vessel for application of water tanks; mild steel is referred to because of its strength, effective cost, and high resistance to breakage compared to higher carbon steel.

Stainless Steel because of its strength and excellent resistance to rust and corrosion, is the general choice for water tank vessels. Since vessels are in contact with water, it might present problems of rust and corrosion, and stainless steel is the best for this challenge. Steel has the best corrosion resistance; its disadvantage is that it is more expensive than copper.

Copper is good because of its high corrosion resistance, but its disadvantage is its high thermal conductivity, leading to increased heat losses.

General because of the following properties mild steel is selected

- Effective cost
- Low thermal conductivity
- High resistance to leakage
- High performance and durability
- Advanced resistance to temperature and water
- Properties of different storage tank materials

Table 3.5: Physical properties of mild steel

Properties at 300 K						Property of K/C_p [W/Km]/J/ kgK]
Substances	Melting point [K]	ρ [kg/m ³]	C_p [J/KgK]	K [W / Km]	$\alpha * 10^6$ [m ² /s]	At 400 K
Copper	1358	8933	385	401	117	393
Aluminum	933	2702	903	237	97.1	240
Mild steel	1810	7832	434	63.9	18.8	58.7
Stainless steel	1670	7913	477	14.6	3.95	16.6
Lead	601	11,340	129	35.3	24.1	34
Nickel	1728	8900	444	90.7	23	80
Iron	1810	7870	447	80.2	23.1	69.5
Glass fiber	343	56-72	-	0.036-0.055	-	-

3.4.2 Design of Hot Water Storage Tank

A cylindrical-shaped tank is considered the most effective for maintaining temperature stratification. The diameter (D), height (H), and volume (V) of the storage tank can be calculated using a specific equation (Gao et al., 2021).

$$v = AL \quad (3.14)$$

$$v = \pi H \frac{D^2}{4} \quad (3.15)$$

The suggested height-to-diameter ratio for most domestic solar water storage tanks is $\frac{H}{D} = 1.5$ to 3.5 (Thermal and Engineering, 2019).

For circular cylindrical shaped storage tank assuming height to diameter ratio $\frac{H}{D} = 2$.

$$H = 2 * D \quad (3.16)$$

Thermal stratification is affected by different factors, such as the flow rate orientation of the tank, whether vertically or horizontally, and aspect ratio. This study considered the aspect ratio because the thermal stratification method is analyzed for a hot water storage tank. A higher quality of temperature stratification is obtained as the aspect ratio increases and the cold-water flow rate decreases. For a vertical hot water storage tank, the best utilization of a hot water storage tank is obtained at aspect ratio 2 with a low flow rate (Khammas, F.A., et al, 2021).

$$v = \pi \frac{D^2}{4} * H \quad (3.17)$$

$$v = \pi \frac{D^2}{4} (2 * D) \quad (3.18)$$

$$v = \pi \frac{D^3}{2} \quad (3.19)$$

A storage tank can be sized based on the hospital's hot water consumption. From the volume of storage tank (V_s).

$$V_s = THWLL \quad (3.20)$$

$$V_s = 38.88m^3 \quad (3.21)$$

Where THWLL is the total hot water load of Limmu Gennet Hospital

In this study, the total hot water demand is $38.9m^3$. So instead of using one large hot water storage tank, two hot water tank is recommended to simplify simulation and provide option during technical problem.

That means having two hot water storage with $19.45m^3$. From equation (3.21), the height and diameter of the water tank are obtained by considering the concept of using two tanks rather than one larger tank. Regarding cost, two smaller tanks are less expensive than one larger tank. The energy loss of a large water tank is higher than that of a smaller or medium because of its length and height. Since each of them operates independently, when one fails to work during problems of incorrect piping condition, poor performance and needs maintenance, the other is used for continuous operation. So, having two independent hot water storage is more energy efficient than one single. Low heat energy is also used in smaller than large ones and is better for handling, space-saving, or the environment.

$$v = \pi \frac{(2r)^3}{2} \quad (3.22)$$

$$v = 4 * \pi * r^3 \quad (3.23)$$

$$v = 19.45m^3 \quad (3.24)$$

$$r = 1.16.$$

From equation (3.16) height of the water storage tank is $h = 4.64m$.

3.4.3 Thickness Optimization Hot Water Tank

Material Cost (CMS): Mild steel is selected as mentioned in the above section, and its related cost gathered from the market is 475 birr/ thickness (mm). That is obtained by Per unit area ($475 * 42.33$). The material cost is obtained by.

$$CMS = (Cost/mm) * (t;mm) \quad (3.25)$$

Heat Loss Cost (HLC): it is amount of heat lost from hot water tank and can be obtained by:-

$$Q_L = U_L A_S \Delta T \quad (3.26)$$

Where: Q_L is amount of heat lost from hot water tank, U_L is the total heat transfer coefficient, ΔT , and is temperature difference through thickness of insulation. From equation (3.24), the internal diameter hot water storage tank is $2.32m$ and the height is $4.64m$ and the total surface storage's area is given by:

$$A_s = \pi D_i h + 2\pi \frac{D_i^2}{4} \quad (3.27)$$

$$A_s = 42.33m^2$$

Assuming the temperature difference between fluid temperature and ambient temperature is 38. The overall heat transfer coefficient is determined as follows.

$$U_l = \frac{K}{t_i} \quad (3.28)$$

Then the rate of heat losses from the storage tank is determined from equation (??), and also using table 3.5 ($k = 63.9W/km$)

$$Q_L = 102.79$$

The cost of heat loss is according to Ethiopian electric generation, transmission, and distribution costs, the tariff for electric energy is 2.628 per *Kwh*.

$$CHL = (cost/kwh) * (Q_l(kwh)) \quad (3.29)$$

The cost of heat loss is according to Ethiopian electric generation, transmission, and distribution costs, the tariff for electric energy is 2.628 per *Kwh*.

$$CHL = 2.628 \text{ per } kWh * 102.78/t_i(mm)Kwh$$

Overall Cost (OC):): total includes materials and heat lost costs.

$$OC = MCS + HLC \quad (3.30)$$

$$OC = [475 * 42.33t_i + 270.13/t_i] \text{ Birr}$$

$$OC = [20106.75t_i + 270.13/t_i] \text{ Birr}$$

To get the numerical value of storage tank thickness for modeling the storage tank, differentiate the total cost equation for thickness and set the value equal to zero.

$$\frac{dTC}{t_i} = 0 \quad (3.31)$$

$$20106.76 - \frac{277.67}{t_i^2} = 0$$

From this equation, the optimum thickness of the storage tank is $t_i = 8.5095mm$. For safety and reliable operation, taking the value of $t_i = 10mm$.

3.4.4 Optimization of Insulation Storage Tank Thickness

Insulation involves using materials to reduce heat transfer between a system and its surroundings. In hot water storage tanks, insulation is used to minimize heat loss from the tank's surface, thereby maintaining purpose energy within the tank. For this purpose, optimizing the insulation materials' thickness is essential. When selecting insulation materials, key factors include low thermal conductivity, resistance to corrosion, non-toxicity, non-flammability, and the ability to withstand long-term use without decomposing (Deshmukh and Blanchet, 2017). The ideal insulation material should also have compressive strength, be suitable for the desired temperature range, possess good thermal conductivity, and have consistent thickness.

Polyurethane, fiberglass, Glass wool, and Rockwool insulation materials contribute to maintaining hot water inside water storage. Among these, polyurethane and fiberglass are hot water tanks' most efficient thermal insulation. The highest temperature occurs at polyurethane, Glass fiber, and Rockwool, respectively, and night heat losses decrease from polyurethane, Glass fiber, and Rockwood, respectively(Deshmukh and Blanchet, 2017).

Among the insulation mentioned above materials, fiberglass is selected because of its Best commercially available insulation materials, lower thermal conductivity, higher resistance to absorption and temperature, and lower cost per unit area.

Insulation Thickness: Determine the cost of insulation thickness for hot water storage; the selected insulation material is glass fiber.

The Cost of Glass Fiber insulation is obtained from the market and is given as 0.40\$ or 20.25 birr per millimeter of thickness per unit area of the tank (m^2). This cost, referred to as GFC, can be calculated using the following formula:

$$GFC = (cost/mm) * t_i(\text{ in } mm) = (20.25 * t_i) \text{ birr} \quad (3.32)$$

Cost of Heat Loss (CHL): Based on the Ethiopian energy context, energy lost from hot water tank is obtained as follow. That is the cost of energy per (kwh) in Ethiopia is equals 2.628 per Kwh . so the cost of heat loss from the storage is determined by the following relation.

$$CHL = (cost/kwh) * Q_L(kwh) = (2.628 * Q_L)kWh \quad (3.33)$$

The rate of heat loss from the storage tank is determined from the following equation.

$$Q_L = U_L A_S \Delta T \quad (3.34)$$

Where: Q_L is the rate of heat loss from the storage tank, U_L is the overall heat transfer coefficient A_S is the surface area of the storage tank, T is the temperature difference through insulation thickness. The total heat loss coefficient (U_L) is the combination of convective heat transfer coefficient ($h_{ins-amb}$) and heat loss coefficient through insulation (U_{ins}).

$$U_L = U_{ins} + U_{ins-amb} \quad (3.35)$$

Heat loss coefficient through insulation is determined by:

$$U_{ins} = K_{ins}/t_i \quad (3.36)$$

The convective heat loss coefficient from insulation to the ambient is determined (Kumar, S., and Mullick, S. C. 2010) by:

$$h_{ins-amb} = 2.8 + 3V_w \quad (3.37)$$

Where K_{ins} and V_w are thermal conductivity glass fiber and average wind speed. The average wind speed of the selected area ($V_w = 2.1m/s$) and thermal conductivity of fiber glass is ($K = 0.036W/mC^\circ$).

The area of the surface including insulation thickness is calculated by

$$A_S = 2\pi * (r + t_i) * h + 2\pi * \frac{D_0^2}{4}, \text{ where } D_0 = D_i + 2t_i \quad (3.38)$$

$$A_S = 42.45m^2$$

The total heat loss coefficient of (U_L) is obtained by combining equations (3.36) and (3.37).

$$U_L = U_{ins} + U_{ins-amb} = \frac{0.036w/mk}{t_{ins}} + 9.1w/m^2k \quad (3.39)$$

By substituting equation (3.36) into equation (3.32).

$$Q_L = \left[\left(\frac{0.036}{t_i} + 9.1 \right) \right]_S^A 1\Delta T \quad (3.40)$$

The area of the storage tank as determined by equation (3.38) is $\frac{A}{S}1 = 42.45m^2$ and the temperature of the hot water storage tank is taken to be $T_s = 60C^\circ$ and the ambient temperature is feed water temperature $T_a = 22C^\circ$

By substituting the above value into equation (3.40) the rate of heat loss from the storage tank in 24 hours becomes.

$$Q_L = \left[\left(\frac{1393.72}{t_i} + 352301.04 \right) \right] Kwh \quad (3.41)$$

$$CHL = (cost/Kwh) * Q_L(Kwh) = (2.628 * Q_L)Kwh$$

Overall cost is the insulation and heat loss cost and determined as follow:

$$CHL = \left[\left(\frac{3662.70}{t_i} + 925847.1 \right) \right] \text{ Birr}$$

Total Cost: Total cost is the insulation cost and heat loss cost and determined as follow:

$$TC = CGF + CHL \quad (3.42)$$

$$TC = \left[\left(\frac{1393.72}{t_i} + 925847.1 + 20.25t_i \right) \right] \quad (3.43)$$

To obtain the thickness of the insulation differentiate the total equation for t_i and set to zero it becomes:

$$\frac{dTC}{dt_i} = 0 \quad (3.44)$$

$$20.25 - \frac{3662.69}{t_i^2} = 0$$

The thickness of the insulation of glass fiber is $t_i \approx 13.45$ for strength and safety 14mm will be taken. The proposed model of hot water storage tank with volumes (V) = $19.45m^3$, height (H) = $4.64m$, and diameter (D) = $2.32m$ with glass fiber insulation thickness of 0.014 was given in figure (3.5)

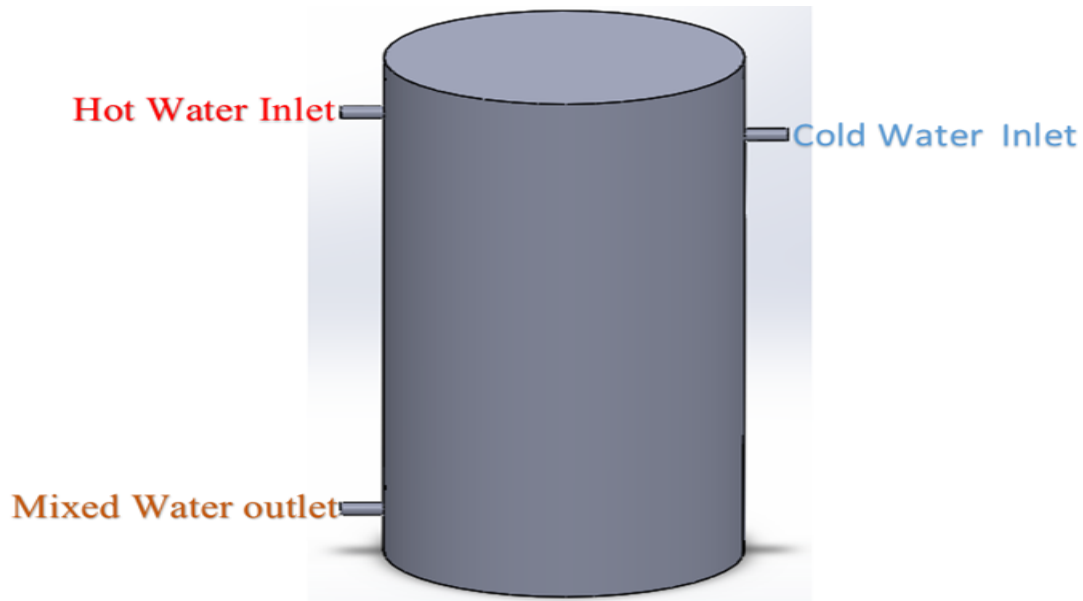


Figure 3.5: Proposed model for the hot water storage tank

Thermal stratification of a hot water tank is based on flow rate rather than the orientation of the position of the inlet and hot liquid water. At an absolute minimum mixing of cold and hot water, thermal stratification of hot water can be maintained. Suppose the inlet pipe of the cold and hot inlet water tank is carefully designed so that the turbulence of liquid water inside the tube is reduced. In that case, thermal stratification can be obtained inside the whole water storage tank with a constant outlet temperature because thermal stratification aims to get a continuous outlet temperature at the outlet side.

3.5 Selection and Design of Paraffin PCMs

3.5.1 Selection of Paraffins as PCMs

The phase change process of PCM depends only on the temperature and is widely used in heat storage and temperature control. PCMs are highly concerned due to their high thermal storage density, compacted thermal storage device building, and approximately isothermal heat release and absorption. This study selected paraffin wax (C_nH_{2n+2}) because of its thermophysical properties, such as low vapor pressure, self-nucleation, high heat density, and extensive range of phase alteration. The phase change temperature ranges from 18 to 71°C, which makes them applicable to thermal energy storage systems. This temperature range is similar to domestic hot water, so paraffin wax is primarily used in hot water applications.

The general thermodynamic properties of PCMs summarized in Appendix A.0.3

Table 3.6: Desirable Thermophysical properties of selected paraffin.

Melting point (°C)	Latent heat of fusion (Enthalpy change) (kJ/kg)	Specific heat (J/kg.°C)		Density (Kg/ m ³)		Thermal conductivity (w/m. oC)	
		Solid	Liquid	Solid	Liquid	Solid	Liquid
59	213	1850	2384	861	778	0.4	0.15

3.5.2 Mechanism of Thermal Energy Storage System

Charging Process: fluid heated in a solar collector having a melting temperature above PCMs is circulated in the system. This fluid enters the tubes of the heat exchanger and shares heat with the PCMs until it maintains the same temperature within HTF, then released at the bottom of the tube. Then, this HTF enters the hot water storage tank through a hot inlet pipe that mixes with cold water temperature coming from the cold-water inlet pipe.

Standby Process: in this case, there is no energy-storing mechanism since the storage tank is fully charged or directly fed to the end user. There is no transfer of HTF inside the arrangement, and it is the transitional period between the charging and discharging process.

3.5.3 Assumption for Latent Heat Thermal Energy Storage System and Design Consideration

In terms of the design consideration for a latent heat thermal energy storage system, factors such as the types of heat transfer units, energy storing capacity of the tank, thermophysical properties of phase change materials, and operating temperature of the system need to be considered.

Design assumption tank insulation to reduce heat losses, temperature of HTF entering the storage tank is equal to the temperature leaving the flat plate collectors, PCMs and HTF have constant thermophysical properties about outlet temperature, uniform initial temperature of the storage within the melting temperature, and negligible thermal conductivity.

3.5.4 Design of Phase Change Materials PCM

Masses of PCM were obtained from the storage capacity of the LHTES system with a PCM medium.

$$Q = \int_{T_1}^{T_2} mC_{p,s}dT + m\Delta H_{pcm} + \int_{T_1}^{T_2} mC_{p,l}dT \quad (3.45)$$

$$Q = m[c_{ps}(T_2 - T_1) + \Delta H_{pcm} + c_{pl}(T_2 - T_1)] \quad (3.46)$$

Then the amount of the mass of PCMs of to be integrated into the storage tank is calculated as follows:

$$Q_{total}(W) = \rho_{pcm,s}C_{p,s}(T_m - T_i) + \Delta H_{pcm} + C_{p,l}(T_0 - T_m) \quad (3.47)$$

$$v_{LHTES_{pcm}} = \frac{Q_{HTF,total}(W)}{\rho_{PCM,s}C_{p,s}(T_m - T_i) + \rho_{PCM,l}\Delta h + \rho_{PCM,l}C_{p,l}(T_0 - T_m)}$$

$$v_{LHTES_{pcm}} = \frac{6205248000}{861 * 1850(59 - 43) + 778 * 213 + 778 * 2384(60 - 59)} = 11.69m^3$$

$$v_{LHTES_{pcm}} = 11.69m^3.$$

Where, v_{pcm} the total volume of PCMs integrated into LTES, $Q_{(HTF,total)}$ is total heat energy stored by water, T_0 , T_m and T_i outlet, melting, and inlet temperature respectively. In this study geometric parameters of PCM storage are determined by taking the aspect ratio of $H/D = 2$ hence diameter and length of LTES are $1.95m$ and $3.89m$.

3.6 Energy Storage Unit

3.6.1 Selection Geometric Parametric of Shell and Tube

To overcome the drawback of low thermal conductivity of PCMs, shells, and tubes are used to exchange heat in latent TES. The geometric parameters of the shell and tube are selected based on a dimensionless number $\frac{r_{0,sh}}{r_{i,sh}} = 1.3$ to 3 is with the tube length $L = 1 - 20m$ (Yang et al., 2021). Depending on this the inner and outer diameters of the shell tube are $0.08m$ and $0.13m$ respectively. So, the geometry is consisting of heat transfer fluid flows into a circular copper pipe surrounded by PCM with an inner $80mm$, outer diameter $130mm$. The diameter shell filled with PCMs is $1950m$ with a height $3890mm$. To minimize the environmental heat losses, it is insulated $30mm$. The total number of pipes is obtained from equation (3.48) equal to 28 pipes.

In this work, the total volume of phase change material used to integrate with LHTES is $5.8m^3$ since two storage tanks are required instead of one large. Each tube in this storage has been filled with HTF $0.078m^3$ and surrounded by $0.21m^3$ of PCMs. The total masses of PCMs used to integrate with the thermal storage tank are determined from the next equation by selecting the porosity of PCM as $\varepsilon = 0.45$.

$$m_{pcm} = (1 - \varepsilon)\rho_{pcm}v_{pcm} \quad (3.48)$$

From equation (3.47) total masses of phase change material needed to be integrated into the storage tank is $2746.59kg$. The total number of shells and tuber is determined by the following:

$$N_{u,total} = \frac{v_{PCM,total}}{v_{PCM,single}} = \frac{5.8m^3}{0.21m^3} = 27.62 \quad (3.49)$$

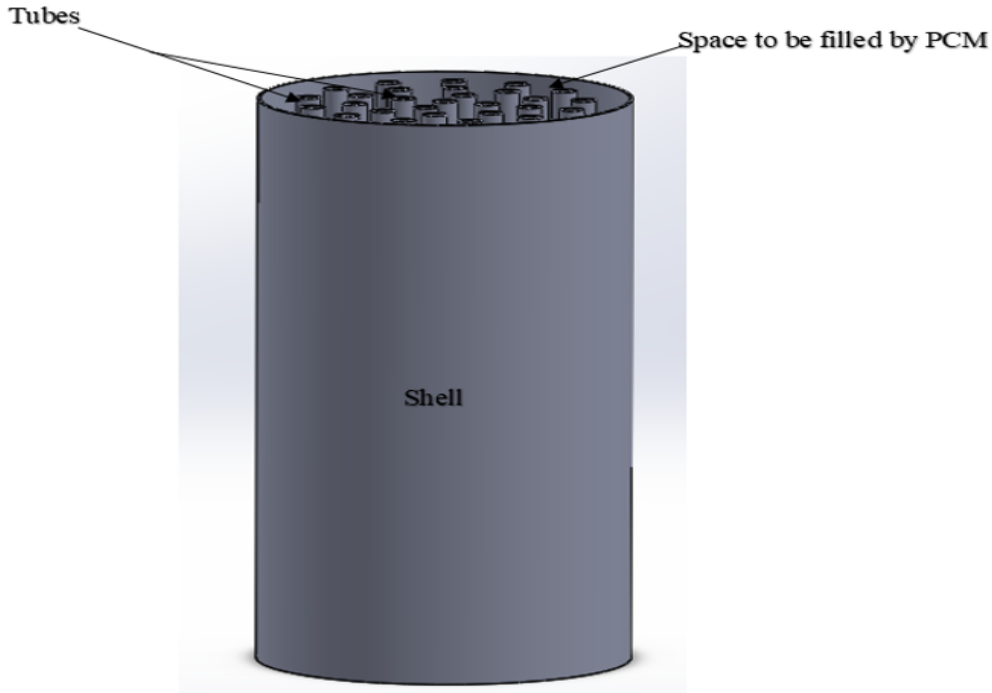


Figure 3.6: Component and inner structure of proposed model for PCMs shell and tube heat exchanger

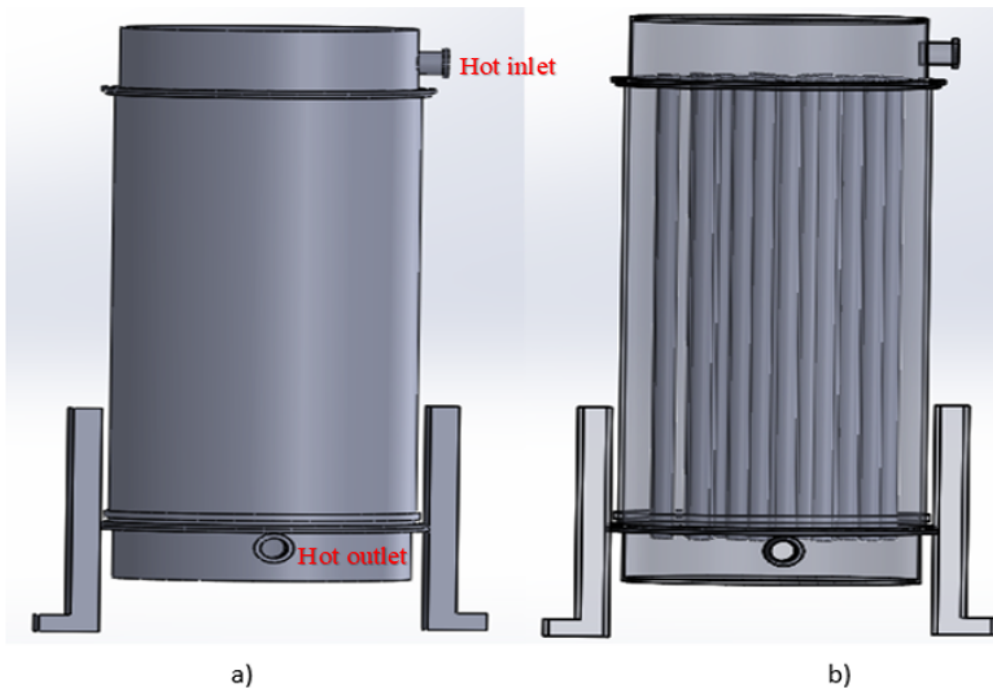


Figure 3.7: Fully assembly of the proposed model for PCMs shell and tube heat exchanger a) indicates solid full structure and b) indicates transparent inner visualization structure

The most essential arrangement of a vertical heat exchanger is its compact design, which is comfortable for limited space. This vertical orientation also provides better fluid distribution that enhances or improves heat transfer efficiency, strengthening the convection of liquid PCM and increasing the nominal conductivity of the material. In this arrangement, gravity is acting party on the flow rate. So, a faster flow rate is obtained compared to horizontal, and a more significant amount of time for the heat exchanger gives better results. The total number of tubes used to incorporate the shell filled with PCM material is calculated by equation (3.49), and their patterns are arranged in the vertical position to enhance the thermal conductivity of PCM filled inside the shell.

3.7 Modeling and Optimization of Hot Water Storage Tank by Thermal Stratification

Improving the efficiency of domestic hot water storage tanks is directly linked to the thermal gradient along the height of the tank. By promoting and maintaining a high level of stratification, where hot and cold water are separated by thermal buoyancy, the overall efficiency of the tank increases (Abdelhak et al., 2015).

They have achieved this stratification by forming a thermocline, a mixing layer between the hot and cold water.

The objective is to keep the thermocline thickness as thin as possible to preserve and stabilize it, minimizing the mixing layer. Thermal stratification ensures that more significant hot water is maintained in the tank, improving storage efficiency. For this purpose, various factors such as the aspect ratio of the tank's height to diameter, the tank's configuration (horizontal or vertical), flow rate, shape of the tank, heat loss to the surroundings, heat conduction between hot and cold layers, and the design and placement of inlet and outlet ports need to be carefully considered and analyzed. By carefully designing and analyzing these factors, the thermocline thickness can be effectively maintained, enhancing the thermal stratification of the hot water storage tank. Careful design and analysis of inlet and outlet ports, as well as the overall design of the hot water storage tank, are essential factors in maintaining the desired thermocline thickness.

Additionally, the selection of the location of inlets and outlets, determining the number of inlets and outlets, placing obstacles inside different parts of the tank, and using stratifiers and baffles can also contribute to enhancing thermal stratification in the hot water storage tank (SHAARAWY, 2014).

3.7.1 Modeling of Inlet Pipe for Inlet Design Optimization

Velocity of water is measure of speed of flowing water through the pipe determined by:

$$u = \frac{Q}{A} \quad (3.50)$$

Where, u velocity, Q flow rate, and A the cross-sectional area of the pipe.

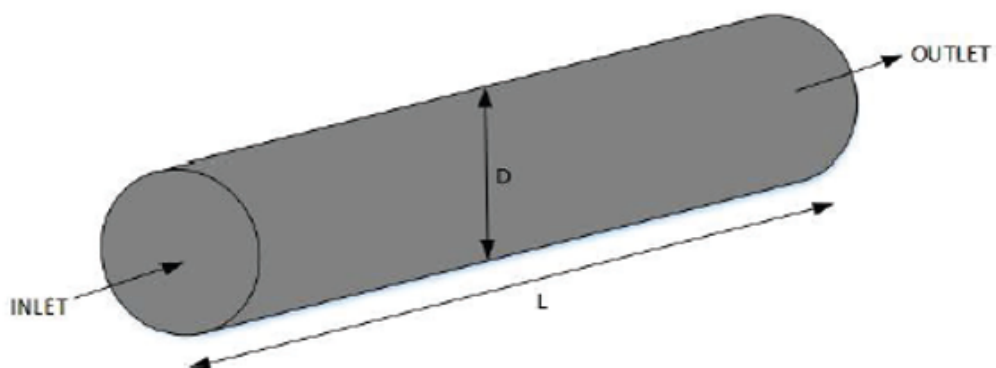


Figure 3.8: Dimension and diagram of the inlet pipe.

For fluid flow simulation in the pipe, only the fluid domain is considered to reduce unnecessary computational effort in modeling and simulating the pipe. The model is based on three-dimensional turbulence across the tube with an internal diameter of $0.045m$ and an external diameter of $0.050m$, with a length of $0.5m$. The flow rate occurs for four hours per day to fill the hot water storage tank

The volumetric flow (\dot{v}) rate is calculated from the following equation.

$$\dot{v} = \frac{V}{t} \quad (3.51)$$

Where, V volume of water and t is time.

From equation, volumetric flow rate is $0.00135m^3/s$, the mass flow rate is obtained by:-

$$\dot{m} = \rho \times \dot{v} \quad (3.52)$$

From equation (3.51), using density of water, $976.86m^3/kg$ mass flow rate is determined to be $1.31kgs$.

Pipe area is determined by:

$$A = \pi r^2 \quad (3.53)$$

Using the above equation area of pipe is calculated to be $0.16m^2$, then velocity of water flow through the pipe is $u = 0.00844m/s$. Reynold's number is used determine the flow characteristic of the fluid flow through the pipe weather the flow is laminar or turbulence. So, the following equation is used to determine Reynold number.

$$R_e = \frac{\rho v L}{\mu} \quad (3.54)$$

Where, μ is dynamic viscosity of the fluid in $kg(m.s)$ or $N.S/m^3$, L is length of the pipe, ρ is density of water in kg/m^3 and v is velocity of fluid in m/s .

Using dynamic viscosity of water $\mu = 8.90 \times 10^{-4}kg(m.s)$, the Reynold's number is $4,731.43$. Many authors stated that flow inside the pipe is turbulent for Reynolds numbers greater than 4000 (Bouzaher et al., 2019). In this work, Reynold's number for inlet velocity is $0.00844m/s$ was found to be $4,731.43$. So that flow was characterized by the turbulence flow regime. To reduce this turbulence flow and enhancing thermal stratification of water storage tanks careful design of the water storage tank for optimization important technique.

In this work, the hot and cold-water inlet pipes top and mixed water outlet pipe at the bottom were modeled with the same diameter and length but different geometries and flow conditions to predict the influence inlet pipe for better thermal stratification.

These inlet pipes were inserted into proposed model for hot water storage shown by Figure (3.5). Two types of flow pipes were; - perforated and normal pipes were modeled and analyzed. These pipes are also modeled by SolidWorks 2020 software and assembled to hot water storage tank and their effects were analyzed.

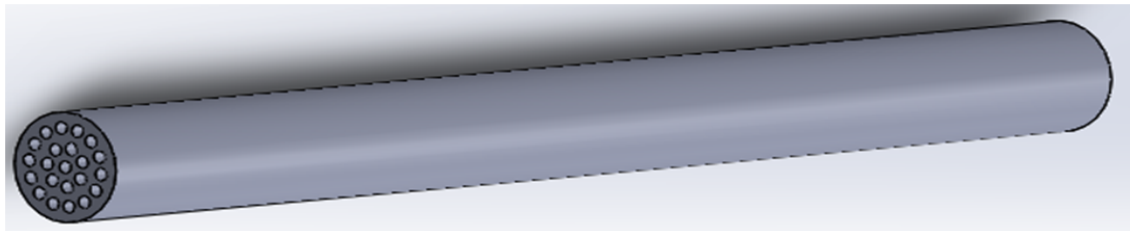


Figure 3.9: Perforated Inlet Pipe

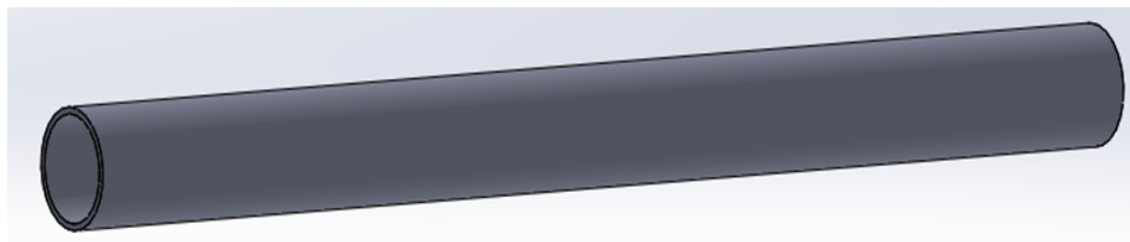


Figure 3.10: Normal Inlet Pipe

3.8 Proposed Solar Water Heating System Integrated with Different Components

The system uses thermosiphon fluid in the collector; within this system, it is heated and expands, becoming less dense, and the tank with water above the collector is more incredible and has higher density, so it flows down to the collector, forcing hot water to go up to the storage-insulated tank during daylight. It uses two thermal storage tanks integrated with PCMs and hot water storage tanks. The solar collectors collect energy from the sun and heat water entering from water sources. Then, the high fluid temperature from flat plate solar collectors becomes stored in a phase change material integrated thermal storage system. The PCMs store heat used for later time (night time).

Finally, hot water with higher temperature from PCMs integrated thermal energy storage and cold water from the water source are mixed in the hot water tank with the required hot water demand for the end user.

All technical data of designed thermal storage and hot water tank are summary table in Appendix A.0.4.

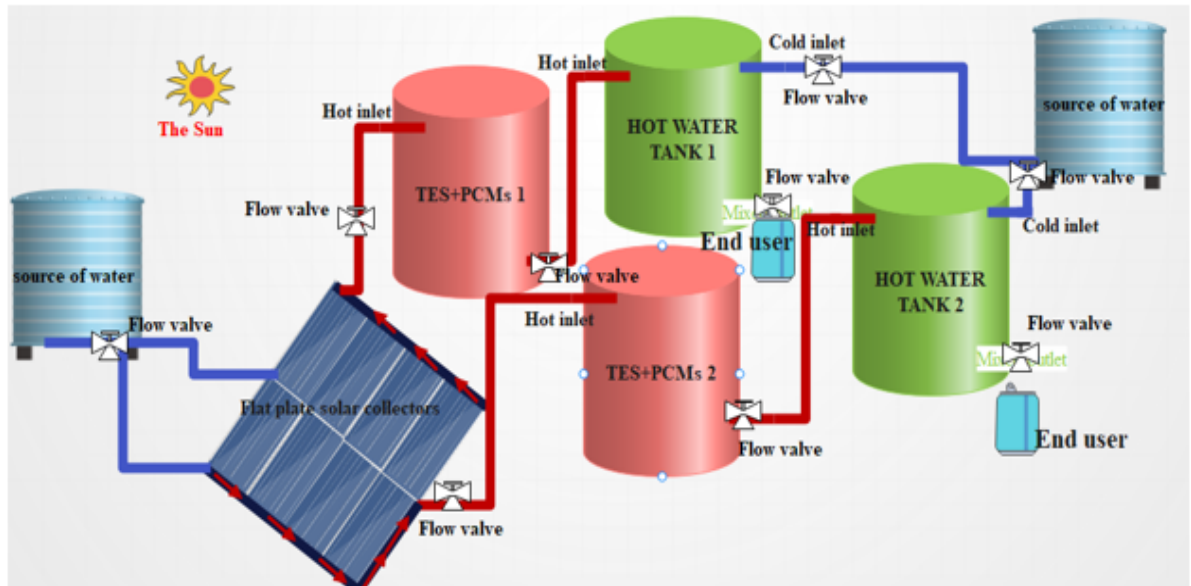


Figure 3.11: Proposed solar water heating system integrated with different component

Chapter 4

Available Solar Radiation

Assessment of Limmu Gennet

The amount of solar radiation for energy drives like heating, cooking, and lighting on the Earth's surface varies depending on local climate environments. It is vital to have accurate information about local solar radiation to design efficient building energy systems. The most reliable data source for calculating the average amount of solar radiation is statistics. However, if this data is unavailable for a specific location, it is possible to estimate the radiation using empirical relationships based on hours of sunshine or cloudiness. Several sources of information on average or potential sunshine hours can be used in such cases. The two chief components of solar radiation are direct beam and diffuse radiation.

Incident Solar Radiation (G_r) is global radiation on a surface that strikes the earth's surface. It is inclined to the collector surface at an angle of β and well-defined in terms of global, beam diffuse, and reflectivity radiation.

Beam Radiation (I_b) refers to the radiant solar energy that strikes the Earth's surface in a straight line from the sun and can be calculated using a simple geometrical relationship between horizontal and tilted.

$$I_b = G_r - I_d \quad (4.1)$$

Diffusion Radiation (I_d) is solar radiation deflected by aerosols, atmosphere, and dust molecules to the sky. The link between diffusion radiation and global radiation can be determined by multiplying the clarity index with global radiation, as expressed in the given equation

$$D_r = G_r * KT. \quad (4.2)$$

Where kT hourly clarity index.

4.1 Basic Sun-Earth Angle Relationship

The relationship between the Earth's location, the situation of the sun, and arriving beam radiation can be designated using various angles.

Latitude (ϕ) is location of some objects to north or south that ranges between $-90^\circ \leq \phi \leq 90^\circ$ north positive and south negative and it is the position of an area relative to north and south.

Hour Angle (W_s) is angular movement of the sun from the observer's local meridian, either east or west, is caused by the Earth's rotation on its axis at a rate of 15° per hour. It is angular distance among the observers meridian whose plane contains the sun and is calculated as the following (Maleki et al., 2017).

$$W_s = \cos^{-1}(-\tan^{-1}\phi \tan\delta) \quad (4.3)$$

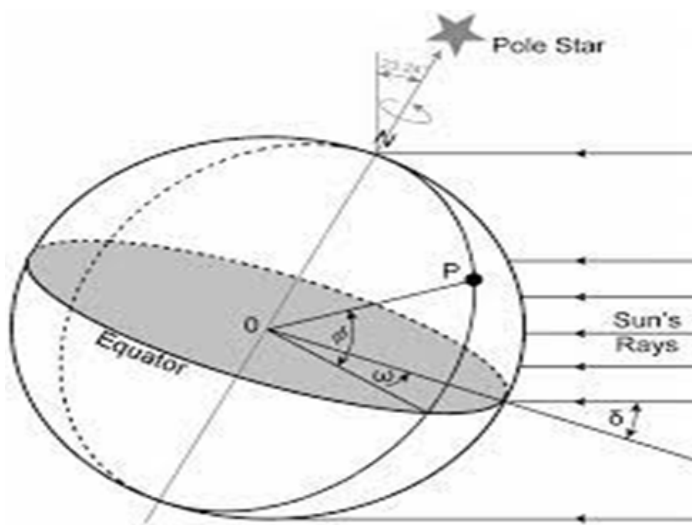


Figure 4.1: Hour angle (Maleki et al., 2017)

The Solar Azimuth Angle (γ), refers to the angular displacement from the south of the projection of beam radiation on the horizontal plane, as shown in Figure (4.2). A displacement to the east of south is considered negative, while a displacement to the west of south is considered positive.

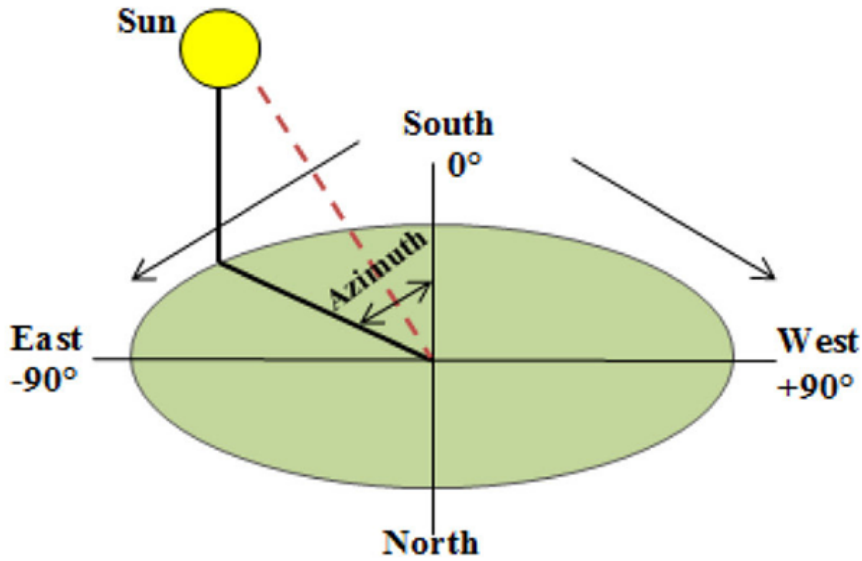


Figure 4.2: Definition solar azimuth angle (Maleki et al., 2017)

The Declination Angle, is the angle at which the sun's position varies from +23.45 degrees to -23.45 degrees throughout the year. The declination angle of any given day can be calculated using Cooper's approximate equation, as mentioned by (Shivalingaswamy and Kagali in 2012).

$$\delta = 23.45 \sin \left[360 \left(\frac{284 + n}{365} \right) \right] \quad (4.4)$$

A solar collector's orientation and tilt angle seriously affect its performance by determining the amount of solar radiation it receives. A tracking system, such as a mechanical tracker, is the most effective way to maximize day-to-day energy capture. The declination angle allows positioning the solar collector at the ideal tilt angle and making adjustments as necessary, ensuring the optimal collector slope for any latitude and surface azimuth angle on any given day of the year. In the northern hemisphere, the best orientation for a solar collector is southward. As for the ideal tilt angle, researchers have not provided a specific figure, but for a solar water heater that maximizes the annual solar fraction of the system, (Shariah et al. 2002) have provided guidelines.

$$\beta = \phi + 10 \quad (4.5)$$

Where, ϕ latitude site is 8.1 and solar collector is oriented facing south and tilt at 18.1 is the recommended orientation for solar heater flat plate collectors.

4.2 Average Monthly Day-to-day Solar Energy on Horizontal Surface

The average daily radiation for the month, the original Angstrom equation-type regression, relates it to the clear-day radiation at the location and the average fraction of possible sunshine hours. In the modified Angstrom equation, values of extraterrestrial radiation on a vertical surface are used instead of clear-day radiation (Ijes and Ijes, n.d.).

$$\frac{H}{H_0} = a + b \left(\frac{n}{N} \right) \quad (4.6)$$

Where, average monthly global energy striking a collector ($MJ/m^2 \cdot \text{day}$),
 H_0 is Regular extraterrestrial energy on the horizontal surface in ($MJ/m^2 \cdot \text{day}$)
 n is the average daily hours per month bright sunshine
 N , Average monthly day length and a and b are values that are constants.
 Average monthly regular extraterrestrial irradiation is obtained by:-

$$H_0 = \left(\frac{24}{\pi} \right) I_{cs} \left[1 + 0.033 \cos \left(\frac{360n}{365} \right) \right] \times \left[\cos \phi_l \cos \delta_{dec} \sin W_s + \left(\frac{\pi W_s}{180} \right) \sin \phi_l \sin \delta_{dec} \right] \quad (4.7)$$

Where, I_{cs} the solar constant ($1367W/m^2$), δ_{dec} angle of declaration, ϕ_l latitude of the site.

The mean sunrise hour angle (W_s) for the specified month and the number of days in the year, counting from January 1st, are also taken into account ($n = 1$ to 365). The solar declination angle and the mean sunrise hour angle can be calculated using specific equations.

Table 4.1: Standard suggested average days for months and values of n by months

Months	n for i^{th} days of the months	For average days of the month		
		Dates	Days of the year (n^{th})	Declination (δ)
January	i	17	17	-20.9
February	$31 + i$	16	47	-13
March	$59 + i$	16	75	-2.4
April	$90 + i$	15	105	9.4
May	$120 + i$	15	135	18.8
June	$151 + i$	11	162	23.1
July	$181 + i$	17	198	21.2
August	$212 + i$	16	228	13.5
September	$243 + i$	15	258	2.2
October	$273 + i$	15	288	-9.6
November	$304 + i$	14	318	-18.9
December	$334 + i$	10	344	-23.0

Sunshine Hours is a climatic indicator that measures the sunshine duration in a given period, typically a day or a year, for a specific location on Earth. It is expressed as an average value over several years. It measures a location's cloudiness rather than insolation, indicating all solar energy received during a specific time. Table 4.2 displays the sunshine hour duration of Limmu Genet for five years, while Table 4.3 presents the five-year average of sunshine hours near the Jimma Zone meteorology agency.

Limmu Genet location:

- Latitude (ϕ) 8.067
- Longitude 39.95
- Altitude 1766 above sea level

Table 4.2: Average monthly sunshine hours of Limmu Gennet (2017-2021)

Years	Jan	Feb	Mar	Apr	May	Jun	Jul	Aug	Sep	Oct	Nov	Dec
2017	8.78	7.07	7.75	8.43	6.31	7.34	3.61	4.52	5.43	7.04	8.65	9.82
2018	8.92	8.32	8.05	7.77	7.60	4.74	4.53	4.26	4.75	7.71	7.22	9.24
2019	9.31	8.70	7.70	6.70	7.65	5.48	3.53	3.37	4.23	8.08	7.14	8.37
2020	8.59	8.40	7.31	7.54	8.15	6.25	2.79	2.93	5.18	7.85	9.13	9.33
2021	9.16	7.75	8.50	6.57	6.71	7.30	2.64	5.06	4.27	7.97	8.50	7.54

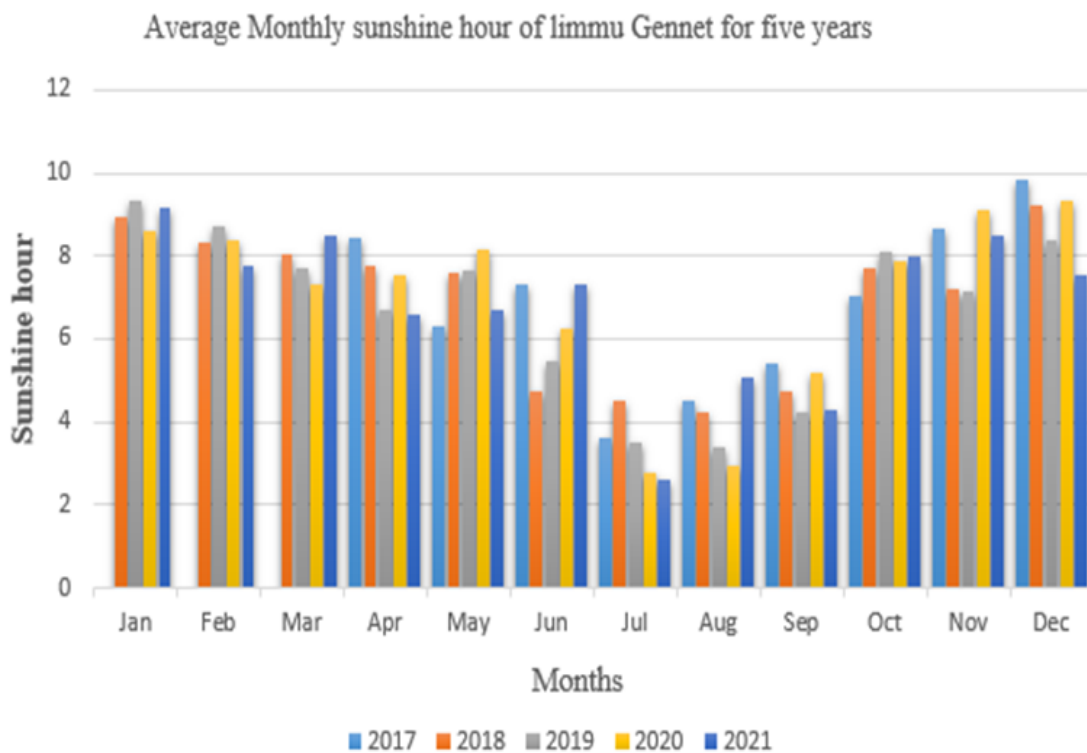


Figure 4.3: Average monthly sunshine of Limmu Genet for five years

Table 4.3: Average sunshine hour duration (2017-2021)

Years	Jan	Feb	Mar	Apr	May	Jun	Jul	Aug	Sep	Oct	Nov	Dev
Average (2017-2021)	8.95	8.05	7.90	7.40	7.28	6.22	3.42	4.03	4.77	7.73	8.13	8.86

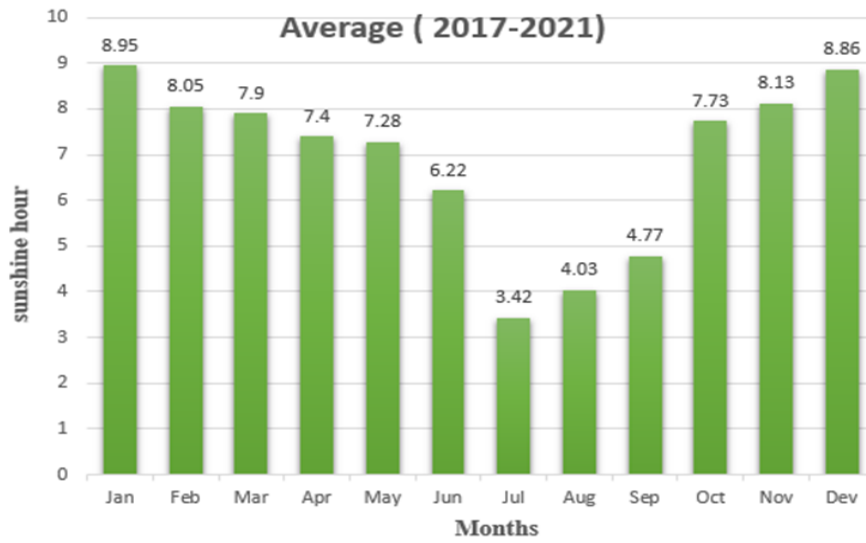


Figure 4.4: Hourly sunshine duration of Limmu Genet (Bar chart)

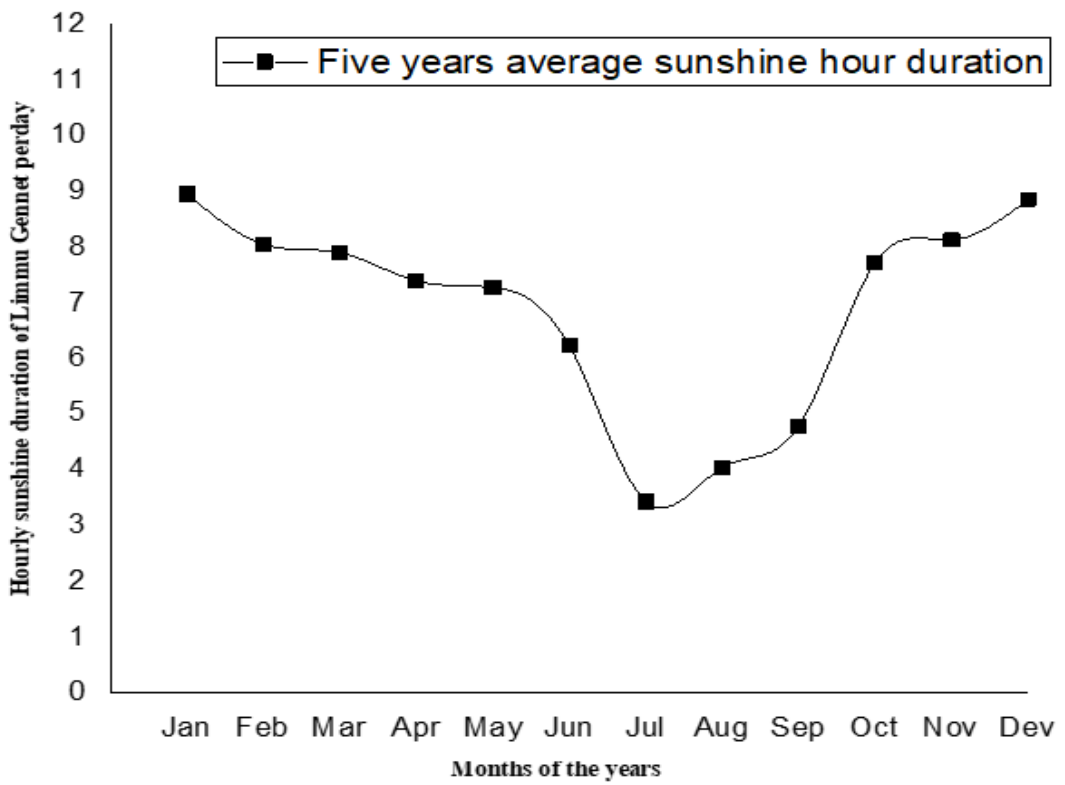


Figure 4.5: Hourly sunshine duration of Limmu Genet (Graph)

Hour angle in degree is determined from equation (4.3) by using Table 4.1 and the latitude of the site. ($\phi = 8.067$).

Table 4.4: Hour Angle (W_s).

Months	Jan	Feb	Mar	Apr	May	Jun	Jul	Aug	Sep	Oct	Nov	Dev
Hour angle	86.9	88.1	89.7	91.3	92.8	93.5	93.2	92.0	90.3	88.6	87.2	86.6

The equation relating the maximum possible sunshine duration (monthly average day length) to the mean sunrise hour angle is as follows:

$$N = \frac{2 \times W_s}{15} \quad (4.8)$$

Where N is the maximum possible sunshine duration in hours and W_s is the mean sunrise hour angle.

Table 4.5: Maximum possible daily hours sunshine duration (N).

Hour angle	86.9	88.1	89.7	91.3	92.8	93.5	93.2	92.0	90.3	88.6	87.2	86.6
Bright sunshine	11.6	11.7	11.9	12.2	12.4	12.5	12.4	12.3	12.0	11.8	11.6	11.5

Coefficients a and b are determined by relationship.

$$a = -0.110 + 0.235 \cos \phi_l + 0.23 \left(\frac{n}{N} \right) \quad (4.9)$$

$$b = 1.449 - 0.553 \cos \phi_l - 0.694 \left(\frac{n}{N} \right) \quad (4.10)$$

Gopinatifian, (1988) suggests that in order to improve the accuracy of the calculated data, it is recommended to consider the latitude, and sunshine duration when calculating the regression coefficients, a and b for any location worldwide.

$$a = -0.309 + 0.539 \cos \phi_l - 0.0693A + 0.29 \left(\frac{n}{N} \right) \quad (4.11)$$

$$b = 1.527 - 1.027 \cos \phi_l + 0.0926A - 0.359 \left(\frac{n}{N} \right) \quad (4.12)$$

Where H is Altitude $1.766km$ above sea level and latitude ($\phi_l = 8.067$).

4.2.1 Monthly Average Diffuse Radiation (H_d) on A Horizontal Surface

The monthly average diffusion radiation per day can be derived using the following equation. The relationship between $\frac{H_d}{H}$ and the clearness index (K_T) has been established based on the average diffuse fraction obtained from the daily diffuse correlations for $\omega_s \leq 81.4001^\circ$ and $0.301 \leq K_T \leq 0.801$.

$$\frac{H_d}{H} = 1.401 - 3.601K_T + 4.201K_T^2 - 2.13K_T^3 \quad (4.13)$$

For $\omega_s > 81.40^\circ$ and $0.30 \leq K_T \leq 0.801$

$$\frac{H_d}{H} = 1.3011 - 3.022K_T + 3.427K_T^2 - 1.8201K_T^3 \quad (4.14)$$

The monthly average clearness index K_T can be calculated by,

$$K_T = \frac{H_T}{H_0} \quad (4.15)$$

Since Limmu Genet has a sunset hour angle above 86.9 degrees for all months through the years, equation (4.14) is valid and used to calculate monthly daily average beam radiation.

The monthly average diffuse radiation H_d on a horizontal surface

Table 4.6: Monthly average diffuse radiation (H_d) on a horizontal surface

Years	Jan	Feb	Mar	Apr	May	Jun	Jul	Aug	Sep	Oct	Nov	Dev
Average(2017-2021)	1.76	2.00	2.20	2.23	2.27	2.36	2.31	2.42	2.23	2.02	1.90	1.72

4.2.2 Monthly Average Global Radiation (H_T) on Horizontal Surface

Table 4.7: Month average everyday global radiation ($kwh/m^2/da$) on horizontal surface

Years	Jan	Feb	Mar	Apr	May	Jun	Jul	Aug	Sep	Oct	Nov	Dev
Average (2017-2021)	5.81	5.85	5.58	5.82	5.79	5.49	3.80	4.43	4.45	5.69	5.62	5.68

4.2.3 Monthly Average Beam Radiation (H_b) on Horizontal Surface

The formula to compute the direct (beam) component of solar radiation on the horizontal surface is as follows.

$$H_{total} = H_{diffuse} + H_{beam} \quad (4.16)$$

To accurately design solar radiation systems, it is crucial to determine the amount of radiation received on a horizontal surface.

Table 4.8: Monthly Average Beam Radiation ($kwh/m^2/day$) on Horizontal Surface

Years	Jan	Feb	Mar	Apr	May	Jun	Jul	Aug	Sep	Oct	Nov	Dev
Average (2017-2021)	4.05	3.85	3.38	3.59	3.52	3.13	1.49	2.01	2.22	3.67	3.72	3.96

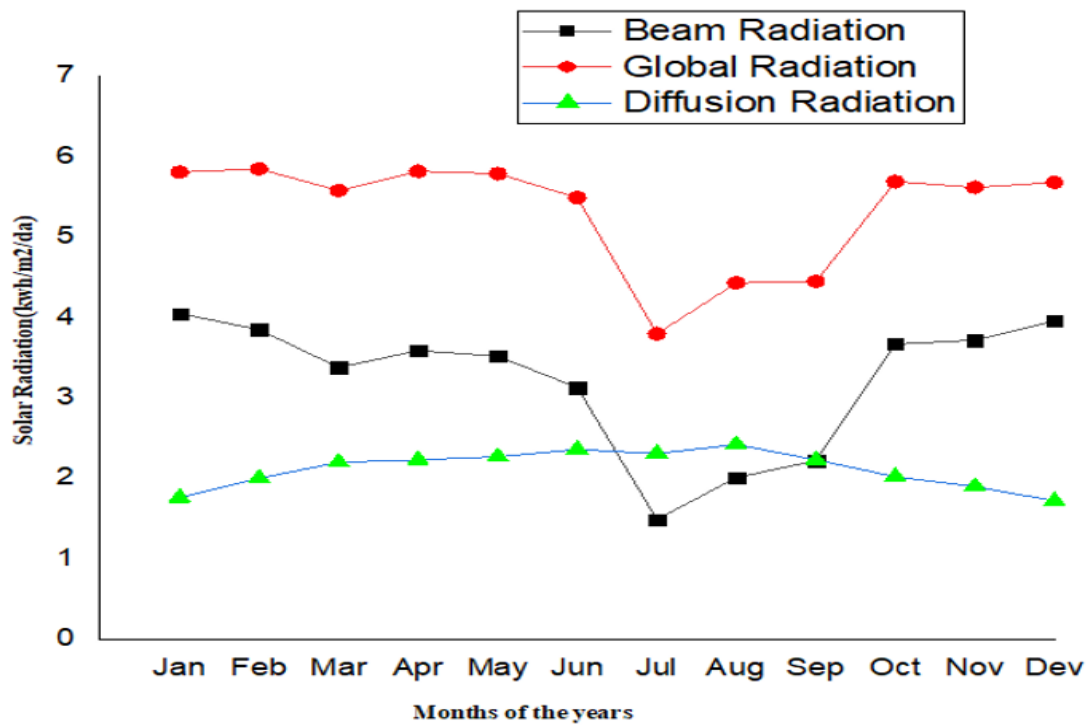


Figure 4.6: Solar radiation of Limmu Genet on the horizontal surface

radiation that will be received on a tilted surface and obtained by comparing the radiation on a horizontal surface to that on a tilted surface using a specific formula. However, obtaining data on total radiation on a horizontal surface is more readily available compared to the beam and diffuse radiation on the collector's plane. Therefore, it is necessary to estimate or calculate these values based on monthly averages of global solar radiation, diffusion radiation, and beam radiation (Deceased and Beckman, n.d.).

4.3 Monthly Average Hourly Global Radiation on a Horizontal Surface

Monthly average hourly global radiation I in ($w.h/m^2$) on horizontal surface can be obtained from monthly average daily global radiation on the horizontal surface H ($\frac{kJ}{m^2}$ per day) from the following relationship (Deceased and Beckman, n.d.).

$$\frac{I}{H} = \frac{\pi}{24}(a + b\cos\omega) \frac{\cos\omega - \cos\omega_s}{\sin\omega_s - \frac{\pi}{180}\omega_s\cos\omega_s} \quad (4.17)$$

$$a = 0.410 + 0.50416\sin(\omega_{sl} - 60) \quad (4.18)$$

$$b = 0.709 - 0.50767\sin(\omega_{sl} - 60) \quad (4.19)$$

Table 4.9: Monthly average hourly global radiation on the horizontal surface I ($\frac{w.h}{m^2}$).

Months	Jan	Feb	Mar	Apr	May	Jun	Jul	Aug	Sep	Oct	Nov	Dec
Solar radiation	683	681	648	666	654	626	434	507	514	606	657	670

4.3.1 Average Monthly Hourly Diffusion Radiation on Horizontal Surface I_d ($\frac{w.h}{m^2}$)

Hourly average monthly diffusion obtained from equation (4.20) by formulas (Deceased and Beckman, n.d.).

$$\frac{I_d}{H_d} = \frac{\pi}{24} \left(\frac{\cos\omega - \cos\omega_s}{\sin\omega_s - \frac{\pi}{180}\omega_s\cos\omega_s} \right) \quad (4.20)$$

Where H_d diffusion radiation

Table 4.10: Diffusion radiation on horizontal the surface I_d ($\frac{w.h}{m^2}$).

Months	Jan	Feb	Mar	Apr	May	Jun	Jul	Aug	Sep	Oct	Nov	Dec	Ave
Solar radiation	203	228	248	248	250	257	254	270	250	229	218	199	238

4.3.2 Average Monthly Hourly Beam Radiation on Horizontal Surface I_b ($\frac{w.h}{m^2}$)

Then hourly beam radiation is determined by:

$$I = I_d + I_b \quad (4.21)$$

Table 4.11: Beam Radiation on Horizontal the Surface $I_b \left(\frac{w.h}{m^2} \right)$

Months	Jan	Feb	Mar	Apr	May	Jun	Jul	Aug	Sep	Oct	Nov	Dec	Ave
Solar radiation	480	453	400	418	404	369	180	237	264	377	439	471	374

4.3.3 Hourly Solar Energy Estimation on Inclined Surfaces

The amount of solar energy interrupted on collectors can be increased by installing at an angle to reduce reflection and cosine losses. The total solar radiation on a tilted surface consists of beam, diffuse, and solar radiation reflected from the ground and surroundings (Mahanta, 2020). Calculating total solar radiation on any arbitrary orientation surface involves considering these factors.

$$I_{Tl} = I_{bl}r_{bl} + I_{dl}r_{dl} + (I_{bl} + I_{dl})r_{rl} \quad (4.22)$$

Beam radiation tilt factor (r_b) is determined by:

$$I_{bh} = I_{bn}\cos\theta_z \quad (4.23)$$

The flux of radiation beams on an inclined surface is calculated by:

Where, $I_{bi} = I_{bn}\cos\theta_i$ and $r_b = \frac{I_{bn}\cos\theta_i}{I_{bn}\cos\theta_z} = \frac{0.85}{0.83} = 1.02$

But Angle of incidence (i) calculated by (Mahanta, 2020):

$$\cos\theta_i = (\cos\phi\beta + \sin\phi\sin\beta\cos\delta\cos\omega + \sin\delta(\sin\phi\cos\beta - \sin\beta\cos\phi)) \quad (4.24)$$

Table 4.12: Average angle of incidence

Month	Jan	Feb	Mar	Apr	May	Jun	Jul	Aug	Sep	Oct	Nov	Dec	Ave
$\cos\theta_i$	0.54	1.0	0.99	0.95	0.92	0.91	0.91	0.94	0.97	0.95	1.0	1.0	0.85

Zenith angle (θ_z) also determined (Deceased and Beckman, n.d.)

$$\theta_z = \cos\phi_l\cos\delta_l\cos\omega_l + \sin\phi_l\sin\delta_l \quad (4.25)$$

Where, ϕ_l , the latitude of the site.

Table 4.13: Average zenith angle

Month	Jan	Feb	Mar	Apr	May	Jun	Jul	Aug	Sep	Oct	Nov	Dec	Ave
$\cos \theta_z$	0.75	0.81	0.85	0.87	0.86	0.85	0.85	0.87	0.91	0.82	0.77	0.74	0.83

The angle hour (ω) is rotation earth around its polar axis within 15° or the sun's angular movement from the local meridian east or west and determined from the following equation.

$$\omega = (TS - 12) * 15^\circ \quad (4.26)$$

Where, TS is local solar time hour

Diffusion radiation tilt factor (r_d is the relation of diffusion energy falling on the inclined surface to the plane surface and determined by:

$$r_d = \frac{1 + \cos\beta}{2} = \frac{1 + \cos 18.1}{2} = 0.98 \quad (4.27)$$

Tilt factor for reflected component (r_r) it is a component of reflection from the ground and the ground object (Mahanta, 2020).

$$r_r = \rho \frac{1 - \cos\beta}{2} = 2 \frac{1 + \cos 18.1}{2} = 0.20 \quad (4.28)$$

Where: ρ is reflection of objects (0.2 for ground and concrete and 0.6 for snow-covered)

Generally average total global solar radiation incident on the inclined surface is 737.12 w/m^2 . by using the next equation.

$$I_T = I_b r_b + I_d r_d + (I_b + I_d) r_r \quad (4.29)$$

Table 4.14: Summary of average temperature five years analysis of the site

Years	2017	2018	2019	2020	2021	Total average
Average (2017-2021)	23	22	21.5	21.5	21	21.8

4.4 Evaluating the Effectiveness of Flat Plate Solar Collectors

These collectors are commonly used in domestic solar fluid heating and solar space heating application. The flat plate However, some new types of collectors that use vacuum insulation can attain greater temperatures up to 100C° Systems typically run and reach their greatest efficiency between the temperature ranges of 30 to 80C° . Since they have beam and diffusion radiation, tracking of the sun is not required and is simple to maintain.

Another advantage of this collector is mechanically simple than other collectors. The development of selective coatings has reduced the temperature of stagnant fluid in flat plate collectors has reached 200C° (Dupeyrat et al., 2011).

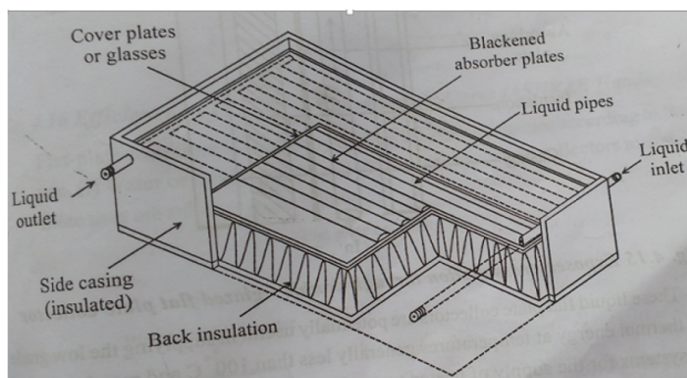
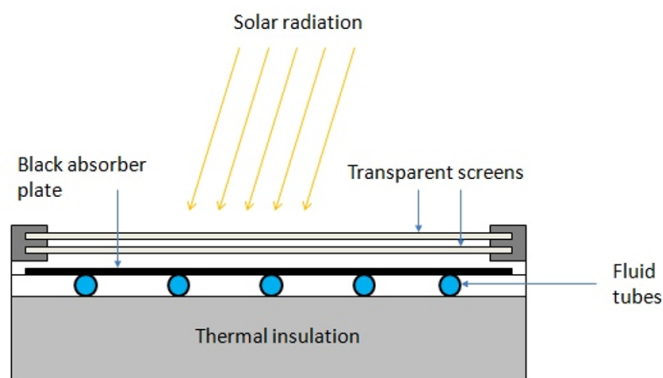


Figure 4.7: Typical liquid flat plate collector (Klevinskis and Buinskas, 2011)

To simplify the complexity of the modeling some parametrizes are taken by assumption at steady state.as the following (Deceased and Beckman, n.d.).

- One-dimensional flow inside back insulation.
- The temperature drop is neglected into cover.
- The sky is blackbody for long-wavelength radiation at corresponding sky temperature.
- The inlet liquid cold-water temperature is approximately equal to the nearby temperature analyzed from metrology agency of the location ($T_a = T_{site,location}$).
- Mean plate temperature (T_{mp}) is $115C^\circ$.
- Mass flow rate (\dot{m}) kg/s is ranging from $0.001 - 0.03$.
- Glass cover emissivity $\epsilon_g = 0.88$, Absorptivity $\epsilon_p = 0.95$.
- Insulations thermal conductivity w/mk 0.04 and thickness is $0.05m$ is respectively.
- The length, thickness, width of the collector respectively is $2m$, $0.03m$, and $1m$.
- Space between the tube and diameter of tube $100mm$ and $60mm$ respectively.

4.5 Mathematical Energy modeling on flat plate solar collectors

Amount of solar energy collected or received on surface of flat plate collector is calculated by:

$$Q_c = I_T \times A_c \quad (4.30)$$

Where I_T total solar radiation in (w/m^2) on the flat of a solar collector, A_c area of collector in m^2 and Q_c amount of solar energy collected by collector.

Considering the transmissivity and absorptivity of the solar collectors glasses the above equation is modified as the following

$$Q_c = I_T(\tau\alpha) \times A_c \quad (4.31)$$

Where α , τ are transmissivity and absorptivity for the collector respectively.

Heat lost to the environment (Q_L)

$$Q_L = U_L A_c (T_c - T_a) \quad (4.32)$$

Where (U_L) overall coefficient heat transfer, T_c , T_a collector and ambient temperature respectively.

Then useful energy collected by flat plate solar collector is difference between amounts of energy received and lost to the surrounding.

$$Q_u = Q_c - Q_L = A_c [I_T \alpha \tau - U_L (T_c - T_a)] \quad (4.33)$$

4.5.1 Theoretical Design of Collector

Efficiency of Collector is effectiveness of collector useful energy per collector area and determined by equation below.

$$\eta = \frac{Q_u}{I_T * A_c} \quad (4.34)$$

By rearranging the above equation to find the outlet temperature:

$$\eta = \frac{\dot{m} C_p (T_0 - T_i)}{I * A_c} \quad (4.35)$$

$$T_0 = \frac{\eta * I * A_c}{\dot{m} * C_p} + T_i \quad (4.36)$$

4.5.2 Determining the Overall Heat Loss Coefficient of Solar Collectors (U_L)

It is determined through several steps in the following section.

Total top loss Coefficient (U_T): It includes convection and radiation heat losses from collectors absorber plate.

1. Convective Heat Transfer Coefficient

a. Losses from absorber to glass cover ($h_{c,conv}$)

The equation determines the convective heat transfer coefficient between the absorber plate and the glass cover when they are inclined at an angle β to the horizontal surface.

$$h_{1conv} = \frac{N_U K}{L} \quad (4.37)$$

Where, N_U is Nusselt number; K , thermal conductivity between the glass cover and absorber plate and L is distance between the absorber and glass covers.

The Nusselt number and its relation to Rayleigh number for tilt angle range from 0 to 75° can be given by:

$$N_U = 1 + 1.440 \left[1 - \frac{1710(\sin 1.80\beta)^{1.6}}{R_a \cos \beta} \right]^* \left[1 - \frac{1710}{R_a \cos \beta} \right]^+ + \left[\left(\frac{R_a \cos \beta}{5830} \right)^{\frac{1}{3}} - 1 \right]^+ \quad (4.38)$$

$$R_a = \frac{g\beta\Delta TL^3}{\alpha\nu} = \frac{g\beta_v\Delta TL^3 pr}{\nu^2} \quad (4.39)$$

$$pr = \frac{\nu}{a} \quad (4.40)$$

$$\frac{1}{\beta\nu} = \frac{T_{mp} + T_c}{2} \quad (4.41)$$

NOTE, + indicate that positive is term in the square bracket is used and zero for negative values. g - is the gravitational constant; ΔT , temperature difference between the plate and glass cover; β_u - volumetric coefficient of expansion of air and L space between cover and plate (Thermal and Engineering, 2019).

Assuming the mean cover plate temperature is $T_c = 35^\circ$ and finding other air properties from the table at the mean temperature T_m between plate and cover at this point becomes,

$$T_m = \frac{T_{mp} + T_c}{2} = \frac{110 + 35}{2} = 72.5^\circ = 345.5K$$

$$\nu = 2.020 \times 10^{-5} m^2/s$$

$$K_a = 0.02899 w/mC^\circ$$

$$T_m = 345.5K$$

$$P_r = 0.7183 \text{ and } g = 9.81 m^2/s$$

Then the Rayleigh number is calculated as the following.

$$R_a = \frac{9.81(110 - 35)(0.025)^3 0.7183}{345.5(2.020 \times 10^{-5})^2} = 5.86 \times 10^4$$

By taking positive terms in the square bracket and zero for the negative terminal of equation (4.38).

$$N_U = 1 + 1.44 \left[1 - \frac{634.4}{55700.2} \right]^* [1 - 0]^+ + \left[\left(\frac{5.86 \times 10^4 \cos 18.1}{5830} \right)^{\frac{1}{3}} - 1 \right]^+ = 3.11 w/m^2k$$

$$N_U = 1 + 1.44(0.011) * [1 - 0]^+ + [2.1 - 0]^+ = 3.11 w/m^2k$$

Using equation (4.42) convective heat transfer coefficient by absorber to the glass cover is:

$$h_{c,ap-c} = \frac{NU \times K_a}{L} = 3.11 * \frac{0.02853}{0,025} = 3.55w/m^2k$$

b. Losses from glass cover to ambient air (h_w)

The heat transfer coefficient from the glass cover to the ambient air is determined based on the local wind velocity occurring on the outside of the glass cover (Kumar, S., and Mullick, S. C.2010).

$$h_{ws} = 5.70 + 3.801v_{speed} \quad (4.42)$$

Where, h_{ws} is in w/m^2k and v_{speed} speedis the wind speed over the glass cover of the solar collector in ms .

The wind velocity of the selected site is $2.08ms$.

Therefore, convective heat transfer coefficient is $h_{ws} = 5.7 + 3.8 \times 2.08m/s = 13.6w/m^2k$

c. Radiative heat transfer coefficient

i. By glass cover to ambient air (h_{1rad})

It is also influenced by the length of wavelength radiation that exchanges heat with the sky at sky temperature. This transfer coefficient from the glass cover to the sky can be calculated using the following relationship (Mahanta, 2020).

$$T_{sky} = T_a - 6 = 0.0552T^{1.5} = 0.0552(22)^{1.5} = 5.7C^\circ \quad (4.43)$$

Then radiative heat transfer coefficient becomes:

$$h_{rad,c-a} = \epsilon_g \sigma \left[\frac{(T_c + 273)^4 - (T_{sky} + 273)^4}{T_c - T_a} \right] = 0.88 \times 5.67 \times 10^{-8} \left[\frac{(35 + 273)^4 - (5.7 + 273)^4}{308 - 278.7} \right] \\ = 5.1w/m^2k$$

ii. By absorber plate to glass cover (h_{2rad})

Radiative heat transfer coefficient by absorber plate to the glass cover becomes:-

$$h_{r,ap-c} = \epsilon f \sigma \left[\frac{(T_{ap} + 273)^4 - (T_c + 273)^4}{T_{ap} - T_c} \right] = 0.88 \times 0.95 \times 5.67 \\ \times 10^{-8} \left[\frac{(110 + 273)^4 - (35 + 273)^4}{383 - 308} \right] = 7.91w/m^2k$$

$$U_t = \left[\frac{1}{h_{c,ap-c} + h_{rad,ap-c}} + \frac{1}{h_{ws} + h_{rad,c-a}} \right]^{-1} \quad (4.44)$$

$$U_t = \left[\frac{1}{3.11 + 7.91} + \frac{1}{13.6 + 5.1} \right]^{-1} = 6.9 \text{ w/m}^2 \text{ k}$$

Then the cover temperature is calculated from the;

$$T_c = T_{ap} - \frac{U_t(T_{sp} - T_a)}{h_{c,ap-c} + h_{r,ap-c}}$$

$$T_c = 110 - \frac{6.9(110 - 22)}{3.11 + 7.91} = 54.9 \text{ C}^\circ$$

Properties of air at mean temperature and new collector temperature $T_c = 55 \text{ C}^\circ$, at $T_m = 82.5 \text{ C}^\circ$ are:

$$T_m = \frac{110 + 54.9}{2} + 82.5 \text{ C}^\circ = 355.5 \text{ K}$$

$$v = 2.108 \times 10^{-5} \text{ m}^2/\text{s}$$

$$k_a = 0.02970 \text{ w/m}$$

$$T_m = 355.5 \text{ K}$$

$$Pr = 0.7148$$

$$Ra = \frac{g\Delta T L^3 pr}{T_m v^2} = \frac{9.81(110 - 55)(0.025)^3 0.7148}{355.5(2.108 \times 10^{-5})^2} = 38164.6$$

$$N_U = 1 + 1.44 \left[1 - \frac{1708(\sin 1.8 \times 18.1)^{1.6}}{38164.6 \cos 18.1} \right] * \left[1 - \frac{1708}{Ra \cos \beta} \right]^+ + \left[\left(\frac{38164.6 \cos 18.1}{5830} \right)^{\frac{1}{3}} - 1 \right]^+$$

$$N_U = 1 + 1.412 + 1.84 = 4.25 \text{ w/m}^2 \text{ k}$$

With this new Nusselt number, $N_U = 4.25$ new cover temperature and other heat transfer coefficient are calculated again.

$$h_{c,ap-c} = \frac{N_U k_a}{L} = 4.25 \times \frac{0.02970}{0.025} = 5.01 \text{ w/m}^2 \text{ k}$$

$$h_{rad,ap-c} = \epsilon_g \sigma \left[\frac{(T_c + 273)^4 - (T_{sky} + 273)^4}{T_c - T_a} \right]$$

$$h_{rad,ap-c} = 0.88 \times 5.67 \times 10^{-8} \left[\frac{(55 + 273)^4 - (5.7 + 273)^4}{328 - 295} \right] = 8.40 \text{ w/m}^2 \text{ k}$$

$$h_{rad,ap-c} = eff \sigma \left[\frac{(T_{ap} + 273)^4 - (T_c + 273)^4}{T_{ap} - T_c} \right]$$

$$h_{rad,ap-c} = 0.88 \times 0.95 \times 5.67 \times 10^{-8} \left[\frac{(110 + 273)^4 - (55 + 273)^4}{383 - 328} \right] = 18.540 \text{ w/m}^2 \text{ k}$$

$$U_t = \left[\frac{1}{h_{c,ap-c} + h_{rad,ap-c}} + \frac{1}{h_{ws} + h_{rad,c-a}} \right]^{-1}$$

$$U_t = \left[\frac{1}{5.01 + 18.54} + \frac{1}{13.6 + 8.40} \right]^{-1} = 11.40 \text{ w/m}^2 \text{ k}$$

Again the cover temperature is calculated from the;

$$T_c = T_{ap} - \frac{U_t(T_{ap} - T_a)}{h_{c,ap-c} + h_{r,ap-c}}$$

$$T_c = 110 - \frac{11.40(110 - 22)}{5.01 + 18.54} = 67.4 \text{ C}^\circ$$

Properties of air at mean temperature and new collector temperature $T_c = 67 \text{ C}^\circ$ at $T_m = 88.7 \text{ C}^\circ$ are

$$T_m = \frac{110 + 67.4}{2} = 88.7 \text{ C}^\circ = 361.7$$

$$v = 2.185 \times 10^{-5} \text{ m}^2/\text{s}$$

$$k_a = 0.03013 \text{ w/mC}^\circ$$

$$T_m = 361.5 \text{ K}$$

$$Pr = 0.7138$$

$$Ra = \frac{g \Delta T L^3 pr}{T_m v^2} = \frac{9.81(110 - 67)(0.025)^3 0.7138}{361.5(2.185 \times 10^{-5})^2} = 27167.6$$

$$N_U = 1 + 1.44 \left[1 - \frac{1708(\sin 1.8 \times 18.1)^{1.6}}{27167.6 \cos 18.1} \right] * \left[1 - \frac{1708}{Ra \cos \beta} \right]^+ + \left[\left(\frac{27167.6 \cos 18.1}{5830} \right) - 1 \right]^+$$

$$N_U = 1 + 1.44(0.98) * (1)^+ + (1.64)^+ = 4.1$$

$$h_{c,ap-c} = \frac{N_U K_a}{L} = 4.10 \times \frac{0.03013}{0.025} = 4.9 \text{ w/m}^2 \text{ k}$$

$$h_{rad,c-a} = \varepsilon_g \sigma \left[\frac{(T_c + 273)^4 - (T_{sky} + 273)^4}{T_c - T_a} \right]$$

$$h_{rad,c-a} = 0.88 \times 5.67 \times 10^{-8} \left[\frac{(67 + 273)^4 - (5.7 + 273)^4}{340 - 295} \right] = 5.46 \text{ w/m}^2 \text{ k}$$

$$h_{rad,ap-c} = eff \sigma \left[\frac{(T_{ap} + 273)^4 - (T_c + 273)^4}{T_{ap} - T_c} \right]$$

$$h_{rad,ap-c} = 0.88 \times 0.95 \times 5.67 \times 10^{-8} \left[\frac{(110 + 273)^4 - (67 + 273)^4}{383 - 340} \right] = 8.99 \text{ w/m}^2 \text{ k}$$

$$U_t = \left[\frac{1}{h_{c,ap-c} + h_{r,ap-c}} + \frac{1}{h_w + h_{r,c-a}} \right]^{-1}$$

Again the cover temperature is calculated from the;

$$T_c = T_{ap} - \frac{U_t(T_{ap} - T_a)}{h_{c,ap-c} + h_{r,ap-c}}$$

$$T_c = 110 - \frac{8.1(110 - 22)}{4.90 + 8.99} = 58.8^\circ \text{C}$$

Properties of air at mean temperature and new collector temperature $T_c = 58.8^\circ \text{C}$ at $T_m = 84.4^\circ \text{C}$ are:

$$T_m = \frac{110 + 58.8}{2} = 84.4^\circ \text{C} = 357.4$$

$$v = 2.143 \times 10^{-5} \text{ m}^2/\text{s}$$

$$k_a = 0.02984 \text{ w/mC}^\circ$$

$$T_m = 357.4 \text{ K}$$

$$Pr = 0.7144$$

$$Ra = \frac{g \Delta T L^3 pr}{T_m v^2} = \frac{9.81(110 - 58.8)(0.025)^3 0.7144}{357.4(2.143 \times 10^{-5})^2} = 34207.31$$

$$N_U = 1 + 1.44 \left[1 - \frac{1708(\sin 1.8 \times 18.1)^{1.6}}{34207.31 \cos 18.1} \right] * \left[1 - \frac{1708}{Ra \cos \beta} \right]^+ + \left[\left(\frac{34207.31 \cos 18.1}{5830} \right) - 1 \right]^+$$

$$N_U = 1 + 1.44(0.98) * [1]^+ + [1.772]^+ = 4.20$$

$$h_{c,ap-c} = \frac{N_U k_a}{L} = 4.2 \times \frac{0.02984}{0.025} = 5.01 \text{ w/m}^2 \text{ k}$$

$$h_{rad,c-a} = \varepsilon_g \sigma \left[\frac{(T_c + 273)^4 - (T_{ask} + 273)^4}{T_{cp} - T_a} \right]$$

$$h_{rad,c-a} = 0.88 \times 5.67 \times 10^{-8} \left[\frac{(58.8 + 273)^4 - (5.7 + 273)^4}{331.8 - 295} \right] = 8.25 \text{ w/m}^2 \text{ k}$$

$$h_{rad,ap-c} = eff \sigma \left[\frac{(T_{ap} + 273)^4 - (T_c + 273)^4}{T_{ap} - T_c} \right]$$

$$h_{rad,ap-c} = 0.88 \times 0.95 \times 5.67 \times 10^{-8} \left[\frac{(110 + 273)^4 - (58.8 + 273)^4}{383 - 331.8} \right] = 8.70 \text{ w/m}^2 \text{ k}$$

$$U_t = \left[\frac{1}{h_{c,ap-c} + h_{rad,ap-c}} + \frac{1}{h_{ws} + h_{rad,c-a}} \right]^{-1}$$

$$U_t = \left[\frac{1}{5.01 + 8.7} + \frac{1}{13.6 + 8.25} \right]^{-1} = 8.40 \text{ w/m}^2 \text{ k}$$

Again the cover temperature is calculated from the;

$$T_c = T_{ap} - \frac{U_t(T_{ap} - T_a)}{h_{c,ap-c} + h_{r,ap-c}}$$

$$T_c = 110 - \frac{8.40(110 - 22)}{5.02 + 8.7} = 56.1 \text{ C}^\circ$$

Properties of air at mean temperature and new collector temperature $T_c = 56.1 \text{ C}^\circ$ at $T_m = 83.1 \text{ C}^\circ$ are:

$$T_m = \frac{110 + 56.1}{2} = 83.1 \text{ C}^\circ = 356.1$$

$$v = 2.129 \times 10^{-5} \text{ m}^2/\text{s}$$

$$k_a = 0.02975 \text{ w/mC}^\circ$$

$$T_m = 356.1 \text{ K}$$

$$Pr = 0.7147$$

$$Ra = \frac{g \Delta T L^3 pr}{T_m v^2} = \frac{9.81(110 - 56.1)(0.025)^3 0.7147}{356.1(2.129 \times 10^{-5})^2} = 35975.6$$

$$N_U = 1 + 1.44 \left[1 - \frac{1708(\sin 1.8 \times 18.1)^{1.6}}{35975.6 \cos 18.1} \right] * \left[1 - \frac{1708}{Ra \cos \beta} \right]^+ + \left[\left(\frac{35975.6 \cos 18.1}{5830} \right)^{\frac{1}{3}} - 1 \right]^+$$

$$N_U = 1 + 1.44(0.98) * [1]^+ + [1.8]^+ = 4.20$$

$$h_{c,ap-c} = \frac{N_U k_a}{L} = 4.2 \times \frac{0.02975}{0.025} = 5.00 w/m^2 k$$

$$h_{rad,c-a} = \epsilon_g \sigma \left[\frac{(T_c + 273)^4 - (T_{ask} + 273)^4}{T_c - T_a} \right]$$

$$h_{rad,c-a} = 0.88 \times 5.67 \times 10^{-8} \left[\frac{(56.1 + 273)^4 - (5.7 + 273)^4}{329.1 - 295} \right] = 8.30 w/m^2 k$$

$$h_{rad,ap-c} = eff \sigma \left[\frac{(T_{ap} + 273)^4 - (T_c + 273)^4}{T_{ap} - T_c} \right]$$

$$h_{rad,ap-c} = 0.88 \times 0.95 \times 5.67 \times 10^{-8} \left[\frac{(110 + 273)^4 - (56.1 + 273)^4}{383 - 329.1} \right] = 8.60 w/m^2 k$$

$$U_t = \left[\frac{1}{h_{c,ap-c} + h_{rad,ap-c}} + \frac{1}{h_{ws} + h_{rad,c-a}} \right]^{-1}$$

$$U_t = \left[\frac{1}{5.0 + 8.6} + \frac{1}{13.6 + 8.30} \right]^{-1} = 8.40 w/m^2 k$$

Again the cover temperature is calculated from the;

$$T_c = T_{ap} - \frac{U_t (T_{ap} - T_a)}{h_{c,ap-c} + h_{r,ap-c}}$$

$$T_c = 110 - \frac{8.40(110 - 22)}{5.0 + 8.6} = 56.0C^\circ$$

Lower (bottom) Loss Coefficient (U_b): ombination of conduction and convection loss coefficient through bottom of absorber is:

$$U_b = \frac{k_i}{t_i} = \frac{0.04}{0.05} = 0.8 w/m^2 k \quad (4.45)$$

K_{insula} thermal conductivity of insulations thickness and t_{insul} is back insulation thickness.

Side Loss Coefficient: Assuming that one dimensional and steady-state flow of heat side loss coefficient is determined by the following equation and it is always less than top loss coefficient.

$$U_e = \frac{k_i}{t_e} \left(\frac{A_1}{A_c} \right) = U_b \left(\frac{A_e}{A_c} \right) \quad (4.46)$$

Where, $A_e = P * t_c$, $P = 2(L * W)$ absorbers perimeter plate and t_c thicknesses of collector thickness.

Therefore A_e becomes

$$A_e = 2(L \times W) \times t_c = 2(2 \times 1) \times 0.03 = 0.12m^2$$

$$U_e = U_b \left(\frac{A_e}{A_c} \right) = 0.8 \times \frac{0.12}{2} = 0.048w/m^2k$$

Total losses of collector are generally the summation of top, bottom, and side becomes:-

$$U_L = U_t + U_b + U_e = 8.40 + 0.800 + 0.048 = 9.25w/m^2C^\circ$$

Then total energy lost by absorber plate per unit area is:-

$$\dot{q}_l = U_L(T_c - T_a) = 9.25w/m^2C^\circ(56 - 22)C^\circ = 314.5w/m^2$$

The useful energy gain is obtained from the following equation.

$$q_u = q_i - q_l$$

$$Q_u = Q_i - Q_L = I_L \alpha_t . A - U_L A (T_c - T_a)$$

$$\frac{Q_u}{A} = q_i - q_l = 737.12w/m^2 - 314.5w/m^2 = 422.6w/m^2$$

$$Q_u = A_c(q_i - q_l) = 2m^2 \times 422.6w/m^2 = 845.5w$$

4.6 Theoretical Collector Efficiency Factors

The multiplier for collector efficiency is the constant parameter for any fluid flow rate and collector design. Research has shown that increasing the distance between the tube center-to-center distances decreases the collector efficiency factor. Conversely, expanding both material thickness and thermal conductivity increases the collector efficiency factor (Supply et al., 2016).

Fin Efficiency Factor: In Figure (4.8), the distance between the tubes is represented as W , the diameter as D , and the sheet thickness as δ . Since sheet metal is a good conductor, the temperature gradient across the sheet is considered negligible. The region between the center line separating the tubes and the tube base is assumed to follow a classical function F , which determines the standard fin efficiency for a straight fin with a rectangular profile, as expressed below, it is determined by the equation taken from (Deceased and Beckman, n.d.) (Thermal and Engineering, 2019).

$$F = \frac{t_{anhm} \left[\frac{m(W-D)}{2} \right]}{m \left(\frac{W-D}{2} \right)} \quad (4.47)$$

$$m = \sqrt{\frac{U_L}{K\delta}} \quad (4.48)$$

$$m = \sqrt{\frac{9.25}{0.4}} = 4.8$$

$$F = \frac{t_{anhm} \left[\frac{4.8(0.1-0.06)}{2} \right]}{4.8 \left(\frac{0.1-0.06}{2} \right)}$$

$$F = \frac{t_{anh}(0.096)}{0.096} = 0.997$$

The copper plate thickness determines the product of the plate thermal conductivity and the plate thickness 0.1mm , $K\delta = 0.4\text{w}/\text{C}^\circ$ and for steel plate 0.1mm thick, $K\delta = 0.005\text{w}/\text{C}^\circ$

Typically, it falls within the range of $K\delta = 0.005$ to $0.4\text{w}/\text{C}^\circ$, with W , W representing the spacing between the tube and D representing the diameter of the tube (Deceased and Beckman, n.d.).

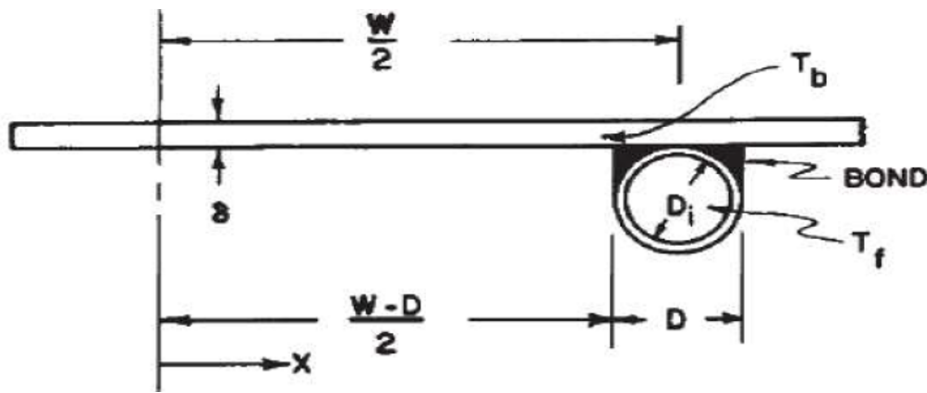


Figure 4.8: Sheet and tubes (Thermal and Engineering, 2019)

The collector efficiency factor (F''): represents the ratio of the actual useful energy gain to the useful gain if the collector absorbing surface had been at the local fluid temperature. It can be calculated using the following equation (Deceased and Beckman, n.d.).

$$F'' = \frac{1/U_L}{w \left[\frac{1}{U_L[D+(W-D)F]} + \frac{1}{bc} + \frac{1}{\pi D_i h_{fi}} \right]} \quad (4.49)$$

$$F'' = \frac{1/9.25}{0.1 \left[\frac{1}{9.25 + (0.1 - 0.06)0.997} + 0 + \frac{1}{\pi * 0.06 * 1500} \right]} = 0.99$$

Where, the bond conductance $\frac{1}{cb}$ is assumed to be very large, so $\frac{1}{cb} = 0$. The heat transfer coefficient inside the tube ranges from 100 to 1500 w/m^2C° , depending on the flow conditions (from laminar to highly turbulent flow). The tube diameter selected is 0.06m (Deceased and Beckman, n.d.)

The collector heat removal factor is a measure of the actual energy gain of the collector compared to the energy gain that would occur if the entire collector surface was at the same temperature as the fluid inlet. It is calculated using the equation provided.

$$FR = \frac{\dot{m}C_p}{A_c U_L} \left[1 - \exp \left(\frac{-A_c U_L F'}{\dot{m}C_c} \right) \right] \quad (4.50)$$

$$FR = \frac{\dot{m}C_p}{A_c U_L} \left[1 - \exp \left(\frac{-A_c U_L F'}{\dot{m}C_c} \right) \right] = 0.87$$

The maximum energy gain in a solar collector occurs when the fluid inlet temperature reaches across the collector. (T_{FI}). The actual increase in usable energy (Q_u) is multiplied by the collector heat removal factor to determine (F_R). The maximum possible energy gain (Mahanta, 2020). In other words, the collector heat removal factor quantifies the collector's efficiency in capturing and utilizing solar energy using an equation taken from Mahanta, 2020 for 4.51 to 4.54.

$$Q_u = A_p F_{FR} [I_T \tau \alpha - U_L (T_{FI} - T_a)] \quad (4.51)$$

At the stagnation temperature (T_s), which means the temperature at which the absorber achieves no HTF. At this point both the collector's useful heat output and efficiency are zero.

$$Q_u = A_p F_R [I_T \tau \alpha - U_L (T_{FI} - T_a)] = 0 \quad (4.52)$$

The following expression then determines the stagnation collector temperature.

$$T_s = T_{FI} = T_a + I_T \frac{F_R (\tau \alpha)}{F_R U_L}$$

$$T_s = T_{FI} = T_i + I_T \frac{F_R (\tau \alpha)}{F_R U_L}, T_a = T_i$$

$$T_s = T_{FI} = 22 + 737.12 \frac{0.87(0.88 \times 0.95)}{0.87 \times 9.25} = 88.6 \approx 89C^\circ$$

The useful energy output of the collector can be expressed by considering the mass flow rate (m) and specific heat capacity c_p of the fluid flowing through the collector.

$$Q_u = \dot{m}C_p(T_{f_0} - T_{f_i}) \quad (4.53)$$

The final outlet fluid temperature can be obtained by rearranging (4.53).

$$T_{f_0} = T_{f_i} + \frac{Q_u}{\dot{m}C_p}$$

$$T_{f_0} = 89 + \frac{845.5}{0.016 \times 4200} = 101.6 \approx 102C^\circ$$

The thermal efficiency The thermal efficiency of the collector can be determined by using the equation that takes into account the mass flow rate and specific heat capacity of the fluid flowing through the collector.

$$\eta^{th} = \frac{Q_U}{A_{IT}} \quad (4.54)$$

$$\eta^{th} = \frac{Q_U}{A_{IT}} = \frac{0.016 \times 4200(102 - 89)}{2 \times 737.12} = \frac{873.6}{1474.24} = 0.593 \approx 0.60 \text{ or } 60\%$$

Chapter 5

CFD Simulation Analysis of Hot Water Storage Tank

The investigation of fluid flow was analyzed using the CFD numerical simulation method to model the physical fluid dynamics problem and solve fluid and thermal behavior inside the storage tank concerning the system's velocity, temperature, and fluid characteristics. CFD is the most powerful tool used to analyze every simulation within every range of initial values, and it transforms fluid flowing into algebraic equations. CFD investigation analysis has three different phases, as analyzed as follows.

- Pre-processing
- Solving
- Post Processing

Generally the following chart summarize step used in each level during CFD simulation analysis.

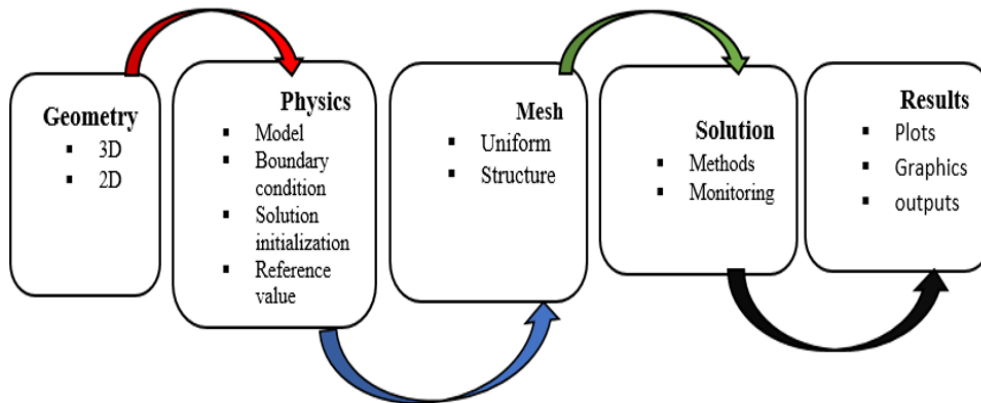


Figure 5.1: Steps of analysis CFD

5.1 Pre-Processing

Preprocessing is transforming a statement of the problem into the idealized and discretized computer model. It was started by identifying flow types as laminar, turbulent, steady, and unsteady. Initial and Boundary conditions, mesh generation, and geometry preparation for meshing were also performed in this phase. The three primary steps to be analyzed were:

- Geometry
- Mesh
- Physics (boundary and initial condition)

5.1.1 Geometry

Before conducting the simulation, CFD geometry must be modelled to import into the fluent flow for starting the simulation process. This work modelled three types of 3D geometry of cylindrical hot water tanks using solid work software. It imported them into the fluent flow to create and identify solid and fluid domains independently. These storage tanks were modelled with the same dimension but with different inlet structures such as normal pipe, perforated pipe, and without pipe. Steady pipe holes were created at the exact location to study the impact of the inlet structure on hot water storage for comparison analyses.

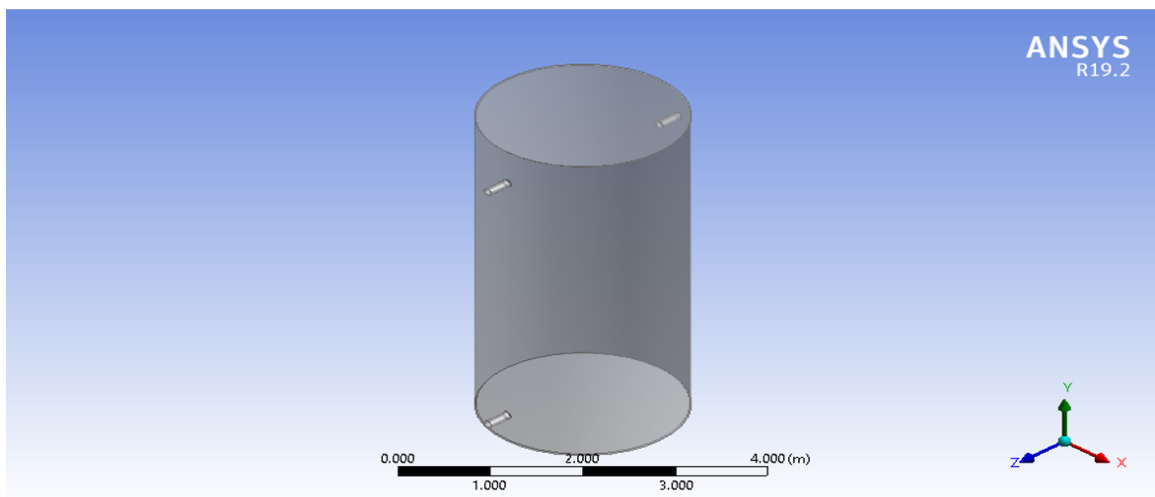


Figure 5.2: CFD geometry model of hot water storage tank designed with a normal pipe inserted.

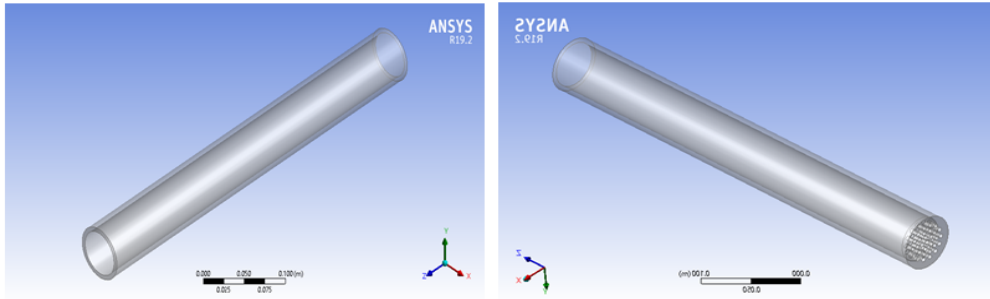


Figure 5.3: a) Normal pipe used in model 1 b) Perforated pipe used in model 2.

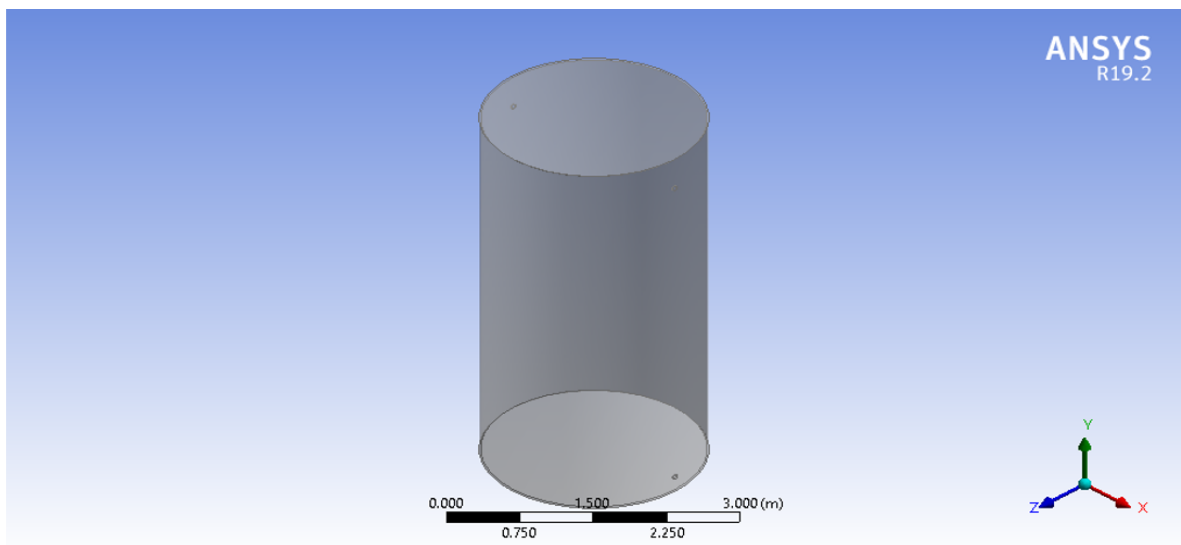


Figure 5.4: CFD geometric model of hot water storage tank constructed without inserting inlet pipe.

5.1.2 Generation of Mesh

Meshing divides the geometry into many elements the CFD solver uses to provide control volumes for fluid flow equations such as the Navier-Stokes equation. Quality of meshing has a significant influence on the accuracy and convergence rate of the solution. In this work, the tetrahedron patch-conforming method is used for three models. The best mesh element size was obtained at 74.75mm , which was obtained after the progress analysis of mesh until nearly the same result was achieved. The same meshing methods were used for model 1, model 2, and model 3. Mesh generation and visualization for different mesh sizes are shown in Figure (5.5).

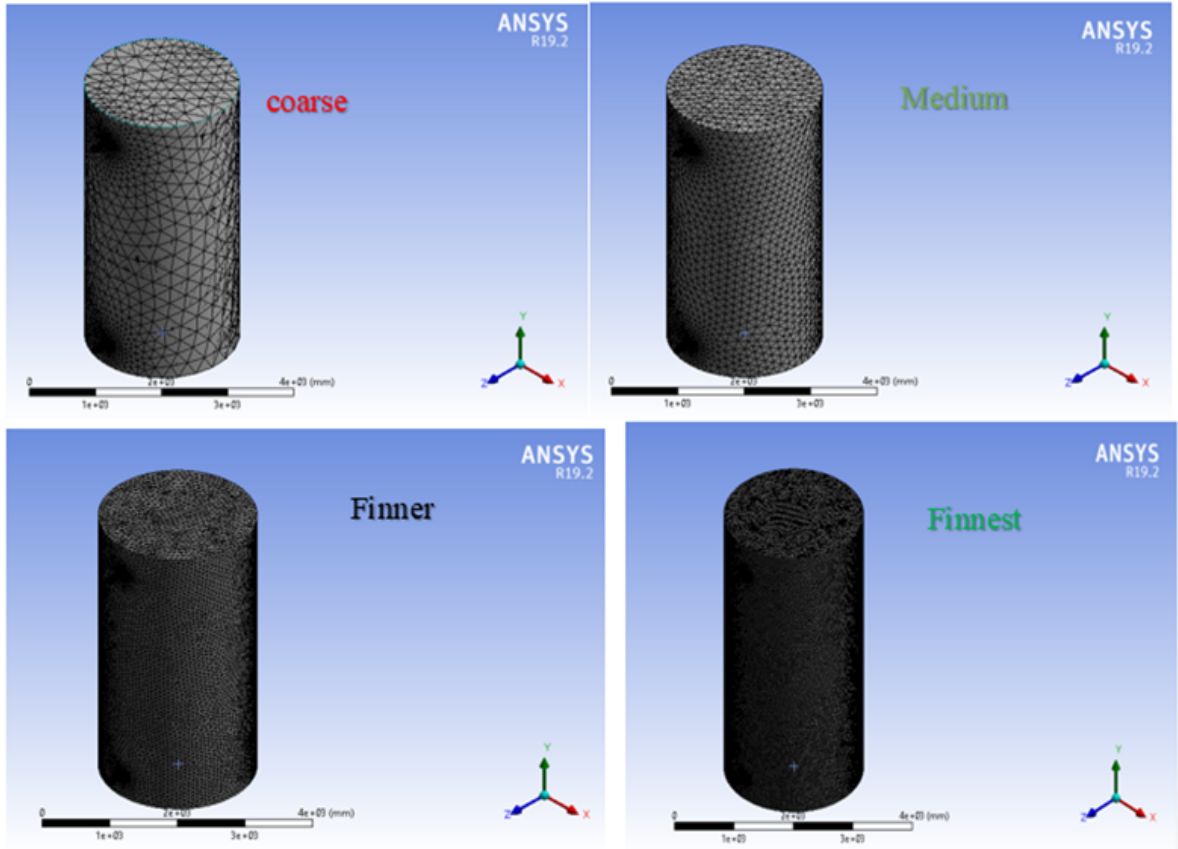


Figure 5.5: Mesh generation and visualization of different mesh sizes.

5.1.3 Mesh Independent Test

Mesh independent test is the method of analyzing variation of result with numbers of element size and node numbers. As mesh element size decreases, the accuracy and convergence of the solution increase. This study analyzed the mesh-independent test with output temperature in the table below.

Table 5.1: Nodes number and elements versus different mesh sizes

Types of mesh	No of nodes	No of elements	Average Output Temperature
Coarse	19267	79953	334.96
Medium	23292	96654	334.81
Fine	37517	158877	333.67
Finer	60197	260504	334.90
Finest	132738	598345	334.99

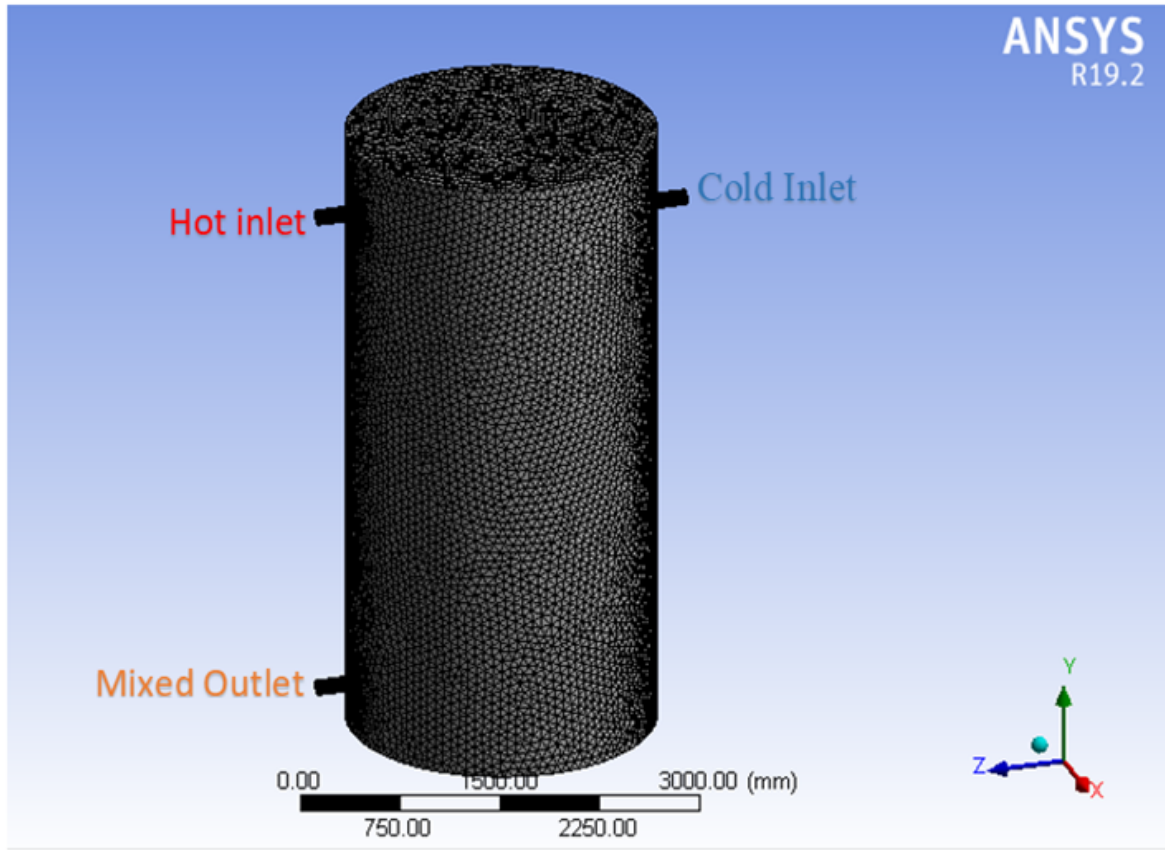


Figure 5.6: The selected Finner mesh element size's view

In figure (5.6) the average output temperature was plotted along the Y-axis, and unit length was plotted along the X-axis. The coarse mesh was not accepted for numerical simulation since the change in average output temperature was high. In the case of medium mesh, less average output temperature is indicated.

However, this mesh is also not accepted because of its low accuracy. In the fine mesh, a high average output temperature was also shown, and this mesh was also not taken for the final simulation. The average output temperature difference is minimal between Finner and the finest mesh. The average output temperature for this mesh was about 0.09. So, the finner mesh with total elements and nodes 260504 and 60197 was selected for numerical simulation to save computational time.

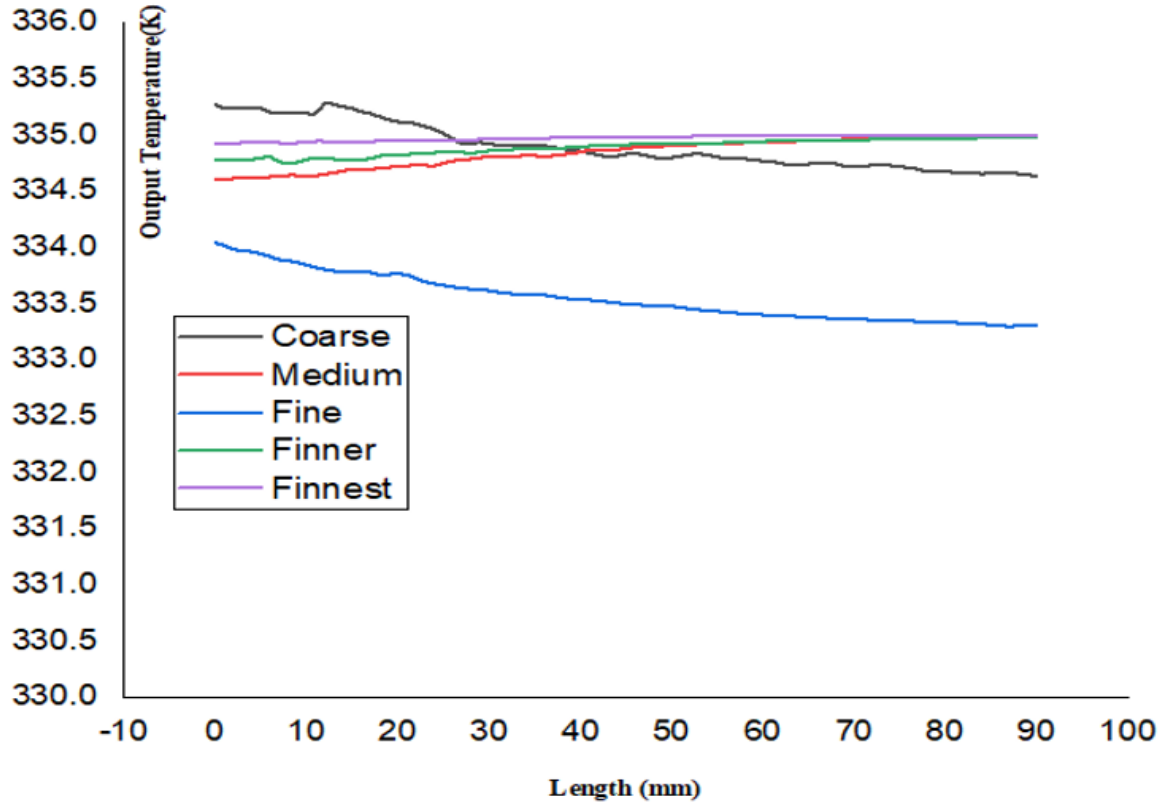


Figure 5.7: Variation of outlet temperature with mesh size elements.

5.2 Boundary and Initial Condition

Based on adiabatic walls assumption, that means no heat flux from the surface. Fluid velocity is zero ($u = 0$), at the wall boundary, with inlet mass flow to the storage tank 1.31 kgs . The initial Cold water and hot inlet temperature were initially charged with $T_i = 295\text{ k}$ and $T_0 = 375\text{ k}$ respectively. The gravitational acceleration due to gravity is equal to 9.81 m/s . Since the physical properties of water changing with a temperature change, the following correlation is used (Bouzaher et al., 2019).

In this work, the calculation was performed based on a temperature range ($293 - 375^\circ\text{ k}$). According to the following information, the physical properties of water are determined from the following equation.

$$\rho = 756.35 + 1.9057T - 0.00365T^2 \quad (5.1)$$

Water specific heat capacity (C_p) in $J/\text{kg.k}$

$$C_{pw} = 5182.1 - 6.4901T - 0.0105T^2 \quad (5.2)$$

Dynamic viscosity μ in (Pas)

$$\mu = 10^{-1} - 8.63 \times 10^{-4}T + 2.21 \times 10^{-6}T^2 - 2.451 \times 10^{-9}T^3 \quad (5.3)$$

Thermal conductivity (λ) in w/mk

$$\lambda_w = -0.581798 + 6.35704 \times 10^{-3}T - 7.96625 \times 10^{-6}T^2 \quad (5.4)$$

Coefficient of thermal expansion (k^{-1}) is determined from the following equation.

$$\beta(T) = -1.908 \times 10^{-3} + 7.319 \times 10^{-6}T \quad (5.5)$$

Where T is the temperature in Kelvin. Based on the above information cold water is characterized by:

- (ρ) is $1007.3 \text{ kg}/\text{m}^3$
- (C_p) $2353.7 \text{ J}/\text{kg}\cdot\text{k}$
- (μ) is $-0.00792(\text{kg}/\text{m}\cdot\text{s})$
- (β) is $0.601 \text{ w}/\text{mk}$

5.3 Governing Equation and Assumption

To simplify the complexity of the equation the following assumption is used.

- Incompressible working fluid
- Neglected viscous and fluid dissipation rate
- 3D turbulence fluid flow motion
- Losses and transport of energy in pipes materials were neglected
- The inner cylinder was perfectly wall and any holes are neglected

Based on the above assumptions, fluid inside hot water storage is governed by computational fluid dynamics (CFD) of Ansys fluent. These equations are given as the following

$$\text{Continuity equation } \frac{\partial p}{\partial t} + \sum_{i=1}^3 \frac{\partial}{\partial x_i} (\rho u_i) = 0$$

$$\text{Momentum equation } \frac{\partial(\rho u_i)}{\partial t} + \sum_{j=1}^3 \frac{\partial}{\partial x_j} (\rho u_j u_i) = -\frac{\partial p}{\partial x_i} + \sum_{j=1}^3 \frac{\partial \tau_{ij}}{\partial x_j} + \rho f_i$$

$$\text{Energy equation } \rho C_p \frac{dT}{dt} = \text{div}(\lambda \overline{\text{grad}T}) + T\beta \frac{dT}{dt} + q + \phi$$

$$\text{Where, } \phi = -\frac{2}{3}\mu(\text{div}\bar{u})^2 + 2\mu S_{ij} \frac{\partial u_i}{\partial x_j}$$

5.4 Selection Turbulence Flow Model

In this study, perforated and regular flow pipes are used to optimize the turbulence flow of water inlets. The length and diameter for both pipes are 500mm and 45mm, respectively. Many authors stated that Reynolds numbers greater than 4000 cause turbulence flow inside the storage tank (Bouzaher et al., 2019). In this work, Reynold's number for inlet velocity is 0.00844m/s was found to be 4,731.43. So, that flow was characterized by the turbulence flow regime. So, thermal stratification of water storage tanks is needed to reduce this turbulence flow characteristics. The standard $k - \epsilon$ model is selected, which is not possible by the laminar model recommended by several authors (Bouzaher et al., 2019).

5.5 Setup

The solution process is generally started by setting an energy model for steady and pressure based on the effect of gravitational force. The realizable $k - \epsilon$ with standard wall functions was selected.

5.6 Defining Material Properties

In the hot storage tank analysis, new materials were assigned to solid and fluid properties. The concrete properties consisted of mild steel and fiberglass as insulation materials. The fluid properties were fluid (liquid water), and its thermo-physical properties of liquid water were calculated in section 5.3, as summarized in the table below.

Table 5.2: Three properties of liquid water and materials (mild steel and fiberglass)

Materials	$(\rho_w)kg/m^3$	$C_{pw}(J/kg.k)$	$(\lambda_w)w/mk$	$\mu(kg/m.s)$
Liquid water	1007.3	2353.7	0.601	0.00792
Mild steel	7832	434	63.9	–
Fiber glass (insulation)	64	39	0.032	–

5.7 Operating and Boundary Conditions

The CFD analysis was started with initial and boundary conditions by creating liquid water with different temperatures as hot and cold inlets. Cold water temperature $T_i = 295K$ and hot water temperature $T_o = 375K$ set as the initial condition. The initial condition of mild steel in this model was the wall heat flux condition in the table below.

Table 5.3: Thermo-physical properties of working fluid (liquid water) and solid materials (mild steel and fiber glass).

	Boundary condition	Liquid water		Adiabatic
		cold	hot	
wall	Temperature	295	375	--
wall	Stationary	No slip	No slip	No slip
wall	Heat Flux	$0\ w/m^2$	$0w/m^2$	$0w/m^2$
wall	Mild Steel	Mild steel		Mild steel

5.8 Solution Methods

In this procedure, the governing equation of continuity, momentum, and energy simulation was solved by the pressure-velocity coupling method in steady-state conditions under a simple algorithm (semi-implicit method equation) using ANSYS FLUENT Software. PISO scheme was selected with a list of green-gauss cell-based, second order is used for both momentum, energy, and pressure equation.

5.9 Solution Initialization

Hybrid initialization was selected for selected variables in the flow field of whole area. This will result in the volume fraction, X , Y , and Z velocity, and pressure being patched in the domain. The number of iterations was set for all models to 20000 and convergence was achieved below this but at a different number. The convergence criteria were taken at the default condition of residual for 10^{-6} for energy and 10^{-3} for all other residuals such as continuity, epsilon, and k and x , y , and z velocities. The solution was converged as residual energy reaches 10^{-7} and continuity 10^{-4} while others reach above 10^{-5} for all models.

Chapter 6

Result and Discussion

6.1 Hot Water Storage Tank CFD Analysis

CFD simulations of model 1, model 2, and model 3 hot water storage tanks were analyzed and compared. SOLIDWORKS2020 model 1 and model 2 were constructed with two different inlet pipes, and model 3 was built without an inlet pipe but with holes by the uses of SOLIDWORKS2020 to study the effect of the inlet on the thermal performance of storage tanks. CFD result of temperature, pressure, and velocity distribution in the storage tank (hot water) indicated in the fluid (liquid water) flow direction on the plane.

6.2 Temperature Distribution or Contours Profiles

The fluid (liquid water) from the two inlets with different temperatures mix at the top of the hot water storage tank, and heat transfer occurs between hot and cold water. Since incomplete thermal mixing of the fluid temperature variation occurs at the mixing region. Figure (6.1) shows the temperature distribution inside hot water storage tanks equipped with three different inlet structures. Model 1 was fitted with the normal inlet pipe, model 2 with perforated pipe, while model 3 was constructed without any inlet pipe, but holes were used as inlets and outlets instead of pipe. The temperature contours of these models were indicated in the cross-sectional views of the planes at different planes along with the outlet. In these sampling planes, the temperature ranges from 295 to 375K. In the case of model 1, as shown in Figure (6.1) , the temperature difference is maximum when hot and cold water meet at the top of the hot storage tank. Model 1 increases within the growing distance from the inlets and mixing intensity decreases with increasing distance. Maximum mixing layers occurred in this model 1. They propagate along the outlet because incoming fluid (liquid water) is directly met with each other (hot and cold) since open holes at both ends direct the entrance of the incoming fluid. The case of model 2 (Figure (6.2)) was constructed with a perforated pipe to obstruct the entry of incoming fluid (both hot and cold) liquid water into the storage tank.

It indicates that uniform temperature distribution formed in this case compared to both model 1 and model 3, and it is recommendable to use this model. In the circumstance of model 3, which was constructed without a pipe as shown, maximum mixing occurred at the top since incoming fluid (hot and cold) directly entered the storage through the holes.

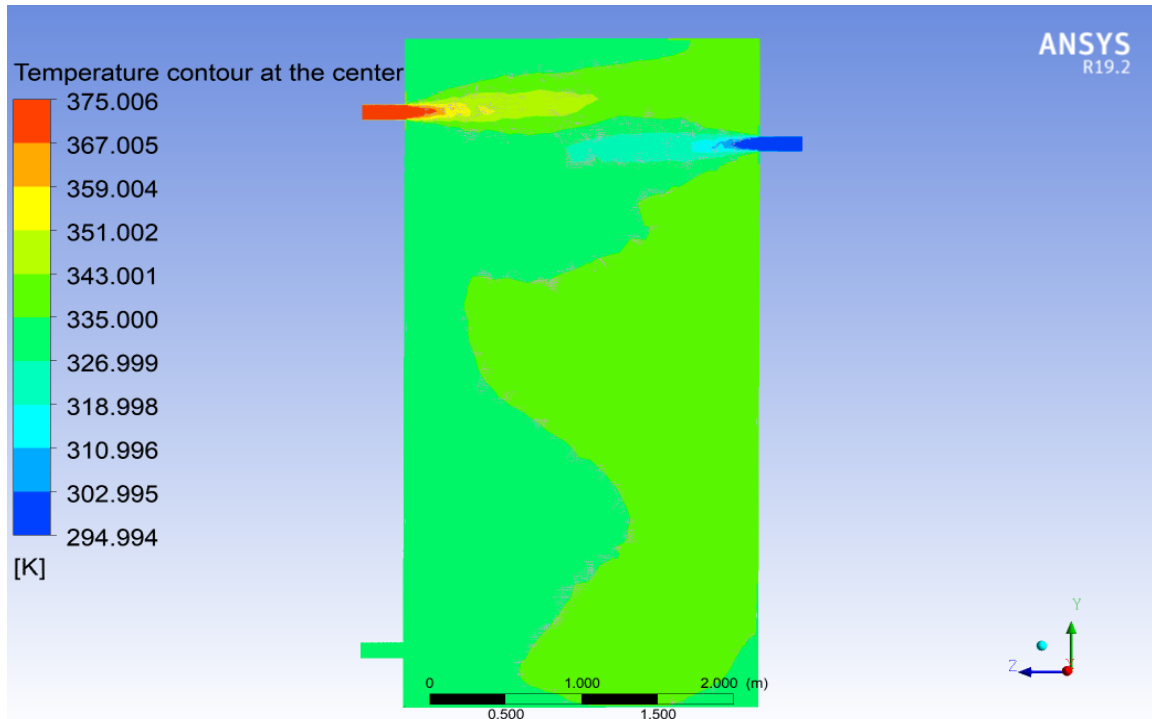


Figure 6.1: Model 1, Normal pipe inserted

From the above Figure (6.1), different temperature distribution profiles were observed on the symmetry plane model 1 constructed with normal inlet pipe. Hot water with a temperature of $375K$ and minimum temperature (cold water) given at both inlets are $295K$, respectively. Inside the storage tank, different temperature distributions have occurred. At the upper part of this model, high turbulence flow of hot and cold liquid water created different temperature layers (around four layers of blue, green, yellow, and mixed). In this model 1, the structure of inlets allows high turbulence throughout the system. The contact between cold and hot water was created because the design of the inlet allows direct penetration of the fluid into the storage tank, which leads to turbulent fluid flow.

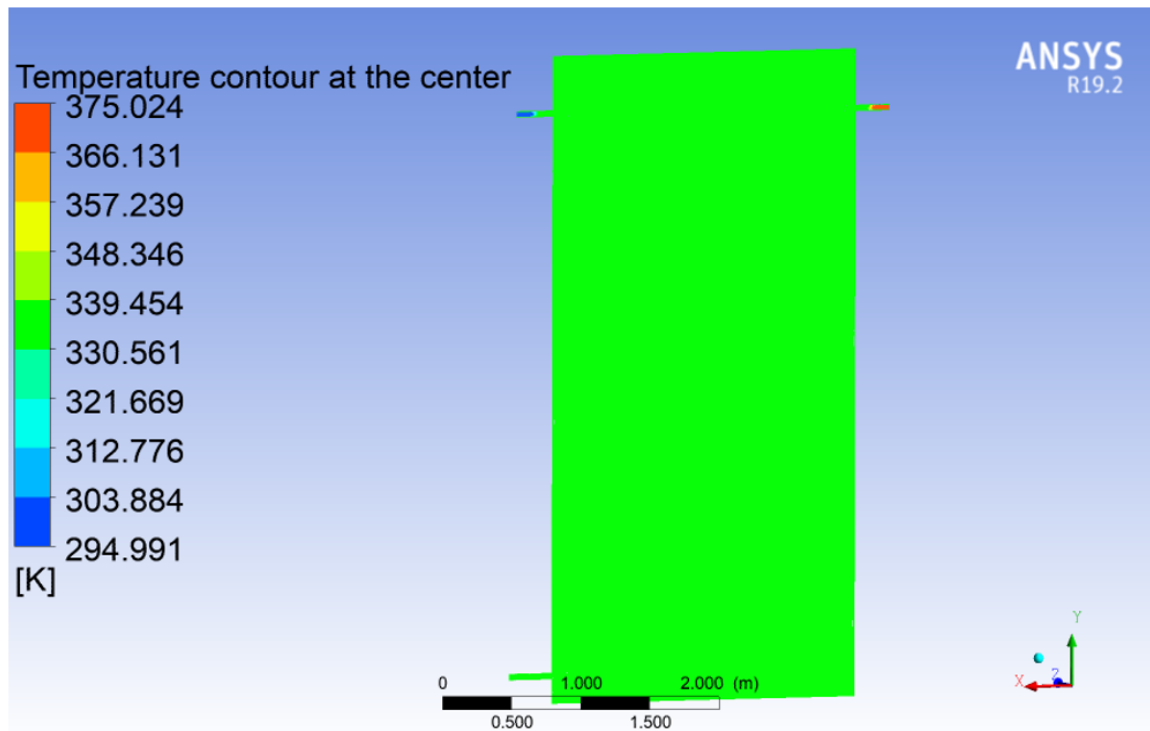


Figure 6.2: Model 2, Perforated Pipe inserted

From the above Figure (6.2), at the same inputs as Figure (6.2), uniform temperature distribution profiles were observed on the symmetry plane of model 2, constructed by perforated inlet pipe. The maximum temperature of $375K$ and minimum temperature of $295K$ at both inlets are $295K$, respectively. Inside the storage tank, uniform temperature distribution formed throughout the system due to the inlet structure of the storage tank. This idea shows that the inlet structure of the hot water storage tank can affect temperature distribution inside the storage tank. Thermal stratification aims to collect constant output temperature at the outlet side by reducing the turbulence flow of the fluid. This study obtains constant output temperature because a perforated inlet pipe is used to overcome turbulence fluid flow inside the storage tank. Unlike model 1 and model 3, uniform temperature was obtained throughout the system. Fully thermally stratified storing energy is obtained by balancing incoming fluid of cold and hot inlet design, reducing pumping power. Constant output temperature was obtained in this model 2, meaning the system depends on an absolute minimum of mixing cold and hot water in the storage tank. The total volume of the storage tank was filled with constant ranging from 330.6 to $339.5K$., which corresponded to the required output demand used for the hospital.

Figure (6.3), similar to figure (6.1), with the same inputs, also different temperature distribution profiles were observed on the symmetry plane of model 3 constructed by a hole as an inlet instead of an inlet pipe. The maximum (hot water) of $375K$ and minimum temperature (cold water) given at both inlets are $295K$, respectively. Different temperature distributions occurred inside the storage tank, like with model 1. At the upper part of this model 3, the high turbulence flow of the water inlet created different temperature layers (around four layers of blue, green, yellow, and mixed) temperature distribution profiles. The poor structure of the inlet also created high turbulence flow at the storage tank, which caused fewer outputs than the other models.

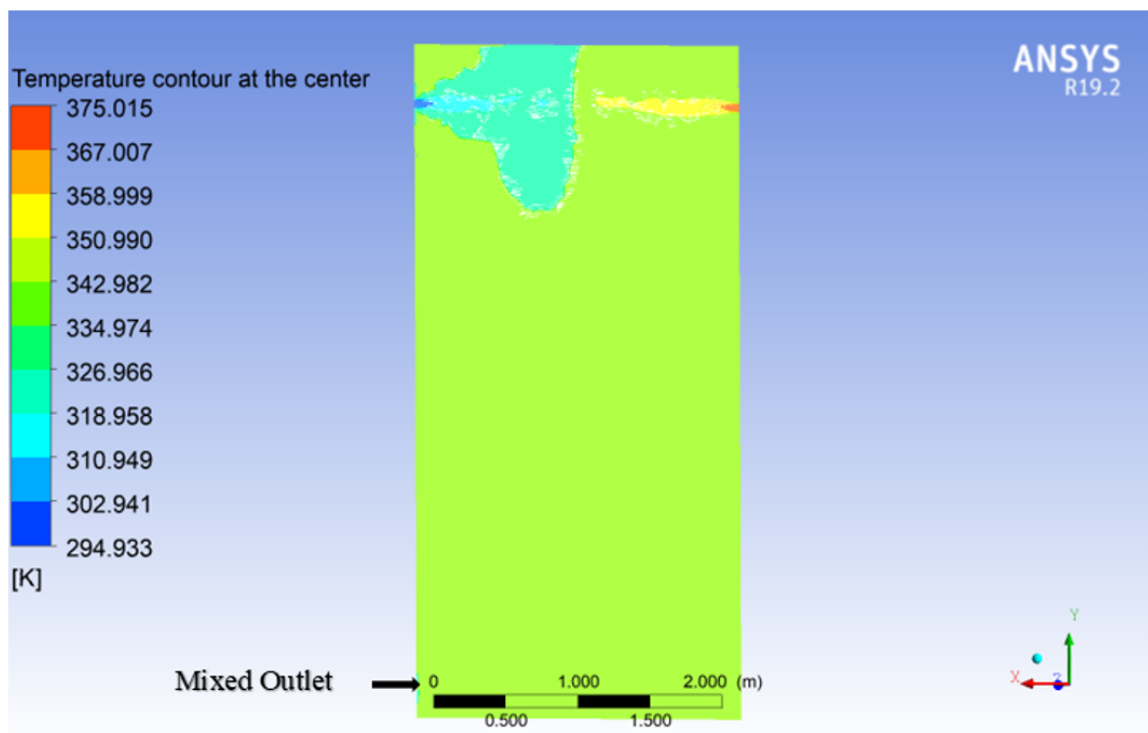


Figure 6.3: Model 3, with holes instead of inlet pipe

6.3 Pressure Contours or Distribution Profiles

The pressure contour (distribution) of Model 1 is shown in Figure (6.4). It was found that pressure distribution was higher at the inlets with lower velocity.

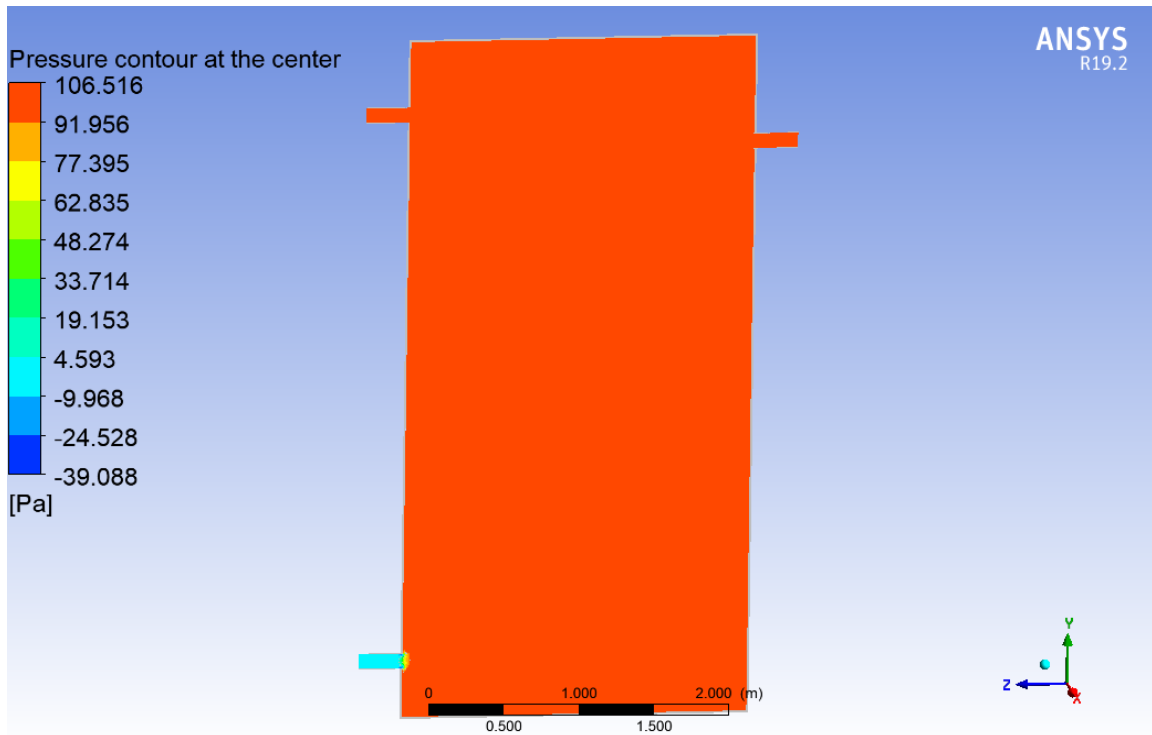


Figure 6.4: Model 1, Pressure contours hot water storage tank constructed normal pipe inserted.

From figure (6.4) the highest pressure occurs at the inlets with lower velocity. At the mixing, the outlet pressure is much lower as mixing fluids are passed out from the mixing region. The most downward pressure was obtained at the outlet, the bottommost section of storage. This area was characterized by distributed flow (turbulent). The maximum pressure found at the inlets was $106.516 Pa$, and the lowest pressure found at the outlet was $9.968 Pa$.

From Figure (6.5), compared to model 1, model 2 was characterized by the highest pressure throughout the system. The pressure decreases from inlets to outlet. The maximum pressure found at the inlets was found to be $4493770.0 Pa$, which was characterized by red colors. This information is caused by the relation between pressure and velocity concept, i.e., pressure and velocity are inversely proportional to each other to keep the algebraic sum of potential energy kinetic energy. This pressure drop resulted from the perforated inlet pipe's design (perforation area). An increase in flow rate causes an increased flow rate through the perforated site. The total pressure drops increased due to the more significant acceleration pressure drop at a higher flow rate through the perforations. The added source term is used to balance this pressure drop in the modelling

energy equation.

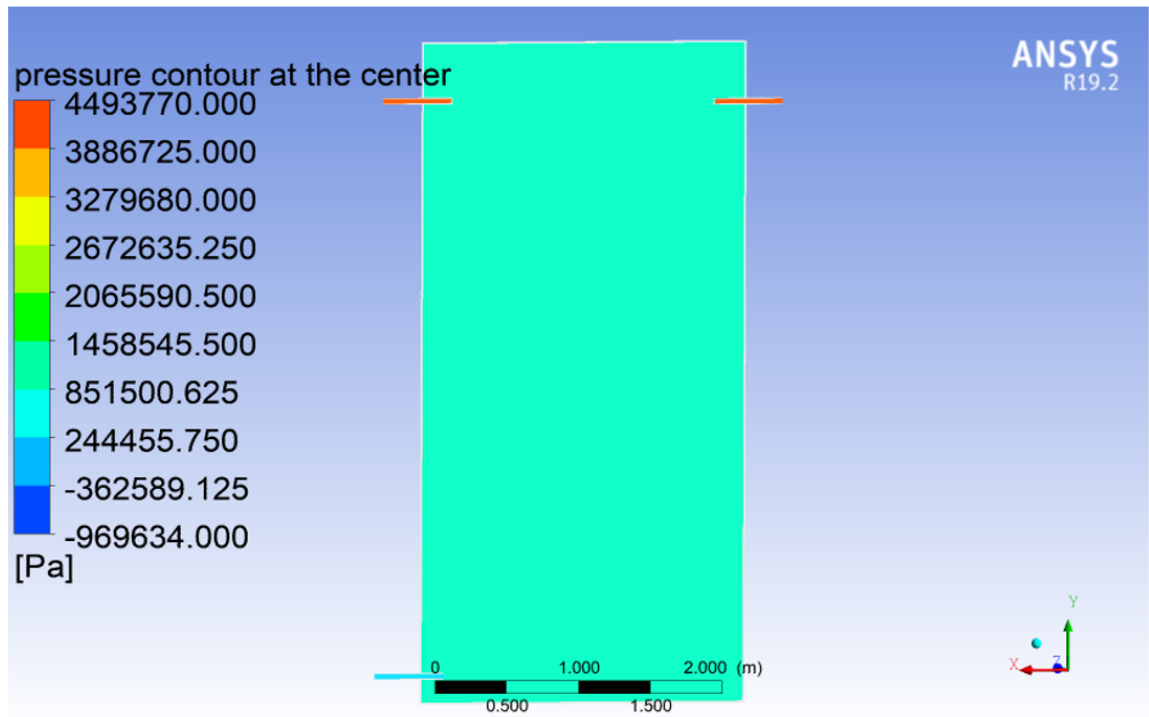


Figure 6.5: Model 2, Pressure contours hot water storage tank constructed perforated pipe inserted.

Figure (6.6) indicates higher pressure distribution compared to Model 1. However, the pressure distribution or contour found in Model 3 was lower compared to Model 2. This indication of destruction of thermal stratification. The maximum pressure was found at both inlets which are characterized by red colors ($1975.83Pa$), while the lowest pressure was $61.483Pa$.

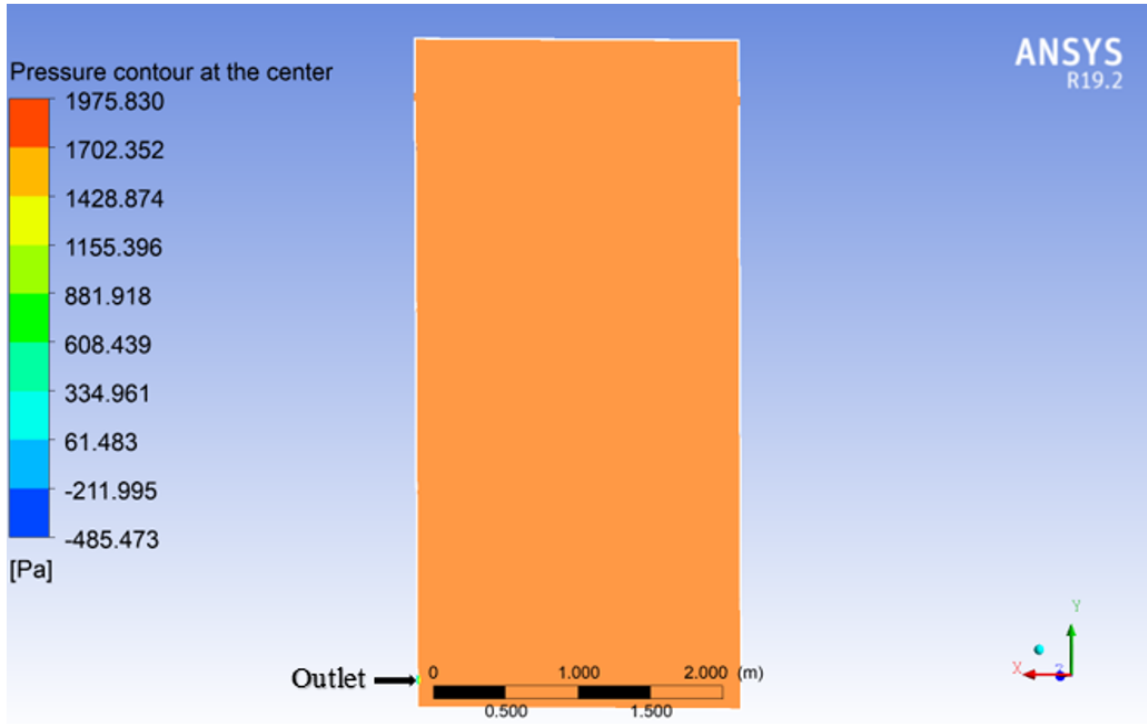


Figure 6.6: Model 3, Pressure contours hot water storage tank holes instead of inlet pipe.

6.4 Streamlines or Velocity Distribution Profiles

Figure (6.7) shows the maximum streamlines or velocity distribution in model 1. Maximum velocity was found at the mixing region as the fluids jets of two inlets struck each other. Around the cylinder wall, streamlines (velocity distribution) were much lower because of the kinetic friction and the adhesive force between the liquid water (fluid) and the structure. This velocity distribution was taken from the CFD post at the maximum number of points of 500 to know the streamlined pattern.

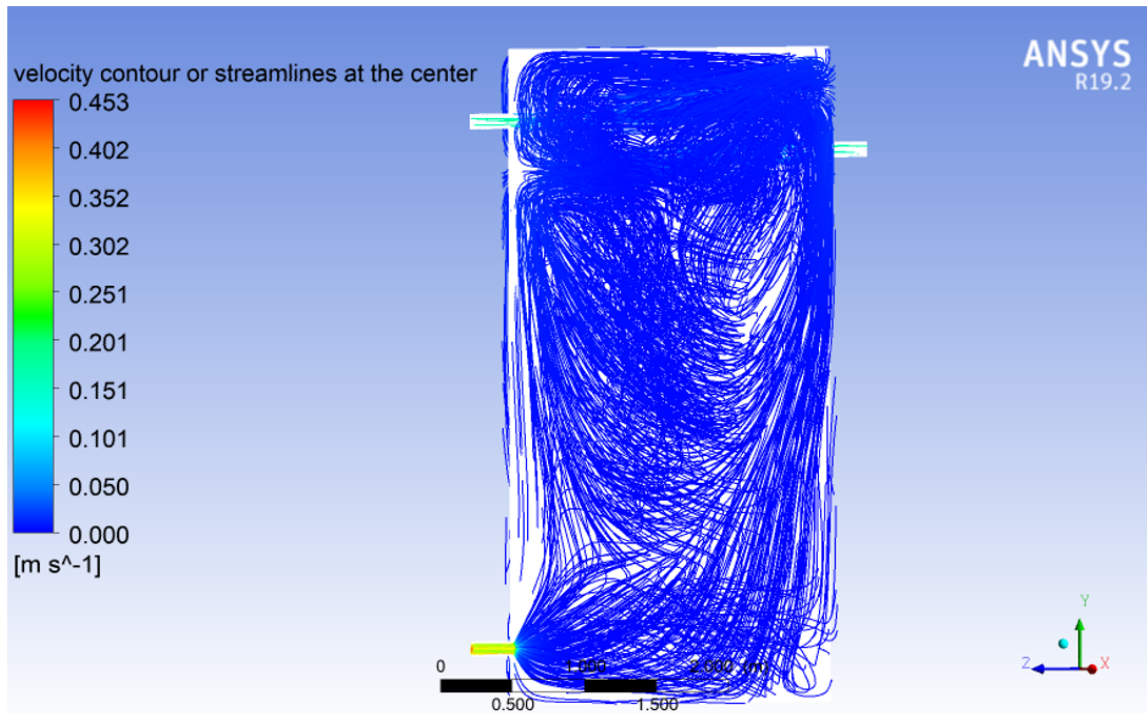


Figure 6.7: Model 1, Streamlines of hot water storage tank with normal inlet pipe.

Figure (6.8)a), shows the velocity distribution of model 2, still maximum velocity distribution was found when two jets of fluid coming from two inlets combined with each others. However, very low velocity distribution was found in this model because of the structure of the inlets at the ends of the exit to the storage tank. This model was characterized by smooth velocity distribution in the storage tank which was used to enhance thermal stratification of this model 2. Larger velocity distribution was characterized by the larger turbulent flow that leads to the destruction of thermal stratification.

As shown in figure (6.8)b) even if maximum number of points of streamlines doubled ($2 * 500$) with that of models 1 and 3 still velocity distribution in model 2 was very smooth. The velocity distribution was decreased from inlets along the mixing to the outlets. This condition was used to collect constant output at the outlet.

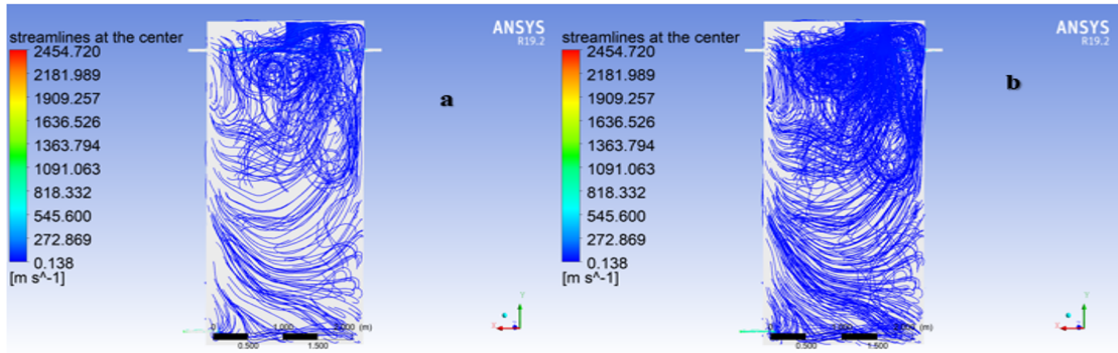


Figure 6.8: Model 2, Streamlines of Hot Water Storage Tank with Perforated Inlet Pipe. This figure shows the doubled velocity distribution of model 2, however still less velocity distribution pattern was found as compared with model 1 and model 3. This indicates that perforated pipes are used as inlets for both cold and hot fluid adjusting the flow patterns of system in this model 2.

Figure (6.9), displays velocity distribution of model 3, maximum velocity is also found when two inlet jets of cold and hot fluid (water) strikes each other. As the mixing continues, the streamlined pattern decreases because of kinetic friction and the adhesive force between the liquid water (fluid) and the structure. The velocity distribution at the outlet pattern becomes larger as seen from the figure below.

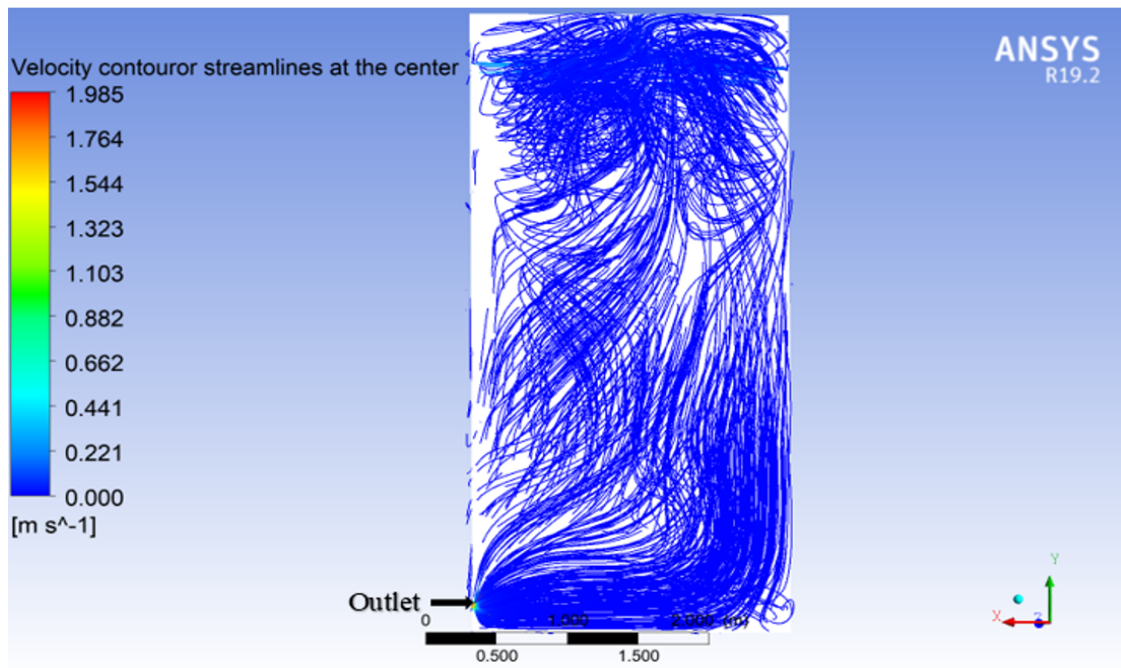


Figure 6.9: Velocity distribution of model 3 HWST holes instead of inlet pipe

6.5 Variation of Outputs with Mass Flow Rates

Variations of outlet temperature by mass flow rates of selected element size for each model were analyzed independently. As the mass flow rate increased, outlet temperature also increased for all models. However, the maximum value was achieved in model 2, while the least was in model 3.

Table 6.1: Mass flow rate vs outlet with normal pipe (model 1)

Mass flow rate (kg/s)	Output mixed water temperature
$\dot{m}_1 = 0.655$	329.9994
$\dot{m}_2 = 1.31$	332.9706
$\dot{m}_3 = 1.9655$	337.4570

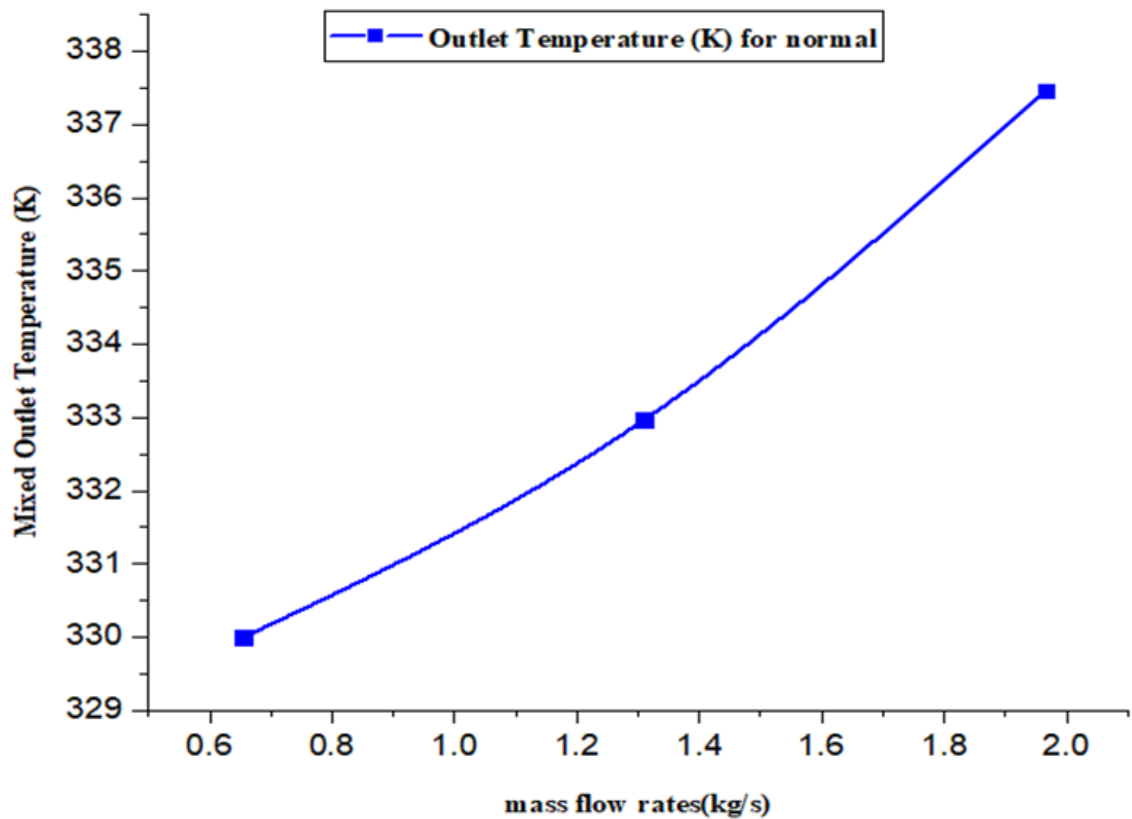


Figure 6.10: Mass flow rate Vs outlet temperature for model 1

Table 6.2: Mass flow rate vs outlet with perforated pipe inserted (model 2)

Mass flow rate (kg/s)	Output mixed water temperature
$\dot{m}_1 = 0.655$	331.6894
$\dot{m}_2 = 1.31$	335.1901
$\dot{m}_3 = 1.965$	339.9691

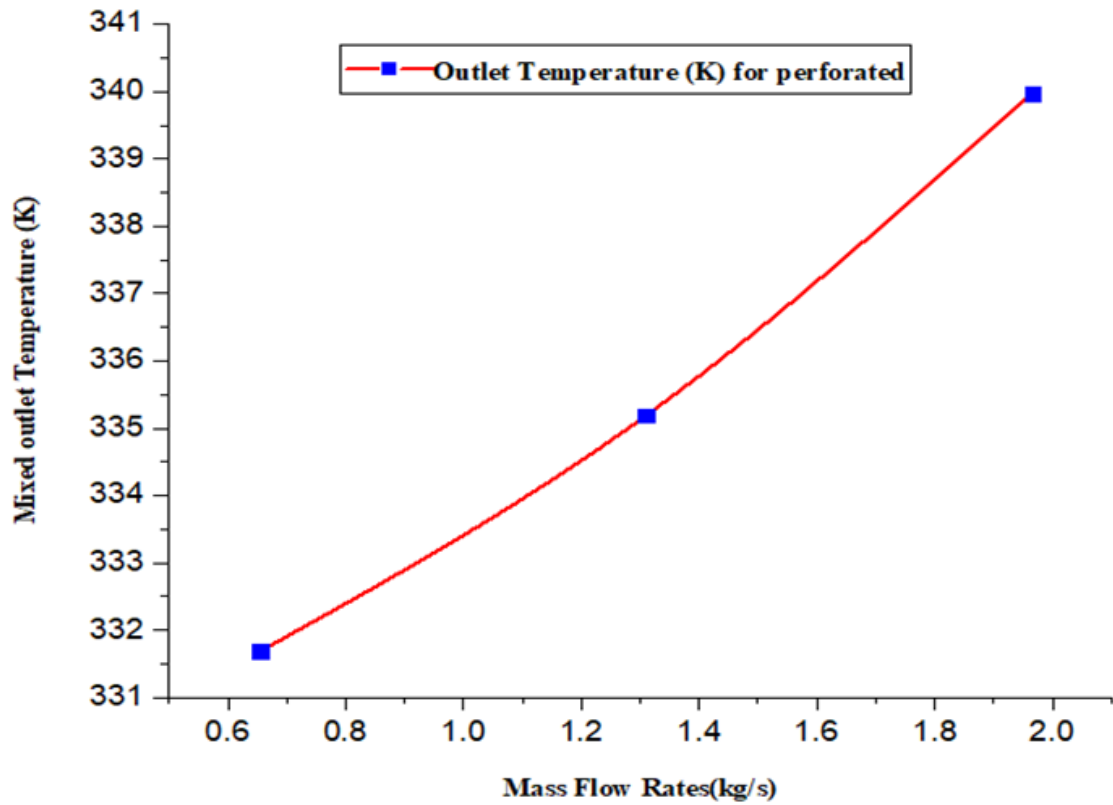


Figure 6.11: Mass flow rate Vs outlet temperature for model 2.

Table 6.3: Mass flow rate Vs outlet without insert pipe (model 3)

Mass flow rate (kg/s)	Output mixed water temperature
$\dot{m}_1 = 0.655$	327.2949
$\dot{m}_2 = 1.31$	330.5676
$\dot{m}_3 = 1.9655$	334.9689

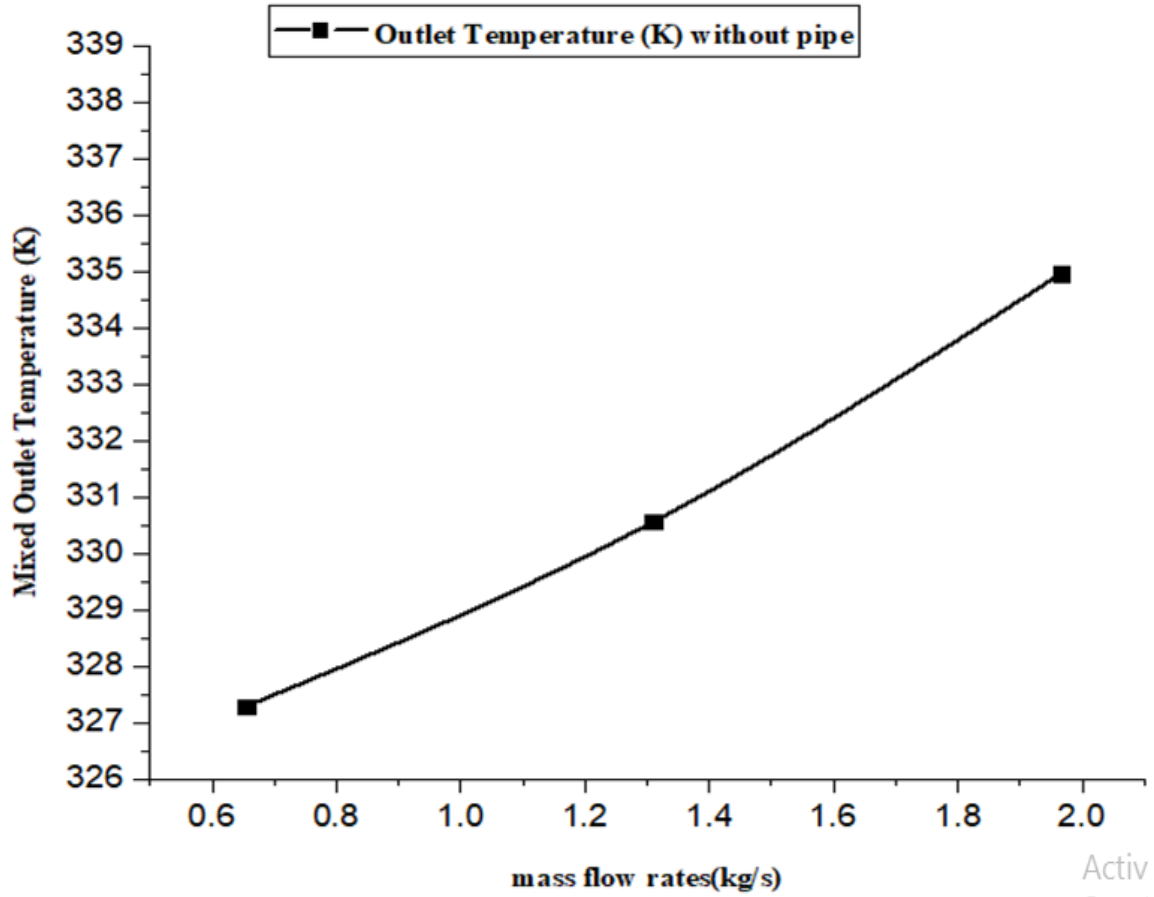


Figure 6.12: Mass flow rate Vs outlet temperature for model 3.

6.6 Comparisons of Hot Water Storage Tank with Stratification and Without Stratification

A thermally stratified hot water storage tank means hot water in which uniform temperature distribution was obtained because of reduced turbulence flow of hot and cold liquid water. In this study, a hot water tank with a perforated inlet pipe was thermally stratified since the structure of this pipe regulates the fluid's inlet flow. Throughout this storage, hot water with uniform temperature was achieved at 335.1901 temperature (K). In the case of the hot water storage tank with a normal inlet pipe inserted, the temperature inside the storage tank was characterized by different temperature distributions inside the storage tank because the inlet structure of this storage tank allows penetration of liquid water into the storage. This results in turbulence of fluid inside the storage tank, which destroys thermal stratification inside the storage tank.

Similarly, the storage tank, without inserting any inlets but instead holes, was used as inlets, and the outlet was also characterized by the formation of different temperature layers inside the storage. In case there was a formation of turbulence flow of inlet liquid water, which destroyed thermal stratification inside the storage tank. In addition to this formation of turbulence flow, the poor structure of these inlets resulted in low output of the system compared to the hot water storage tank designed with both normal inserted inlet pipe and perforated inlet pipe.

Comparison analysis of each model was performed by analyzing the mass flow rate of each model against outlet temperature. As shown in the following table, the maximum outlet temperature was obtained in model 2, and the minimum result was achieved in model 3 compared to each other.

Table 6.4: Mass flow rate vs outlet for each model

Flow rates hot fluid (kg/s)	Without inlet pipe	With normal pipe	With perforated pipe
$\dot{m}_1 = 0.655$	327.2949	329.9994	331.6894
$\dot{m}_2 = 1.31$	330.5676	332.9706	335.1901
$\dot{m}_3 = 1.965$	334.9689	337.4570	339.9691

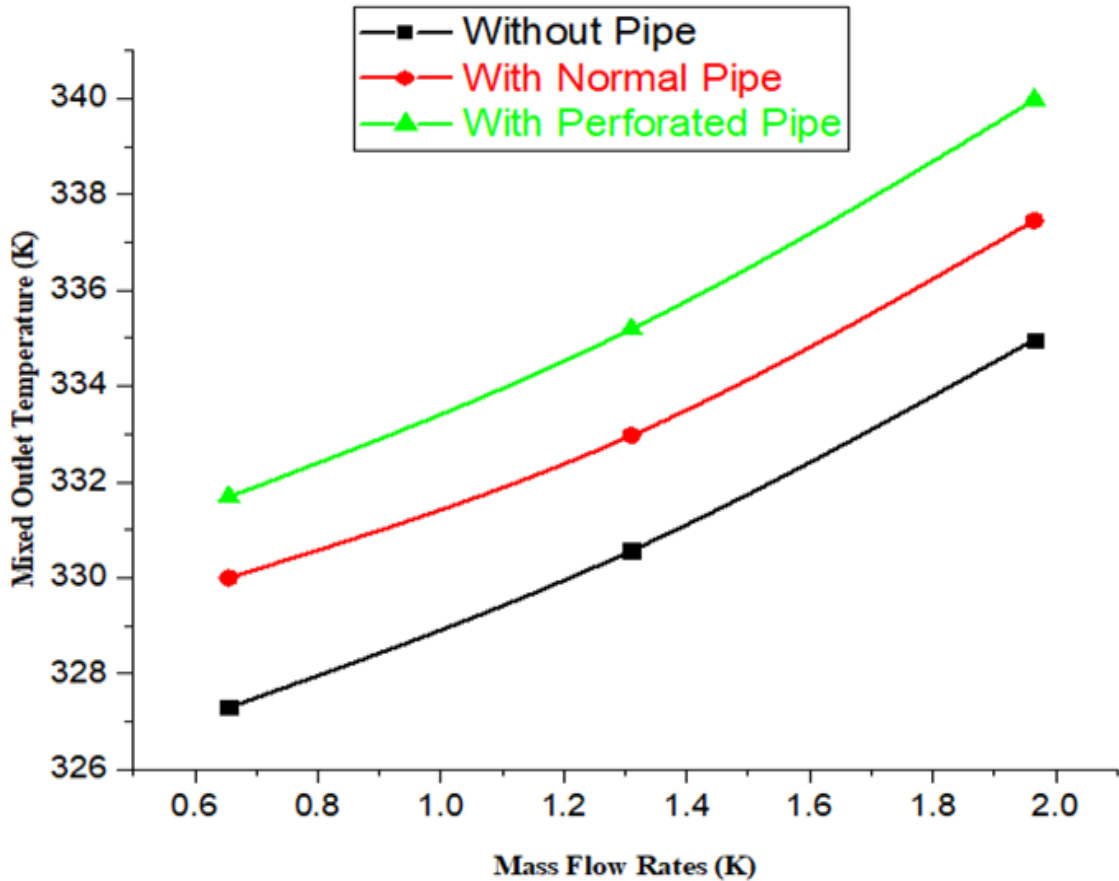


Figure 6.13: Mass flow rate Vs outlet temperature for each model

From the above graph, it is clear that as the mass flow rate increased, outlet temperature also increased for all models. However, model 2 had more incredible performance overall model because of the modified structure of the inlets. Model 1 had more outstanding performance than Model 3. From this comparison, the conclusion can be drawn that the hot water storage tank with a perforated inlet pipe inserted was characterized by low turbulence flow, which was used to enhance thermal stratification inside the storage tank.

Another method of comparison was the efficiency of the system. The efficiency of most water heaters was known by their uniform energy factor that was based on the amount of energy the water heater had. The standard that the efficiency of water storage corresponded to 58 – 60%, which was determined by the following equation.

$$\eta_{th} = \frac{\text{Effective output}}{\text{power input}} = \frac{m\Delta cp(T_0 - T_i)}{mcp(T_{f0} - T_i)} \quad (6.1)$$

In equation (6.1), the efficiency of a hot water storage tank designed with a normal pipe inserted was 53.1%, while for a hot water storage tank with a perforated pipe inserted was 56.2%. Similarly, the efficiency of a hot water storage tank designed without inserting any inlet pipes but instead using holes as inlets was 49.9%.

From these designs, the hot water storage tank designed with a perforated inlet was optimized from 53.1% to 56.2% compared to the normal inserted pipe. Similar to the hot water storage tank without inserting an inlet, it was optimized from 49.9% to 56.2%. The best output temperature was achieved from a hot water storage tank with perforated inlet pipe, which was thermally stratified because of reduced turbulence flow of fluid inlets. Generally, a hot water storage tank with a normal inlet pipe and without an inserted inlet pipe had no stratification. In contrast, a hot water storage tank with a perforated pipe inserted was a stratified storage tank, as its efficiency and thermal performance indicated.

6.7 Comparisons of Thermal Stratification Hot Water Storage Tank with Experimental Results

For validity of this study CFD results of thermally stratified hot water tank (model 2) was selected and compared with experiment results of (Louanate et al., 2020) and the result of study has good agreement with the experimental result. The experiment used hot water storage tank made up of stainless steel with dimension 400mm height and 220mm diameter as thermal energy storage. The inlet and outlet diameter were 50mm for both cold water at the bottom and top water at the top (Louanate et al., 2020). The results of this work was compared with experimental result taken from the above dimension.

Figure (6.14) shows comparison between experimental results taken from related work and this work. The figure shows that CFD results of this work and experimental result of the relate work have good agreement with each other. However, as figure indicate CFD result shows greater performance over experimental results.

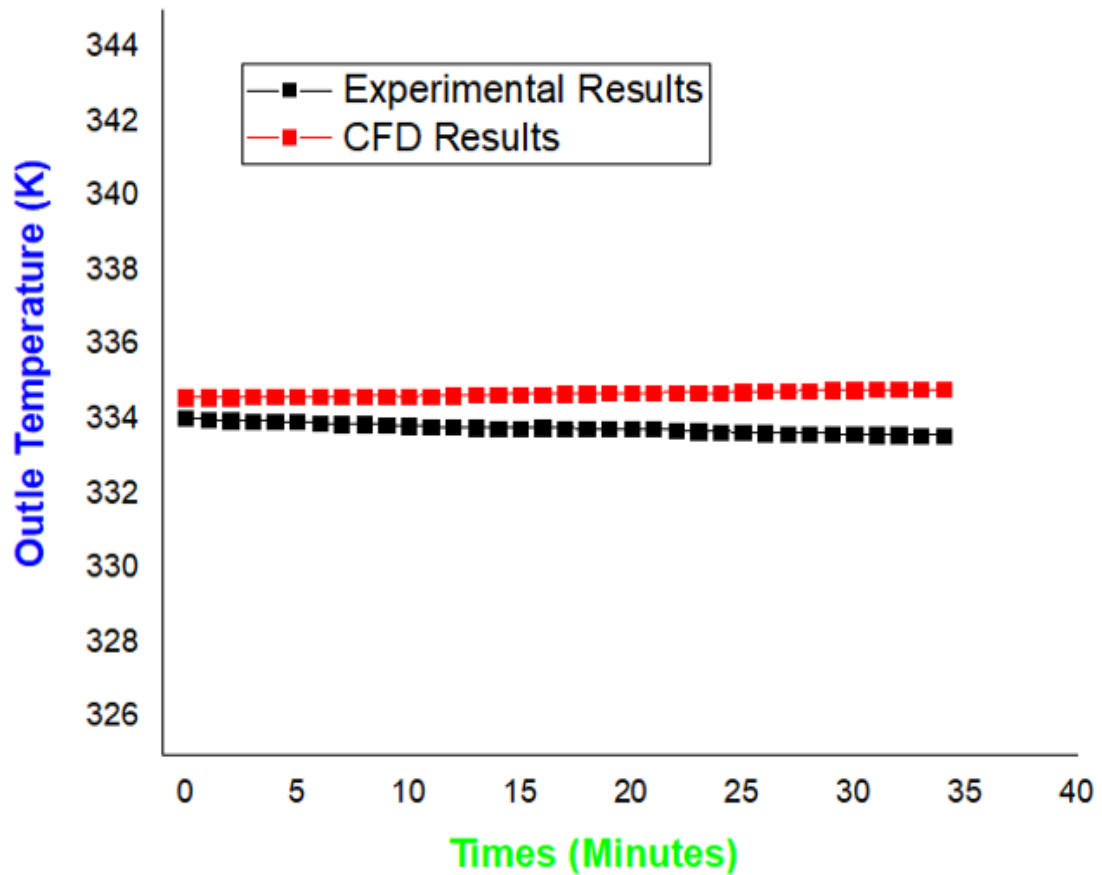


Figure 6.14: Comparison of CFD results with experimental results

Chapter 7

Conclusion and Recommendations

7.1 Conclusion

Design and 3-D modeling of the thermal energy storage tank and hot water storage tank were carried out in this study. Thermal energy storage was designed for storing HTF containing high temperatures from flat plate solar collectors. Paraffin wax PCMs are used as a heat storage medium. The total mass of the PCMs was 2746.59kg with a total volume of 5.8m^3 and a total number of 28 pipes as shell and tube heat exchangers. In the case of hot water storage, three types of hot water storage were modelled with the same dimension but different inlets to investigate the inlet effects on the hot energy storage system. From CFD analysis results, the following conclusion was achieved:

- Model 1 was designed with a normal inlet pipe inserted, and was characterized by different temperature around six layers inside hot water storage formed by the turbulent flow of fluid. It indicates that the hot water tank's inlet design affects the system's thermal performance.
- The uniform temperature only one layer distribution was achieved within model 2, designed with a perforated pipe inlet. Because of this, the best output that lined up with the expected was obtained in this model.
- Temperature distribution inside model 3, designed without inserting inlets, was also distinguished by six different temperature layers, especially at the top of the storage. These different temperature layers were formed because of the inlet structure; incoming fluid water was high at the start and then gradually decreased along the bottom of the storage. In this model, the outlet was less compared to the two.
- Design of hot water storage tank designed with perforated inlet was optimized from 53.1% to 56.2% compared to normal inserted pipe. Similar when compared to the hot water storage tank without inserting inlet it was optimized from 49.9% to 56.2%. Constant output temperature was achieved inside the hot water storage tank design with a perforated inlet pipe since thermal stratification was maintained because of the inlet design.
- Generally, from this CFD simulation result, thermal storage inside of hot water storage is affected by the inlet structure of the storage system.

7.2 Recommendations

Interested researchers can address the following recommendations for future works to extend and solve more problems.

- Someone can work on experimental validation to make the study more attractive and reliable.
- Up and downward inlet pipes for hot storage tanks can be designed to investigate their effects on the system performance by CFD simulation.
- The cost analysis can be done to complete the system entirely.
- This study can be used as an input for the design optimization of PCMs integrated into hot water storage tanks to predict their effects on the system efficiency.

References

- Hasen, Y. (2019). *Investigating the Thermal Performance of a Solar Water Heating System Integrated with Phase Change Material as a Thermal Energy Storage: A Case of Adama Hospital Medical College* (Doctoral dissertation, ASTU).
- White, M., Read, M. G., and Sayma, A. I. (2018). Optimisation of cascaded organic Rankine cycle systems for high-temperature waste-heat recovery.
- Jankowiak, C., Zacharopoulos, A., Brandoni, C., Keatley, P., MacArtain, P., and Hewitt, N. (2019). The role of domestic integrated battery energy storage systems for electricity network performance enhancement. *Energies*, 12(20), 3954.
- Herrando, M., Pantaleo, A. M., Wang, K., and Markides, C. N. (2019). Solar combined cooling, heating and power systems based on hybrid PVT, PV or solar-thermal collectors for building applications. *Renewable Energy*, 143, 637-647.
- Abokersh, M. H., Osman, M., ElBaz, O., ElMorsi, M., and Sharaf, O. (2018). Review of the phase change material (PCM) usage for solar domestic water heating systems (SDWHS). *International journal of energy research*, 42(2), 329-357.
- Karim, A., Burnett, A., and Fawzia, S. (2018). Investigation of stratified thermal storage tank performance for heating and cooling applications. *Energies*, 11(5), 1049.
- Duffie, J. A., Beckman, W. A. (2013). *Solar engineering of thermal processes*. John Wiley and Sons.
- Abu-Hamdeh, N., and Alnefaie, K. (2019). Techno-economic comparison of solar power tower system/photovoltaic system/wind turbine/diesel generator in supplying electrical energy to small loads. *Journal of Taibah University for Science*, 13(1), 216-224.
- Basu, A. K., Tatiya, S., Bhatt, G., and Bhattacharya, S. (2019). Fabrication processes for sensors for automotive applications: A review. *Sensors for automotive and aerospace applications*, 123-142.
- Majumdar, R., and Saha, S. K. (2019). Effect of varying extent of PCM capsule filling on thermal stratification performance of a storage tank. *Energy*, 178, 1-20.
- Bouzaher, M. T., Bouchahm, N., Guerira, B., Bensaci, C. E., and Lebbi, M. (2019). On the thermal stratification inside a spherical water storage tank during dynamic mode. *Applied Thermal Engineering*, 159, 113821.
- Rasha, R. (2020). *Solar water heating systems with thermal storage for application in Newfoundland* (Doctoral dissertation, Memorial University of Newfoundland).

- Lasmar, A. (2018). *Modeling a hot water storage tank for thermal energy storage using encapsulated phase change materials (PCMs)* (Doctoral dissertation, Memorial University of Newfoundland).
- Bazri, S., Badruddin, I. A., Naghavi, M. S., Seng, O. K., and Wongwises, S. (2019). An analytical and comparative study of the charging and discharging processes in a latent heat thermal storage tank for solar water heater system. *Solar Energy*, 185, 424-438.
- Bouhal, T., Fertahi, S., Agrouaz, Y., El Rhafiki, T., Kousksou, T., and Jamil, A. (2017). Numerical modeling and optimization of thermal stratification in solar hot water storage tanks for domestic applications: CFD study. *Solar Energy*, 157, 441-455.
- Rauf, S., and Saha, S. K. (2019). Thermal performance of multitube latent heat storage using a metal matrix for solar applications: numerical study. *Heat Transfer Research*, 50(6).
- Bouzaher, M. T., Bouchahm, N., Guerira, B., Bensaci, C. E., and Lebbi, M. (2019). On the thermal stratification inside a spherical water storage tank during dynamic mode. *Applied Thermal Engineering*, 159, 113821.
- Wang, Z., Zhang, H., Dou, B., Zhang, G., and Wu, W. (2019). Influence of inlet structure on thermal stratification in a heat storage tank with PCMs: CFD and experimental study. *Applied Thermal Engineering*, 162, 114151.
- Theeb, M. A., Alhamdo, M. H., and Fahad, R. S. (2020). Thermal effects of using various metal disks inside liquid-PCM thermal storage system. *J. Mech. Eng. Res. Dev*, 43(5), 218-230.
- Huang, H., Wang, Z., Zhang, H., Dou, B., Huang, X., Liang, H., and Goula, M. A. (2019). An experimental investigation on thermal stratification characteristics with PCMs in solar water tank. *Solar Energy*, 177, 8-21.
- Neri, M., Chiavazzo, E., and Mongibello, L. (2020). Numerical simulation and validation of commercial hot water tanks integrated with phase change material-based storage units. *Journal of Energy Storage*, 32, 101938.
- Rasha, R. (2020). *Solar water heating systems with thermal storage for application in Newfoundland* (Doctoral dissertation, Memorial University of Newfoundland).
- Louanate, A., El Otmani, R., Kandoussi, K., and Boutaous, M. H. (2020). Non-isothermal crystallization kinetics of paraffin wax as a phase changing energy storage material. *Physica Scripta*, 95(10), 105003.

- Dileep, K., Raj, A., Dishnu, D., Saleel, A., Srinivas, M., and Jayaraj, S. (2020). Computational fluid dynamics analysis on solar water heater: Role of thermal stratification and mixing on dynamic mode of operation. *Thermal Science*, 24(2 Part B), 1461-1472.
- Wang, Z., Zhang, H., Dou, B., Zhang, G., Wu, W., and Zhou, L. (2020). An experimental study for the enhancement of stratification in heat-storage tank by equalizer and PCM module. *Journal of Energy Storage*, 27, 101010.
- Avargani, V. M., Norton, B., Rahimi, A., and Karimi, H. (2021). Integrating paraffin phase change material in the storage tank of a solar water heater to maintain a consistent hot water output temperature. *Sustainable Energy Technologies and Assessments*, 47, 101350.
- Malec, A., Cholewa, T., and Siuta-Olcha, A. (2021). Influence of cold water inlets and obstacles on the energy efficiency of the hot water production process in a hot water storage tank. *Energies*, 14(20), 6509.
- Kumar, K., and Singh, S. (2021). Investigating thermal stratification in a vertical hot water storage tank under multiple transient operations. *Energy Reports*, 7, 7186-7199.
- Diro, S., Erko, B., and Fikirie, K. (2019). Production and adoption constraints of improved coffee varieties in Jimma zone, Southwest Ethiopia. *Journal of Scientific Agriculture*, 3, 33-40.
- Fuentes, E., Arce, L., and Salom, J. (2018). A review of domestic hot water consumption profiles for application in systems and buildings energy performance analysis. *Renewable and Sustainable Energy Reviews*, 81, 1530-1547.
- Gedlu, S. (2019). *Potential Use Of Solar Thermal As An Alternative Energy Source For Adama General Hospital And Medical College* (Doctoral dissertation, ASTU).
- Deshmukh, G., Birwal, P., Datir, R., and Patel, S. (2017). Thermal insulation materials: A tool for energy conservation. *J. Food Process. Technol*, 8(04), 8-11.
- Alva, G., Liu, L., Huang, X., and Fang, G. (2017). Thermal energy storage materials and systems for solar energy applications. *Renewable and Sustainable Energy Reviews*, 68, 693-706.
- Xie, L., Tian, L., Yang, L., Lv, Y., and Li, Q. (2017). Review on application of phase change material in water tanks. *Advances in Mechanical Engineering*, 9(7), 1687814017703596.

- Kumar, S., and Mullick, S. C. (2010). Wind heat transfer coefficient in solar collectors in outdoor conditions. *Solar energy*, 84(6), 956-963.
- Pan, C., Vermaak, N., Wang, X., Romero, C., and Neti, S. (2021). A fast reduced model for a shell-and-tube based latent heat thermal energy storage heat exchanger and its application for cost optimal design by nonlinear programming. *International Journal of Heat and Mass Transfer*, 176, 121479.
- Mousavi Maleki, S. A., Hizam, H., and Gomes, C. (2017). Estimation of hourly, daily and monthly global solar radiation on inclined surfaces: Models re-visited. *Energies*, 10(1), 134.
- Shivalinga swamy, T., and Kagali, B. A. (2012). Exact Eigenstates of a Relativistic Spin less Charged Particle in a Homogeneous Magnetic Field. *Physics Education*.
- Skeiker, K. (2009). Optimum tilt angle and orientation for solar collectors in Syria. *Energy Conversion and Management*, 50(9), 2439-2448.
- Yadav, A. K., and Chandel, S. S. (2013). Tilt angle optimization to maximize incident solar radiation: A review. *Renewable and Sustainable Energy Reviews*, 23, 503-513.
- Gana, N. N., and Akpootu, D. O. (2013). Angstrom type empirical correlation for estimating global solar radiation in north-eastern Nigeria. *The International Journal Of Engineering And Science*, 2, 58-78.
- Gopinathan, K. K. (1988). A general formula for computing the coefficients of the correlation connecting global solar radiation to sunshine duration. *Solar energy*, 41(6), 499-502.
- Duffie, J. A., Beckman, W. A., and Worek, W. M. (1980). Solar engineering of thermal processes (Vol. 3). *New York etc.: Wiley*.
- Mahanta, D. K. (2020, December). Mathematical Modeling of Flat Plate Solar Collector. In *2020 IEEE International Conference on Power Electronics, Drives and Energy Systems (PEDES)* (pp. 1-5). IEEE.
- Khammas, F. A., Mustafa, A. T., and Khalifa, A. J. N. (2021). Temperature stratification in a thermal storage tank: The effect of flow rate and aspect ratio. *J. Eng. Sci. Technol*, 16, 1066-1081.

Appendix A

Appendix

A.0.1 Analyzed average monthly sunshine hours of Limmu Gennet for five years

Months	n^{th}	$\delta(^{\circ})$	$ws(^{\circ})$	$N (hrs.)$	$n (hrs)$	n/N	a	b	$H_o(kW$ $h/m^2/d)$	$H(kwh$ $/m^2/d)$	$K_T = \frac{H_T}{H_o}$
Jan	17	-20.9	86.9	11.6	8.95	0.77	0.33	0.40	9.1	5.81	0.64
Fe	47	-13	88.12	11.7	8.05	0.69	0.30	0.43	9.8	5.85	0.60
Mar	75	-2.4	89.66	11.9	7.90	0.66	0.29	0.44	10.3	5.58	0.54
Apr	105	9.4	91.34	12.2	7.40	0.61	0.28	0.45	10.5	5.82	0.55
May	135	18.8	92.76	12.4	7.28	0.59	0.27	0.46	10.7	5.79	0.54
Jun	162	23.1	93.47	12.5	6.22	0.50	0.25	0.49	11.1	5.49	0.5
Jul	198	21.2	93.15	12.4	3.42	0.28	0.18	0.57	11.2	3.80	0.34
Aug	228	13.5	91.95	12.3	4.03	0.33	0.20	0.56	11.5	4.43	0.39
Sep	258	2.2	90.31	12.0	4.77	0.40	0.22	0.53	10.3	4.45	0.43
Oct	288	-9.9	88.63	11.8	7.73	0.66	0.29	0.44	9.8	5.69	0.58
Nov	318	-18.9	87.23	11.6	8.13	0.70	0.31	0.42	9.3	5.62	0.60
Dec	344	-23	86.56	11.5	8.86	0.77	0.33	0.40	8.9	5.68	0.64

A.0.2 The monthly average daily solar radiation on the horizontal surface (H_o)

Hour angle	86.9	88.1	89.7	91.3	92.8	93.5	93.2	92.0	90.3	88.6	87.2	86.6
Declination	-20.9	-13	-2.4	9.4	18.8	23.1	21.2	13.5	2.2	-9.6	-18.9	-23.0
(H_o)	9.1	9.8	10.3	10.5	10.7	11.1	11.2	11.5	10.3	9.8	9.3	8.9

A.0.3 General thermodynamic characteristics of PCMs(Zhang et al., 2018)

Thermo-physical properties	<ul style="list-style-type: none"> ✓ High specific heat, High conductivity, high density, and thermal conductivity ✓ Required melting temperature range ✓ Small volume changes in phase transformation and small vapor pressure at operating temperatures reduce the containment problem ✓ Congruent melting
Chemical properties	<ul style="list-style-type: none"> ✓ Complete reversible cycle ✓ Chemically stable with no degradation after a large number of freezing melting cycles. ✓ Encapsulation materials ✓ No corrosiveness, not poisonous, not volatile and anti-flammable ✓ Compatibility with materials, encapsulation with container
Kinetics properties	<ul style="list-style-type: none"> ✓ High nucleation rate to prevent liquid phase super cooling ✓ High rate of crystal development to suit the needs of the storage system's heat recovery
Economic properties	<ul style="list-style-type: none"> ✓ Cost-effective ✓ Commercially available for large scale-practice
Environmental properties	<ul style="list-style-type: none"> ✓ Low environmental impact ✓ Nonpolluting through service life and having recycling potential

A.0.4 Summary technical data designed thermal and hot water tank.

Phase Change Material Integrated Thermal Storage Tank	
Volume (V)	$11.6m^3$
Number of storage	2
Diameter (m)	1.95
Height (m)	3.89
Mass (kg)	2746.59
Number of tubes	28
Insulation thickness (m)	0.03
Phase Change Material	Paaraffin wax
Hot Water Storage Tank	
Material	Mild steel
Volume (V)	$38.88m^3$
Diameter (m)	4.64
Diameter (m)	2.32
Height (m)	4.64
Thickness (m)	0.01
Number of hot water tank	2
Insulation material	Fiber glass
Capacity (kwh)	6205.25
Solar Collector	
Types	Flat plate
Numbers (V)	217
Area (m^2)	2
Fluid temperature outlet (k)	375
Useful energy gained (w)	845.5
Overall heat transfer coefficient (w/m^2C°)	9.25
Total energy lost (w/m^2)	314.5
Collector efficiency	60%
Collector area (m^2)	2

A.0.5 Questionnaire

This questionnaire is required for academic research study purpose and you are politely asked to fill the following form. Fill the box with sign X in the provided space.

1. Number of beneficiaries from the hospital? _____
2. What is the main source of energy for water heating?
Wood biomass electrical coal kerosene other _____
3. How much money per week do you spend for heating?
Up to 1000 1001 – 2000 2001-3000 3001-4000 above 4000
4. When using wood biomass what do you think the main problem?
Smoke Supply Cost Labor If other specify _____
5. If using electric energy what is advantage and disadvantages?

_____.
6. Do you use solar energy for water heating?
a) Yes why? _____
b) No why? _____
7. How many numbers of bed room the hospital occupies? _____ numbers of bed in each room _____.
8. How many numbers of laundry the hospital has? _____.
9. How many numbers of restaurant the hospital has? _____.
10. How many numbers of restaurant the hospital has? _____.
11. How numbers of households benefited from the hospital? _____.
12. How much liters of hot water consumed per a day in the hospital? _____.
13. Do buy solar water heating system for water heating system? _____.